DEPOSITION OF SUSPENSIONS IN LAMINAR FLOW IN THE ENTRANCE REGION OF CHANNELS WITH DIFFUSIVE, ELECTROSTATIC AND GRAVITATIONAL EFFECTS

BY

THOMAS ANTHONY KORJACK

A DISSERTATION

PRESENTED IN PARTIAL FULFILLMENT OF THE

REQUIREMENTS FOR THE DEGREE OF

DOCTOR OF ENGINEERING SCIENCE IN

MECHANICAL ENGINEERING

AT

NEW JERSEY INSTITUTE OF TECHNOLOGY

Newark, New Jersey
1978

ABSTRACT

This investigation entailed the consideration of the deposition of suspensions in laminar flow in the entrance region of a parallel-plate channel, and both converging and diverging channels, under the combined influences of diffusive, electrostatic and gravitational effects. The fluid phase was assumed to be incompressible, steady and laminar; the particle phase was assumed to be steady, laminar, dilute, and with negligible lift force.

The complete solution of the problem involved solving the boundary layer equations for the completely viscous fluid phase, and the particulate momentum, continuity and potential equations for the particle phase. Since the resulting equations are non-linear partial differential equations, numerical techniques were utilized to obtain solutions.

The flow characteristics of the particulate phase along with the deposition rate of the solid particles were investigated under varied flow conditions. Deposition due to surface adhesion,gravity and electrostatic charge was considered.

It was found that an appreciable amount of particle deposition can result because of gravity on the solid particles especially on the bottom wall which showed a much higher deposition rate than the top wall. Moreover, when

the combined influence of gravity and electrostatic charge was considered, it was found that a much higher deposition rate occurs on the bottom wall as compared to the case without the electrostatic charge effect.

Furthermore, it was observed that the deposition lessened with increased convergence angle; however, a much higher deposition rate was found on the bottom wall with increased divergence(diffuser) angle due to the separation phenomenon of the boundary layer.

APPROVAL OF DISSERTATION

DEPOSITION OF SUSPENSIONS IN LAMINAR FLOW IN THE ENTRANCE REGION OF CHANNELS WITH DIFFUSIVE, ELECTROSTATIC AND GRAVITATIONAL EFFECTS

BY

THOMAS ANTHONY KORJACK

FOR

DEPARTMENT OF MECHANICAL ENGINEERING
NEW JERSEY INSTITUTE OF TECHNOLOGY

BY

FACULTY COMMITTEE

APPROVED: _____ CHAIRMAN

_____

_____

_____

_____

NEWARK, NEW JERSEY
1978

To my beloved wife and my dear mother,

for their patience and encouragement

ACKNOWLEDGEMENTS

The author wishes to express his sincere and grateful gratitude to his advisor and project director, Professor Rong-Yaw Chen, who provided many valuable suggestions, continuous guidance and encouragement throughout the course of the entire investigation.

The author wishes also to express his sincere gratitude to Professors J. S. Hsieh, R. P. Kirchner, H. Pawel and R. I. Andrushkiw, who have kindly read through the original manuscript and provided valuable suggestions.

Further acknowledgement is given to the Mechanical Engineering Department of the New Jersey Institute of Technology for the teaching fellowship appointments during the 1974-1975, 1975-1976 academic years.

The research assistantship supported by the Army Research Center during 1977-1978 is gratefully acknowledged.

TABLE OF CONTENTS

LIST OF FIGURES

NOMENCLATURE

a	radius of a particle
C_D	drag coefficient for a sphere
D_p	particle diffusivity
E	electric field intensity
E^*	dimensionless electric field intensity
f_w	adhesive force per unit mass of particles at the immediate vicinity of the wall
f_L	lift force per unit mass of particles acting on a particle by fluid shear
f_i	i th component of body force for fluid phase
f_{pi}	i th component of body force for particle phase
F	inverse of relaxation time for momentum transfer given by equation (3-2)
h	half the channel width
K_m	an effectiveness parameter accounting for a momentum transfer from the freely suspended particles to the fluid
K_{np}	particle Knudsen number
L_p	fluid-particle interaction length
m_p	mass of a particle
$\dot{m}1$	rate of mass flow of the solid particles deposited on the bottom wall
$\dot{m}2$	rate of mass flow of the solid particles deposited on the top wall
N_s	surface adhesion parameter

$\dot{m}$ total rate of mass flow of the solid particles deposited on the walls

$\dot{M}^*1$ dimensionless rate of deposition of particles on the bottom wall

$\dot{M}^*2$ dimensionless rate of deposition of particles on the top wall

$\dot{M}^*$ total rate of deposition of particles on the walls

N_{DF} diffusion-response number which is the square root of the ratio of relaxation time to diffusion time

N_{ED} electro-diffusion number which is the ratio of displacement by electrostatic repulsion to that by diffusion

N_m momentum-transfer number which is the ratio of relaxation time to transport time

N_R Reynolds number

N_{scp} particle Schmidt number

p static pressure of the fluid

p_o static pressure at inlet

q electric charge per particle

R dimensionless density of the particle cloud (concentration)

t time variable

u,v axial and vertical component of fluid velocity

u_p,v_p axial and vertical component of particle velocity

u_o inlet velocity (uniform)

U,V dimensionless axial and vertical component of fluid velocity

U_i i^{th} component of the velocity of the fluid phase

U_{pi} i^{th} component of the velocity of the particle phase

U_p, V_p dimensionless axial and vertical component of particle velocity

W_i i^{th} component of the electric potential

W^* dimensionless electric field potential

WP dimensionless half diffuser width as defined in Appendix B

x,y axial and vertical coordinates respectively

X_i i^{th} component of the space coordinate

X,Y dimensionless axial and vertical coordinates

Greek Letters

N_α, N_β, N_η dimensionless groups as defined in Appendix B

δ_{ij} Kronecker-Delta

Δ_{ij} deformation tensor (for the fluid phase) as defined by equation (3-2a)

$(\Delta_p)_{ij}$ deformation tensor for the particle phase as defined by equation (3-4a)

ε_o permittivity of free space

θ half the diffuser angle

ρ density of the fluid phase

$\bar{\rho}$ density of the material constituting the fluid phase

ρ_p density of the particle cloud (concentration)

$\bar{\rho}_p$ density of the material constituting the particle phase

ρ_{po} inlet density of the particle cloud

$\bar{\mu}_f$ viscosity of the material constituting the fluid phase

μ_f viscosity of the fluid of suspension

μ_{f2} viscosity defined by equation (3-2a)

ζ_f bulk viscosity of the fluid phase

ζ_p bulk viscosity of the particle phase

μ_p viscosity of the particulate phase in suspension, $\mu_p \tilde{\sim} \rho_p D_p$

μ_{p2} viscosity defined by equation (3-4c)

ν kinematic viscosity of the fluid of suspension

ν_p kinematic viscosity of the particulate phase in suspension, $\nu_p \sim D_p$

τ relaxation time, $F^{-1} = \tau$

Ω_f dilatation tensor of the fluid phase defined in equation (3-2c)

Ω_p dilatation tensor of the particle phase defined in equation (3-4b)

σ sticking probablility accounting for electrical and viscous forces

σ_w sticking probability accounting for adhesive forces at the wall

Superscripts

* dimensionless quantities as defined

Subscripts

c	for centerline condition
f	for fluid phase
o	initial condition
p	for particle phase
w	for wall condition

1. INTRODUCTION

Two phase fluid-solid particle suspension flow exists in various situations and it is of extreme importance in many applications. Among these are dust collectors, fluidized beds, pneumatic conveyors, air compressors, fluid scrubbers, aerosol sprays, rocket exhausts containing solid propellants, furnace exhausts, blood flows, respiratory tracts and many others. The flow of suspensions resulting in depositions is the primary cause of fluidic contamination. Hence, reliability prediction depends upon an in depth knowledge of the contamination process itself whereby performance and plugging characteristics can be obtained for better fluidic control.

An important problem investigated recently was the significance of parameters affecting the deposition process in laminar flow where perfect symmetry was assumed. It was found that an appreciable amount of particle deposition can result because of the electrostatic charge on the particles. Because of symmetrical flow, gravitational influences were of course neglected. Although there have been many investigations related to particle depositions, all have been for turbulent flows, fully developed laminar flows, or for symmetrical laminar entrance flows neglecting gravitational influences.

The objective of this study is to investigate numerically the unsymmetrical laminar entrance flow of suspensions under a gravitational field. Since experimental work in most cases utilizes particles (such as 10 or more micro meter in size) for which the gravity effect is very significant, this analysis will serve as a practical model for experimental data analysis.

Thus, a mathematical model for the entrance solution of suspensions in laminar flow with significant gravity effects or with both electrostatic charge and gravitational effects has been developed for the deposition process on both the top and bottom walls of channels. Due to gravitational considerations (influences), the particulate phase will follow an unsymmetricalflow pattern whereas the fluid phase, being the incompressible carrier, will follow a symmetrical pattern.

The characteristics of the rate of deposition curves for different flow parameters with gravitational forces will also be considered. In particular, for the convergent and divergent channels, the effect of the angle of divergence or convergence with gravity on the rate of deposition of the solid particles will be investigated. Moreover, the case when a parallel plate channel is connected to a divergent channel will also be considered.

Consequently,the case when a parallel channel is connected to a diffuser will be investigated. Here it is meant by channel, the constant area one,i.e.,the parallel-plate channel and by diffuser is meant the straight wall diffuser.

In this study,the particle cloud was treated as a continuum whereby the flow of suspensions was regarded as a mixture of two interpenetrating continuous fluids. The particulate concentration was assumed low enough(dilute suspension) such that the particles have negligible effect upon the fluid phase. The fluid phase was assumed to be viscous throughout the entire flow field, and both the fluid phase and the particle phase were assumed to be in two-dimensional, steady flow.

Since the resulting governing equations and boundary conditions are non-linear partial differential systems, finite difference and other numerical techniques were used to solve the parallel,converging and diverging channels.

All the numerical work was carried out on an IBM 370 computer with an accuracy of four significant figures for the various channel flow configurations.

In Chapter 2, a brief literature survey on the deposi-tion of particles in multiphase flow was studied. The

laminar flow of suspensions in the entrance region of a parallel-plate channel under a gravitational field was studied in chapter 3; that of the divergent and convergent channels with uniform and nonuniform inlet conditions in chapter 4. Conclusions and suggested recommendations for future study are given in chapters 5 and 6 respectively.

2. LITERATURE SURVEY

Internal flows of suspensions of particles have been studied by many authors. Tan and Hsu [36] presented the problem of mass transfer of aerosols with axial diffusion in laminar flow through a cylindrical tube. They considered two cases: In the first case all of the particles entered the channel inlet only and none formed within the channel itself; in the second case, no particles enter the channel and "formation in flight" occurs within the channel. This second case occurs when air containing a radioactive rare gas enters the channel through a high-efficiency filter located at the channel inlet. As the radioactive gas flows through the channel, it decays giving rise to the steady production of a certain number of daughter atoms per unit volume. Unlike the radioactive gas, the daughter atoms adhere to the wall and hence are lost by diffusion. This dispersion of atoms may be considered to be an "atomic aerosol" since it has the same property as sub-micron aerosols in that they can be collected at a surface. It was found that for Peclet numbers, N_β ($N_\beta = 2V_m r_o/D_p$, where V_m = mean flow velocity, r_o = inner radius of tube, D_p the coefficient of diffusion) less than 100, the effect of axial diffusion is still significant at μ ($= D_p X/V_m r_o^2$) < 0.04. Also, the effect may be neglected at an axial

distance from the tube inlet greater than two and a half times that of the tube diameter for $1 < N_{\beta} < 100$.

Stukel and Soo [35] investigated the hydrodynamics of a suspension in turbulent motion over the inlet of a channel formed by two flat plates made for various flow velocities, plate gap widths and mass flow ratios of solids in air. Experiments were carried out in a 30 cm x 30 cm section wind tunnel with flow velocities up to 36 m/sec., plate gap widths of 0.64, 2.54 and 5.08 cm, and mass flow ratios up to 0.1 kg particles/kg air.

The nature of the developing turbulent boundary layer is such that the density of particles is higher at the wall than at the core due to the presence of charge on the particles (induced by surface contacts). Furthermore, a particle slip velocity brought about by the lack of particle to particle collisions in the suspension was observed at the wall, analagous to rarefied gas motions. It was concluded that similarity laws for the scaling of equipment for air pollution control should include the momentum transfer number and the electroviscous number in addition to the Reynolds number.

The general case of a fully developed pipe flow of a suspension in a turbulent fluid with electrically charged particles or with significant gravity effect, or both and

for any inclination of the pipe with the direction of gravity was formulated by Soo and Tung [33]. The significant parameters defining the state of motion were: pipe flow Reynolds number, Froude number, electro diffusion number, diffusion response number, momentum transfer number and particle Knudsen number.

Comparisons with experimental results were made for both gas-solid and liquid-solid suspensions. It was shown that the gravity effect becomes significant in the case of large pipe diameters and large particle concentrations.

Soo and Tung [34] took into account the effect of sedimentation taken from previous studies of the fully developed flow of a suspension of particles in a turbulent fluid.

Additional considerations from previous studies were the diffusion and settling under field forces, and the sticking probability of a particle at the wall and that to a bed of similar particles. The transient conditions gave the rate of build up of a bed of deposited particles. The method was applicable to pipes at any inclination to the direction of gravity.

Friedlander and Johnstone [13] found that when a stream of gas carrying suspended particles flows in turbulent motion past a surface, the particles are deposited

due to the radial fluctuating component of velocity. They found that the net rate of deposition depends on both the rate of transport of the particles to the wall and the rate of re-entrainment.

Soo and Rodgers [32] studied the occurrence of deposition due to field forces. They identified a sticking probability, σ, which depends upon material properties when all particles drifting to the wall stick or settle at the wall, $\sigma = 1$; $\sigma = 0$ for complete re-entrainment. This sticking probability is related to the force of adhesion of particles to a surface.

Corn [10] showed that adhesive forces are either electrical or liquid (viscosity and surface tension) in origin. The electrical forces include contact potential differences and dipole effects, space charge and electronic structure. The gravity effect alone produces settling, but the fact that a particle may again be re-entrained gives $\sigma < 1$. Another sticking probability σ_w concerns adhesion of particles at the immediate vicinity of the wall.

Chua and Wang [8] performed an experimental investigation of the deposition of submicron particles from steady flows in a branched tube. At all flow rates, the deposition rates along the inner walls were observed to

have a maximum at the branch point and a second maximum at approximately two diameters distance from the branch point.

Simultaneous diffusion and sedimentation of aerosol particles in two dimensional channels have been studied theoretically by Ingham [16] and [17]. Both plug (uniform) and fully-developed flow were considered with the emphasis on the case when diffusion effects are larger than or of the same order as sedimentation effects due to gravity. The theoretical investigation assumed complete adhesion of particles on the surface and the effect of the developing velocity profile in the entrance was not investigated.

Chen and Comparin [7] and Chen [6] investigated theoretically the diffusive deposition of particles in the entrance of circular tubes and two-dimensional channels, respectively. These analyses also assumed a complete adhesion of particles on the surface. It was found that the deposition depends on the Schmidt number (ν/D) of the flow. For a dimensionless distance, $(4x/\mu)/(u_o h/D)$ greater than 0.0001, the deposition in the entrance region approaches that of uniform flow for Schmidt numbers less than 0.01 and approaches that of Poiseuille flow greater than 100. The symbol x is axial distance from inlet, h width (i.e. depth) of channel, u_o uniform inlet velocity, D coefficient of diffusivity and ν the kinematic viscosity of the fluid.

Theoretical analyses on deposition in the entrance of a channel was investigated by Comparin et al. [9] and Eldighidy et al. [12] and in a diffuser by Comparin et al. [9]. In these analyses, the diffusion, electrostatic charge and adhesive force effects were investigated and it was found that the electrostatic charge effect played an important role in the deposition of particles. Eldighidy et al. [12] further found that the surface adhesion has a smaller effect on the rate of deposition than that due to electric charge. Furthermore, it was found that the angle of divergence has a great effect on the rate of deposition in a diffuser flow. By increasing the diffuser angle, the pressure gradient increases and also the rate of deposition increases. However, at larger diffuser angles separation takes place earlier and the rate of deposition increases rapidly in the presence of electric charge. However, in the absence of electric charge the rate of deposition decreases rapidly with increasing diffuser angle.

Experimental studies on the sticking probability of molecular clusters of Fe_2O_3 to solid surfaces by Zagainov et al. [39] showed that the sticking probability of such small particles was dependent on the surface material and the particle size. Analyses of data indicated a sticking probability of the order of 10^{-5}.

Recently, Savilionis et al. [27] presented a paper on charged aerosol deposition in straight and curved conducting tubes. The experimental study employed charged silicon carbide (1.4 μm) and titanium dioxide (0.22 μm) particles with $8x10^{-18}$ to $1.6x10^{-15}$ coulomb per particle at low Stokes numbers of $4x10^{-5}$ to $6x10^{-3}$ and Reynolds numbers ranging from $2x10^{3}$ to 10^{4}. The inlet and exit charge flow were measured by a collecting copper screen. By assuming charge flow to be proportional to the mass flow rate, it was found that the ratio of local to inlet concentration was in excellent agreement with Wilson's theory [37] that $\rho_p/\rho_{po} = 1/(1 + T_x/\gamma_i)$ where x is the axial distance down the tube and γ_i the tube radius. The constant T is $\rho_{po}q^2\gamma_i/(6\pi\mu a\varepsilon u_o)$ where q is the electric charge per particle; particle radius a, the electrical permittivity ε, and μ the viscosity of the fluid. Very small amounts of additional deposition were found in a tube with a 90 degree bend.

Comparin et al. [9] studied experimentally the deposition of contaminants in fluidic devices. They found that serious changes in performance and plugging can be expected in such devices.

Yang and Peddieson [38] discussed the continuum theory of solid-fluid suspensions including solid-phase viscosity. They applied that theory to the solution of

problems of one-dimensional, plane, parallel flow. The Stokes' drag formula was assumed to govern the interphase force and both components were assumed to obey Stokes' law of viscosity. They assumed no-slip condition for the dispersing phase and slip condition for the dispersed phase at a solid surface. The resulting equations were used to solve three steady-flow problems: (1) plane Poiseuille flow, (2) plane Couette flow, and (3) vertical film flow. They further assumed an incompressible Newtonian fluid with intermediate pressure, and that the solid phase contributed nothing to the pressure of the mixture.

Closed form solutions were obtained for these problems and were used to evaluate the velocity profiles, skin friction coefficients, and flow rates of both phases for a variety of numerical values of the parameters arising in the problem. Their results showed that the inclusion of the solid-phase viscosity and the amount of particle slip allowed at the channel walls have important consequences in the problems solved. Yang and Peddieson [38] treated the particle cloud in their analysis as a continuum, whereby the suspension can be regarded as a mixture of two interpenetrating continuous fluids.

A matter of further investigation would be to analyze analytically the deposition of contaminations with significant gravitational considerations particularly in fluidic devices or in splitter regions taking into account entrance

regions and various channel flow configurations typifying realistically a possible operational fluidic device.

The analysis that ensues will consider the electro-hydrodynamic flow system of charged solid particles each of mass m_p, carrying charge q, moving between grounded straight wall plates. The flow will be two-dimensional in the subsonic range in an electric field. Viscous forces encountered by particles drifting toward the walls are taken into account. In this case, the electrostatic forces acting on the particle cloud are entirely due to image charges of the conducting walls and the space charge of the particle cloud.

3. LAMINAR FLOW OF SUSPENSIONS IN THE ENTRANCE OF A PARALLEL-PLATE CHANNEL WITH DIFFUSIVE ELECTROSTATIC AND GRAVITATIONAL EFFECTS

In this chapter, a numerical scheme is presented to study the Laminar flow of suspensions in the entrance of a two-dimensional parallel-plate channel including the rate of deposition of solid particles on the channel walls due to diffusive, electrostatic and gravitational effects.

The suspension flow is laminar and is considered to be (incompressible carrier) incompressible which is also a good approximation for compressible flow at very low Mach numbers. Also, the case of low particulate concentration (dilute suspension) will be considered such that the particles have relatively no effect on the fluid phase.

Assumptions made are:

(1) Incompressible, steady flow

(2) Two-dimensional laminar boundary layer flow

(3) Dilute suspension ($K_m = 0$, $\rho > \rho_p$) having negligible effect on the fluid phase

(4) Fluid-particle interaction by Stokes drag law.

(5) Negligible particle-particle interaction

(6) Negligible axial component of the electric field and negligible axial diffusion

(7) Negligible change in channel width resulting from the deposited layer

(8) Negligible lift force on the particles

(9) Negligible material density of the fluid phase in comparison to that of the solid particles

(10) No chemical reactions

Rectangular Cartesian coordinates will be utilized in this analysis such that the x-axis will be formed in the streamwise direction along the centerline of the channel and the y-axis in the vertical direction as shown in Fig. (3.1).

3.1 Governing Equations

Fluid Phase

$$\frac{\partial \rho}{\partial t} + \frac{\partial}{\partial x_j}(\rho U_i) = 0 \qquad (3\text{-}1)$$

$$\rho\left\{\frac{\partial U_i}{\partial t} + U_j \frac{\partial}{\partial x_j}(U_i)\right\} = -\left[1 - K_m \frac{\rho_p}{\rho_p}\right] \frac{\partial P}{\partial x_i} + \frac{\partial}{\partial x_j}\{\mu_f \Delta_{ij} + \mu_{f2} \Omega_f \delta_{ij}\} + \rho f_i - \frac{1}{2} \bar{\rho} K_m \frac{\rho_p}{\bar{\rho}_p}\left\{\frac{\partial}{\partial t}(U_i - U_{pi}) + U_{pj}\frac{\partial}{\partial x_j}(U_i - U_{pi})\right\} - \frac{9}{2\sqrt{\pi}} \sqrt{\mu\rho}\, K_m \frac{\rho_p}{\bar{\rho}_p} \int_{t_o}^{t_p} \left[\frac{d}{d\tau}(U_i - U_{pi})\right] (t_p - \tau)^{-1/2} d\tau$$

$$- K_m \rho_p F(U_i - U_{pi}) \qquad (3\text{-}2)$$

where K_m is an effectiveness parameter accounting for the momentum transfer from the particles to the fluid, μ_{f2} =

$\zeta_f - \frac{2}{3}\mu_f$ (3-2a) such that ζ_f is the bulk viscosity, Δ_{ij} is the deformation tensor defined as,

$$\Delta_{ij} = \frac{\partial U_j}{\partial x_i} + \frac{\partial U_i}{\partial x_j} \qquad (3\text{-}2b)$$

Ω_f is the dilatation tensor defined as

$$\Omega_f = \frac{\partial U_i}{\partial x_i} , \qquad (3\text{-}2c)$$

f_i is the body force.

The first term on the right hand side of eq (3-2) gives a correction for the volume occupied by the solid particles, the fourth term accounts for the reaction due to accelerating the apparent mass of the particles relative to the fluid, the fifth term represents the reaction due to the Basset force (resistance force opposing steady state motion) on the particles, and the sixth term is due to the drag of the particles on the fluid.

Since the Basset term constitutes an instantaneous flow resistance, it becomes substantial when the solid particle is accelerated at a high rate whereby the drag force becomes many times that due to steady state drag. It should also be noted that the solid particles, due to its inertia, do not necessarily follow the streamline of the fluid i.e., the particle lines (paths) and streamlines of the fluid do not necessarily coincide. Thus,

$$\frac{d}{dt_p} = \frac{\partial}{\partial t} + U_{pi} \frac{\partial}{\partial x_i} \quad \text{for the solid particle}$$

and

$$\frac{d}{dt} = \frac{\partial}{\partial t} + U_i \frac{\partial}{\partial x_i} \quad \text{for the fluid.}$$

Also, F is the time constant for momentum transfer $[t^{-1}]$ or simply referred to as the inverse relaxation time. It is due to the drag force such that for the Stokes law regime,

$$F = 9\bar{\mu}/9a^2\bar{\rho}_p \tag{3-2d}$$

Particulate Phase

$$\frac{\partial \rho_p}{\partial t} + \frac{\partial}{\partial x_i}(\rho_p U_{pi}) = 0 \tag{3-3}$$

$$\rho_p\left[\frac{\partial}{\partial t}(U_{pi}) + U_{pj}\frac{\partial}{\partial x_j}(U_{pi})\right] = \frac{\partial}{\partial x_j}\left[\mu_p(\Delta_p)_{ij} + \mu_{p2}\Omega_p\delta_{ij}\right]$$

$$+ \rho_p f_{pi} + \rho_p F(U_i - U_{pi}) \tag{3-4}$$

$$\frac{\partial^2 W_i}{\partial x_i^2} = -\frac{\rho_p q}{\epsilon_o m_p} \tag{3-5}$$

where $(\Delta p)_{ij}$ is the deformation tensor defined as

$$(\Delta p)_{ij} = \frac{\partial U_{pj}}{\partial x_i} + \frac{\partial U_{pi}}{\partial x_j} \quad , \tag{3-4a}$$

Ω_p is the dilatation tensor defined as

$$\Omega_p = \frac{\partial U_{pi}}{\partial x_i} \quad , \tag{3-4b}$$

$$\mu_{p2} = \zeta_p - \frac{2}{3}\mu_p \qquad (3\text{-}4c)$$

such that ζ_p is the bulk viscosity of the particles, f_{pi} is the ith component of the body forces of the particles.

By shear (deformation) tensor and dilatation of the particle phase is meant that the shear and dilatation occurs only for the particle cloud.

In this analysis, it is presumed that the drag on a solid particle is mainly due to the difference between the velocities of the particles and the stream. Hence, the velocity of each solid particle due to its own thermal state is extremely low and thus the particulate phase does not contribute to the static pressure of the system.

The effectiveness correction, K_m, is of extreme significance for the case when the solid particles are either accelerated by the fluid ($K_m = 1$), or decelerated by the fluid ($K_m < 1$). But for a dilute suspension, $K_m = 0$, i.e., $\rho >> \rho_p$ as in this analysis.

Assuming steady, two-dimensional flow with boundary layer simplifications along with other assumptions previously mentioned, equation (3-1) and (3-2) reduce simply to (see Appendix A):

(a) Fluid Phase

$$\frac{\partial u}{\partial x} + \frac{\partial v}{\partial y} = 0 \qquad (3\text{-}5)$$

$$u_o = \frac{1}{2h} \int_{-h}^{h} u\,dy \qquad (3\text{-}6)$$

$$u \frac{\partial u}{\partial x} + v \frac{\partial u}{\partial y} = - \frac{1}{\rho} \frac{dp}{dx} + \frac{\mu}{\rho} \frac{\partial^2 u}{\partial y^2} \qquad (3\text{-}7)$$

(b) Particle Phase

$$\frac{\partial (\rho_p u_p)}{\partial x} + \frac{\partial}{\partial y} (\rho_p v_p) = 0 \qquad (3\text{-}8)$$

$$u_p \frac{\partial u_p}{\partial x} + v_p \frac{\partial u_p}{\partial y} = F(u - u_p) + \frac{D_p}{\rho_p} \frac{\partial}{\partial y} \left(\rho_p \frac{\partial u_p}{\partial y}\right) \qquad (3\text{-}9)$$

$$u_p \frac{\partial v_p}{\partial x} + v_p \frac{\partial v_p}{\partial y} = F(v - v_p) - \left(\frac{q}{m_p}\right) \frac{\partial W}{\partial y} - g \qquad (3\text{-}10)$$

$$\frac{\partial^2 w}{\partial y^2} = - \frac{\rho_p q}{\varepsilon_o m_p} \qquad (3\text{-}11)$$

where $F = 9\bar{\mu}/2a^2\bar{\rho}_p$ for spherical particles in the Stokes' range, and W is the vertical component of the electrical potential. The vertical component of the electric field intensity, E, is related to W by, $E = \partial W/\partial y$.

In these equations, the subscript p denotes properties of the particle phase. Equations (3-5) and (3-8) can be combined to yield,

$$u \frac{\partial \rho_p}{\partial x} + v \frac{\partial \rho_p}{\partial y} = - \frac{\partial}{\partial x} [\rho_p (u_p - u)] - \frac{\partial}{\partial y} [\rho_p (v_p - v)] \qquad (3\text{-}12)$$

Letting

$$J_{px} = \rho_p (u_p - u)$$

$$J_{py} = \rho_p (v_p - v)$$

and assuming that

$$\frac{\partial J_{px}}{\partial x} << \frac{\partial J_{py}}{\partial y}$$

$$u \frac{\partial \rho_p}{\partial x} + v \frac{\partial \rho_p}{\partial y} = - \frac{\partial J_{py}}{\partial y} \qquad (3\text{-}12a)$$

From Fick's Law,

$$J_{py} = -\left(\frac{q}{m_p}\right) \frac{\rho_p}{F} \frac{\partial W}{\partial y} - D_p \frac{\partial \rho_p}{\partial y} - \frac{\rho_p g}{F} \qquad (3\text{-}12b)$$

Thus, the diffusion equation is,

$$u \frac{\partial \rho_p}{\partial x} + v \frac{\partial \rho_p}{\partial y} = \frac{\partial}{\partial y} \left(\frac{q}{m_p} \frac{\rho_p}{F} \frac{\partial W}{\partial y}\right) + \frac{\partial}{\partial y} \left(D_p \frac{\partial \rho_p}{\partial y} + \frac{\rho_p g}{F}\right) \qquad (3\text{-}13)$$

Equation (3-13) represents the steady state diffusion equation including the electrical and gravitational effects.

The rate of deposition on the channel walls can be obtained by consideration of the conservation of mass of the particle phase,

$$- \frac{\partial}{\partial x} \int_{-h}^{h} \rho_p u_p dy = [\sigma v_p \rho_p + \sigma_w f_w \rho_p / F]_{y = h \text{ upper wall}}$$

$$+ [-\sigma v_p \rho_p + \sigma_w \rho_p f_w / F]_{y = -h \text{ lower wall}} \qquad (3\text{-}14)$$

where the term,

$$- \frac{\partial}{\partial x} \int_{-h}^{h} \rho_p u_p dy,$$

represents the total deposition rate; the first term on the

right hand side of eq. (3-14) represents the deposition rate on the top wall and the second term on the right hand side of eq. (3-14) represents the deposition rate on the bottom wall. Also, σ is the probability that the particles falling towards the wall will stick to the wall and σ_w is the sticking probability which accounts for the adhesive forces at the wall, f_w. The term $(\sigma\rho_p V_p)$ is the rate of deposition of particles per unit area due to electric charge; the term $(\sigma_W \rho_p f_w/F)$ is the rate of deposition of particles per unit area due to surface adhesion which depends upon material and surface properties.

Equations (3-5) to (3-9), (3-13) and (3-14) can be nondimensionalized (see Appendix B) as follows:

$$\frac{\partial U}{\partial X} + \frac{\partial V}{\partial Y} = 0 \tag{3-15}$$

$$\int_{-1}^{1} U dY = 2.0 \tag{3-16}$$

$$U \frac{\partial U}{\partial X} + V \frac{\partial U}{\partial Y} = - \frac{dP}{dX} + \frac{1}{N_R} \frac{\partial^2 U}{\partial Y^2} \tag{3-17}$$

$$U_p \frac{\partial U_p}{\partial X} + V_p \frac{\partial U_p}{\partial Y} = \frac{1}{N_m} (U - U_p) + \frac{1}{N_\beta R} \frac{\partial}{\partial Y} (R \frac{\partial U_p}{\partial Y}) \tag{3-18}$$

$$U_p \frac{\partial V_p}{\partial X} + V_p \frac{\partial V_p}{\partial Y} = \frac{1}{N_m} (V - V_p) - \frac{1}{N_\beta N_m} \frac{\partial W^*}{\partial Y} - \frac{N_\eta}{N_\beta N_m} \tag{3-19}$$

$$N_\beta [U \frac{\partial R}{\partial X} + V \frac{\partial R}{\partial Y}] = \frac{\partial^2 R}{\partial Y^2} + \frac{\partial R}{\partial Y} \frac{\partial W^*}{\partial Y} - 4 N_\alpha R^2 + N_\eta \frac{\partial R}{\partial Y} \tag{3-20}$$

$$\frac{\partial^2 W^*}{\partial Y^2} = -4N_\alpha R \tag{3-21}$$

$$\dot{M}^* = \underbrace{[R\{\sigma V_p + \frac{N_s}{N_\beta}\}]}_{\text{top wall}} + \underbrace{[R\{\frac{N_s}{N_{\hat{\beta}}} - \sigma V_p\}]}_{\text{bottom wall}} \tag{3-22}$$

The Fraction of Penetration, given by, $\frac{1}{2}\int_{-1}^{1} RU_p dY$, represents the ratio of the mass flux of solid particles leaving a given section to the mass flux of particles entering the channel. Upon inlet, this ratio is simply one whereas if $\chi \to \infty$, the penetration approaches zero.

Also, the Fraction of Deposition, given by $1 - \frac{1}{2}\int_{-1}^{1} RU_p dy$ represents the ratio of the mass flux of solid particles that are deposited between the inlet and a given section to the mass flux of particles entering the channel. This ratio is sometimes simply referred to as the deposition of solid particles, where upon inlet, this ratio is zero; whereas if $\chi \to \infty$ the deposition approaches one.

Thus, by definition,

$$\dot{M}^* \equiv -\frac{d}{dX}\int_{-1}^{1} RU_p dy \tag{3-22a}$$

Eq. (3-20) is the Diffusion Equation while eq. (3-21) is the Poisson Equation.

The unknowns in the above equations (Equations (3-15) through Equation (3-22) are:

$$U,\ V,\ P,\ U_p,\ V_p,\ R,\ W^* \text{ and } \dot{M}^*.$$

The solution depends upon the Reynolds number N_R, the momentum transfer number N_m, the diffusive Peclet number N_β, the gravity flow parameter N_η, the electrostatic charge parameter N_α and the boundary conditions.

Developing flow in the entrance region of a two-dimensional channel was solved by Bodoia [4] employing the implicit finite difference method. His results for $X < 0.18\ N_R$ where $(X = X/h)$ can be approximated within 4 percent error by:

The dimensionless centerline velocity,

$$U_c = u_c/u_o = N + 1/N \tag{3-23}$$

where

$$N = N(x) = 0.48\left(\frac{N_R}{x}\right)^{0.54} + 3.0\ \left(\frac{N_R}{x}\right)^{-.75} \tag{3-24}$$

The velocity profile,

$$U = U_c[1 - Y^N] \tag{3-25}$$

where N_R = Reynolds number = $u_o h/\nu$.

These approximate expressions were used to obtain the vertical velocity V such that,

$$V = -\frac{dU_c}{dX}\,[Y - Y^{N+1}/(N+1)] + U_c(dN/dX)Y^{N+1}[(N+1)\ln(Y) - 1]/(N+1)^2 \tag{3-25a}$$

3.2 Boundary Conditions

The width of the parallel-plate channel is 2h, the centerline is at y = 0, the lower wall is at y = -h, and the upper wall is at y = h.

At x = 0 (at the channel inlet) for $-h \leq y \leq h$

$$u_p = u_o \text{ (uniform)}$$
$$v_p = w = o \qquad (3\text{-}26)$$
$$\rho_p = \rho_{po} \text{ (uniform)}$$

At y = -h (at the lower wall of the channel) for $X > 0$,

$$w = o \qquad (3\text{-}27)$$

$$u_p = L_p \left(\frac{\partial u_p}{\partial y}\right)_{y=-h} \quad \text{Particle slip condition} \qquad \text{(Case I) (3-28)}$$

or

$$\begin{cases} u_p = \sigma_s u_o (1 - xF/u_o) + L_p \left(\frac{\partial u_p}{\partial y}\right)_{y=-h} & \text{For } x < u_o/F \\ u_p = L_p \left(\frac{\partial u_p}{\partial y}\right)_{y=-h} & \text{For } x \geq u_o/F \end{cases} \qquad \text{(Case II) (3-28)}$$

$$D_p \left(\frac{\partial \rho_p}{\partial y}\right)_{y=-h} = \left\{-\sigma v_p \rho_p + \frac{\sigma_w f_w \rho_p}{F} - \left(\frac{q}{mp}\right) \frac{\rho_p}{F} \frac{\partial W}{\partial y} - \frac{g \rho_p}{F}\right\}_{y=-h} \qquad (3\text{-}29)$$

At y = h (at the upper wall of the channel) for x > 0

$$w = 0 \qquad (3\text{-}30)$$

$$u_p = -L_p \left(\frac{\partial u_p}{\partial y}\right)_{y = h} \quad \text{Particle slip condition} \qquad \text{(Case I) (3-31)}$$

or
$$\begin{cases} u_p = \sigma_s u_o (1 - xF/u_o) - L_p \left(\frac{\partial u_p}{\partial y}\right)_{y = h} & \text{For } x < u_o/F \\ u_p = L_p \left(\frac{\partial u_p}{\partial y}\right)_{y = h} & \text{For } x \geq u_o/F \end{cases} \qquad \text{(Case II) (3-31)}$$

$$D_p \left(\frac{\partial \rho_p}{\partial y}\right) = -\left(\sigma v_p \rho_p + \frac{\sigma_w f_w \rho_p}{F} + \left(\frac{q}{mp}\right) \frac{\rho_p}{F} \frac{\partial W}{\partial y} + \frac{g \rho_p}{F}\right)_{y = h} \qquad (3-32)$$

The particle cloud density at each wall given by Eqs. (3-29) and (3-32) are obtained from equations (3-13) and (3-14), that is, the diffusion equation and the conservation of mass of the particle phase.

Cases I and II take into account the general notion that at a solid boundary, solid particles may have finite velocities even though the gas phase attains zero velocity there except at very low pressures.

Case I is the regular slip condition; but the slip velocity of the particles at the wall, given by Case II for $x < u_o/F$ takes into account the distance that the solid particles will travel before they are decelerated to the slip velocity given for $x \geq u_o/F$.

A factor of $\sigma_s (1 \leq \sigma_s \leq 0)$ is multiplied to this additional slip velocity, $(1 - xF/u_o)$, so that the particles on the wall will not have a higher velocity than the particles near the wall.

The boundary conditions can be nondimensionalized as follows:

<u>At $\chi = 0$</u> (at the channel inlet)

$$\left.\begin{aligned} U_p &= R = 1 \\ V_p &= W^* = 0 \end{aligned}\right\} \quad \text{(uniform)} \tag{3-33}$$

<u>At $Y = -1$</u> (at the lower wall of the channel)

for $\chi > 0$,

$$W^* = 0 \tag{3-34}$$

$$U_p = K_{np}\left(\frac{\partial U_p}{\partial Y}\right)_{Y = -1} \quad \text{(Particle slip condition)} \quad \text{(Case I)} \tag{3-35}$$

$$\text{or} \begin{cases} U_p = \sigma_s(1 - \chi/N_m) + K_{np}\left(\frac{\partial U_p}{\partial Y}\right)_{Y = -1} & \text{for } \chi < N_m \\ U_p = K_{np}\left(\frac{\partial U_p}{\partial Y}\right)_{y = -1} & \text{for } \chi \geq N_m \end{cases} \quad \text{(Case II)} \tag{3-35}$$

$$\left(\frac{\partial R}{\partial Y}\right)_{Y = -1} = -R(X, -1)\left[\left(\frac{\partial W^*}{\partial Y}\right)_{Y = -1} + \sigma N_\beta V_p(X, -1) - N_s + N_\eta\right] \tag{3-36}$$

At Y = 1 (at the upper wall of the channel)

for $\chi > 0$,

$$W^* = 0 \tag{3-37}$$

$$U_p = -K_{np}\left(\frac{\partial U_p}{\partial Y}\right)_{Y=1} \quad \text{(Particle slip condition)} \quad \text{(Case I)} \tag{3-38}$$

or

$$\left.\begin{aligned} U_p &= \sigma_s(1 - \chi/N_m) - K_{np}\left(\frac{\partial U_p}{\partial Y}\right)_{Y=1} \quad \text{for } \chi < N_m \\ U_p &= -K_{np}\left(\frac{\partial U_p}{\partial Y}\right)_{Y=1} \quad \text{for } \chi \geq N_m \end{aligned}\right\} \quad \text{(Case II)} \tag{3-38}$$

$$\left(\frac{\partial R}{\partial Y}\right)_{Y=1} = -R(X, 1)\left\{\left(\frac{\partial W^*}{\partial Y}\right)_{Y=1} + \sigma N_\beta V_p(X, 1) + N_s + N_\eta\right\} \tag{3-39}$$

3.3 Method of Solution

The governing equations (3-15) to (3-22) and boundary conditions (3-33) to (3-39) are written into finite difference expressions using the spatial coordinates as shown in Fig (3.1).

A mesh is superimposed on the flow field internal to the channel itself. Twenty-one mesh points in the Y-direction and up to 141 mesh points in the X direction were used.

Each increment in the Y direction was held constant at $\Delta Y = 0.1$. However, the increments in the χ direction varied downstream as $\Delta X = 0.001$, 0.01, 0.1, 0.2 and 0.3 giving a total axial distance of 8.5 times the channel width or simply $\chi = 17$.

By use of the finite difference scheme superimposed upon the flow field, a matrix equation of the form,

$$A_i X_{i+1} = B_i$$

is generated where A_i is the coefficient matrix at axial position i and B_i is the column vector also at axial position i.

X_{i+1} is the variable column vector at axial position i + 1. This matrix equation is sparse and unsymmetric. A computer program has been written to solve this matrix

equation utilizing Gaussian elimination with partial pivoting and the Crout reduction technique.

The subroutines formulated for the elimination procedure were LINAEQ which in turn calls upon other subroutines such as LUDECO, ELIMIN and REFINE.

A matrix size of 78 x 78 was used and an accuracy of 4 significant figures was realized in the computations.

Berezin [2] and Quarmby [26] indicated that the general condition of stability was

$$(\Delta X/N_R)/(\Delta Y) \quad < 0.5$$

for

$$\Delta X = 0.001,\ 0.01,\ 0.1,\ 0.2,\ 0.3$$

$$\Delta Y = 0.1$$

and

$$N_R > 60,$$

this condition is satisfied.

3.4 Results and Discussion

In this section, the particulate phase will be considered only since the fluid phase was examined and discussed in detail by Quarmby[26] and others. Two main subdivisions was investigated for the particulate phase:

(1) Flow of suspensions with deposition due to gravity and surface adhesion only.

(2) Flow of suspensions with deposition due to the combined effects of gravity, surface adhesion and electric charge.

3.4.1 Flow of suspensions with simultaneous action of diffusion and gravity. Since this study of the laminar flow of suspensions deals with particles of a size where the gravitational influence is the predominant one, this section will treat the deposition process where electricity is ignored; however, the general case including electricity is examined later.

Fig. (3.3) illustrates the influence of the surface adhesion parameter (N_S = 0.1 and 10 shown) on the concentration distribution. At low surface adhesion force, the particles concentrate near the bottom wall, and the concentration is highest at the wall itself. However, as the surface adhesive force is increased, the particle concentration becomes less at the bottom wall and shows a point

of maximum concentration between the centerline of the channel and the bottom wall.

Fig. (3.4) shows the effect of the gravity flow parameter N_η (N_η = 0.1 and 1 shown) on the deposition rate of the bottom and top walls. Although the gravitational parameters are not high, their effects are quite significant causing a sharp increase of deposition on the bottom and a decrease of deposition on the top wall.

Fig. (3.5) shows the axial distribution of the rate of deposition of solid particles on both the bottom and top walls of the channel due to significant gravitational effects. As can be seen most of the particles are deposited on the bottom wall showing a peak approximately 3.5 plate gap widths down the channel from inlet due to high gravity flow; whereas, the top deposition rate is almost negligible.

Fig. (3.6) and Fig. (3.7) illustrate the effect of the particle Knudsen number, K_{np}, (shown K_{np} = 0.1, 0.2) upon the rate of deposition on both the bottom and top walls of the channel. As can be seen, increasing the particle Knudsen number causes a lesser deposition gradient in the particle slip region for the bottom wall. In these two figures, the gravity effect was held constant at N_η = 4.5.

Fig. (3.8) indicates the influence of the surface adhesion parameter, N_s, with moderate gravitational influences ($N_\eta = 1$). Clearly, with $N_s = 5$ indicates a sudden decrease in the particle slip region with a moderating decrease further downstream. The gravitational effect is again seen by a higher bottom wall deposition than the top.

Fig. (3.9) shows the axial velocity distribution of the particles U_p with significant gravitational influences and large particle Knudsen number. Certainly, the centerline velocity is increasing with almost negligible drop of zero velocity gradient with respect to channel width.

Fig. (3.10) illustrates the effect of the momentum transfer number on the rate of deposition of the solid particles on both the top and bottom walls of a channel. As the momentum transfer number increases, the deposition rate decreases particularly on the bottom where the maximum deposition occurs due to gravity. The top deposition rate decreases more rapidly with increasing momentum number with a maximum at inlet.

3.4.2 Flow of suspensions with combined action of diffusive, electrostatic and gravitational influences. Since deposition caused by dipoles or space charges can be equally problematic in fluidic devices as seen in the

literature survey especially when dealing with gas-particle suspensions, the case when electricity along with diffusive, gravitational influences will now be discussed.

Fig. (3.11) illustrates the distribution of the particle concentration, R, due to surface adhesion (N_s = 0.1, 10) along with electrical and gravitational effects. At high gravity flow parameters (here N_η = 4.5), the gravitational force overrides the electrical force (N_α = 2), causing a continual increase in concentration near the bottom wall with low adhesion. At high adhesion, the concentration of solid particles becomes greatest towards the bottom wall but comparatively less in the immediate vicinity of the wall itself.

Fig. (3.12) shows the axial distribution of the rate of deposition of solid particles on both the bottom and top walls of the channel due to both gravity and electricity. An increase in the gravity flow parameter (here N_η = 1.6, 4.5) causes a greater peak in the rate of deposition at the bottom wall, and a smaller peak at the top. The electrical field (here N_α = 2) certainly increases the deposition on the top wall as compared to the case when no electrical field exists as seen from Fig. (3.5).

Fig. (3.13) indicates the influence of the momentum transfer number, N_m, upon the rate of deposition for the

top and bottom walls. An increase in N_m (here N_m = 1 & 5) causes a decrease in deposition rate on both walls. In this figure, the gravitational effect is low with N_η = 0.05.

Fig. (3.14) illustrates the Electrostatic Charge parameter effect with constant gravity flow parameter upon the rate of deposition on both the bottom and top walls of the channel. An increase of electric charge clearly marks a greater peak of deposition rate with a particular increase of deposition at the bottom again due to the gravitational field.

As can be seen, an increase in either gravity or electrical parameters clearly causes a large deposition rate at the bottom wall. However, in the absence of an electric field, the deposition is comparatively low at the top wall as compared to the situation when there exists an electric field.

Fig. (3.15) shows the effect of the electrostatic charge parameter, N_α, on the deposition rate of the top and bottom walls of the parallel-plate channel in a weak gravitational field (here, N_η = 0.05). Clearly, the higher the electric field induced by the contact potential difference the dipole effect and the space charge, the higher the deposition rate. Again, since in the presence of a

gravitational field, although not well pronounced, the deposition rates clearly indicate an increase for the bottom over the top wall.

Fig. (3.16) illustrates the symmetrical effect of both the Fraction of Penetration and Fraction of Deposition induced by both electrical fields (here N_α = 1 & 2) and gravitational field (here N_η = 1). Since the fraction of penetration is a ratio of the mass flow of solid particles penetrating a given region to the mass flow of solid particles entering that region, this figure clearly indicates that more particles will deposit on the walls if the electric field is increased, thus inducing a greater total deposition.

Fig. (3.17) and Fig. (3.18) represent the axial electric potential distribution where the electrostatic charge parameter, N_α, is 1 and 2 respectively, and the gravity flow parameter, N_η, is 1.0 for both. Clearly, the further downstream, the less potential and space charge which further indicates a maximum deposition rate occuring in the entrance region of the parallel-plate channel.

The influence of the electrostatic charge parameter, N_α, with very high diffusive Peclet number $N_\beta = 10^7$, is illustrated in Fig. (3.19). The bottom deposition rate increases with much higher magnitude for N_α = 1 showing a

steady increase of deposition particularly after the particle slip region; however, for N_{α}= 0, the bottom deposition rate increases in the particle slip region to a point of much less magnitude whereby thereafter, the rate becomes relatively constant. The top deposition decreases rapidly in the particle slip region and then remains relatively constant. The electrostatic flow causes the greater deposition rate. Here, the gravity flow parameter was five whereby the effect was clearly seen on the top deposition showing a very small change when N_{α} = 1.

Fig. (3.20) illustrates the comparison of various surface adhesion flows made by this study with both fully-developed and Plug flow analyzed by Ingham[17] . When the surface adhesion is 1, the deposition is much less than both fully-developed and Plug flows since more particles are re-entrained into the main stream. However,when the adhesive force becomes 10, the deposition becomes greater than fully-developed flow but yet less than Plug flow.

Moreover,as can be seen, when the adhesive force is 1000, the deposition is greater than both Plug and fully-developed flow with the exception of the immediate entrance region where the deposition is less than Plug flow due to the magnitude of the normal velocity component of the fluid phase which causes the flow to emanate away from the walls towards the centerline counteracting the gravitational force.

4. LAMINAR FLOW OF SUSPENSIONS IN THE ENTRANCE REGION OF CONVERGENT AND DIVERGENT CHANNELS WITH DIFFUSIVE, ELECTROSTATIC AND GRAVITATIONAL EFFECTS

The problem of laminar flow in a radial diffuser, a converging channel and tube has been investigated analytically by many investigators.

Schlichting [28] discussed the flow in convergent and divergent channels for some special cases. He found that in a divergent channel, the shape of the velocity profiles was markedly affected by the Reynolds number and by the angle of divergence.

Blasius [3] investigated the two-dimensional and axisymmetrical flow through channels with small angles of divergence. He showed that laminar flow can support only a very small pressure increase without the incidence of separation.

The laminar diffuser flow of suspensions as a two-phase flow problem has been investigated by Eldighidy et al. [12] but not with unsymmetrical, gravitational considerations. In this chapter a mathematical model is presented to investigate the laminar flow of suspensions in the entrance region of convergent and divergent channels and in parallel, convergent and divergent arrangements with

diffusive, electrostatic and gravitational effects. Particular emphasis will be placed upon the rate of deposition of the solid particles on the bottom and top walls of the channels.

The diverging channel problem will be investigated from inlet downstream to where the point of separation occurs beyond which boundary layer equations are no longer applicable; the converging channel problem will be investigated from inlet downstream to where the gap width is one half the inlet width beyond which incompressibility effects become less accurate.

4.1 Governing Equations

With the same assumptions as in Chapter 3, the governing equations will be the same as before for the parallel-plate channel flow described in section 3.1 with the exceptions of equation (3-6) and (3-14) which will include h(x) instead of h. Consequently, equation (3-16) will be written as (see Appendix B),

$$\int_{-H^*}^{H^*} U dY = 2H^* \qquad (4\text{-}1)$$

However, since the fluid phase alone will be considered as symmetrical flow, equation (4-1) can be expressed as,

$$\int_{o}^{H^*} U dY = H^* \qquad (4\text{-}2)$$

4.2 Boundary Conditions

Two different cases for the boundary conditions of the divergent and convergent channel flow will be considered. The first case is for a single divergent or convergent channel assuming uniform boundary conditions at the inlet. The second case will be for a divergent channel connected with a parallel-plate channel.

For uniform inlet conditions, @ $x = 0$ for $-h(x) \leq y \leq h(x)$

$$
\begin{aligned}
u &= u_p = u_o \qquad \text{uniform} \\
v &= v_p = 0 \\
\rho_p &= \rho_{po} \qquad \text{uniform} \\
p &= p_o \qquad \text{uniform} \\
W &= 0
\end{aligned}
\tag{4-3}
$$

Now, @ $y = -h(x)$ (at the lower wall of the channel)

for $(x > 0)$

$$w = 0$$

$$u_p = L_p \left(\frac{\partial u_p}{\partial y}\right)_{y = -h(x)} \qquad \text{particle slip condition (Case I)}$$

$$\text{or} \begin{cases} u_p = \sigma_s u_o (1 - xF/u_o) + L_p \left(\frac{\partial u_p}{\partial y}\right)_{y = -h(x)} & \text{for } x < u_o/F \\ u_p = L_p \left(\frac{\partial u_p}{\partial y}\right)_{y = -h(x)} & \text{for } x \geq u_o/F \end{cases} \quad \text{(Case II)} \quad (4\text{-}4)$$

$$D_p \left(\frac{\partial \rho_p}{\partial y}\right)_{y = -h(x)} = \left\{-\sigma v_p \rho_p + \frac{\sigma_w f_w \rho_p}{F} - \left(\frac{q}{m_p}\right) \frac{\rho_p}{F} \frac{\partial w}{\partial y} - \frac{g \rho_p}{F}\right\}_{y = -h(x)} \quad (4\text{-}5)$$

@ y = 0 (at the centerline)

(x > 0)

$$\frac{\partial u}{\partial y} = 0 \quad \text{symmetry} \qquad (4\text{-}6)$$

$$v = 0 \qquad (4\text{-}7)$$

@ y = h(x) (at the upper wall)

$$u = v = 0 \quad \text{no slip condition} \qquad (4\text{-}8)$$

$$w = 0 \qquad (4\text{-}9)$$

$$u_p = -L_p \left(\frac{\partial u_p}{\partial y}\right)_{y = h(x)} \quad \text{Particle slip condition} \quad \text{Case I}$$

$$\text{or} \begin{cases} u_p = \sigma_s u_o (1 - xF/u_o) - L_p \left(\frac{\partial u_p}{\partial y}\right)_{y = h\ x)} & \text{for } x < u_o/F \\ u_p = L_p \left(\frac{\partial u_p}{\partial y}\right)_{y = h(x)} & \text{for } x \geq u_o/F \end{cases} \quad \text{(Case II)} \quad (4\text{-}10)$$

$$D_p \left(\frac{\partial \rho_p}{\partial y}\right)_{y = h(x)} = -\left(\sigma v_p \rho_p + \frac{\sigma_w f_w \rho_p}{F} + \left(\frac{q}{m_p}\right) \frac{\rho_p}{F} \frac{\partial w}{\partial y} + \frac{g \rho_p}{F}\right)_{y = h(x)} \quad (4\text{-}11)$$

Referring to Appendix B, the boundary conditions can be nondimensionalized as follows:

@ $\chi = 0$ for $-1 \leq Y \leq 1$

$$U = U_p = 1 \quad \text{uniform}$$
$$V = V_p = 0$$
$$R = 1 \quad \text{uniform} \tag{4-12}$$
$$P = 0$$
$$W = 0$$

@ $Y = -H^*$ (at the lower wall)

($\chi > 0$)

$$w = 0$$

$$U_p = K_{np}\left(\frac{\partial U_p}{\partial Y}\right)_{Y = -H^*} \quad \text{Particle slip condition} \qquad \text{Case I}$$

or

$$\left.\begin{aligned} U_p &= \sigma_s(1 - \chi/N_m) + K_{np}\left(\frac{\partial U_p}{\partial Y}\right)_{Y = -H^*} \quad \text{for } \chi < N_m \\ U_p &= K_{np}\left(\frac{\partial U_p}{\partial Y}\right)_{Y = -H^*} \quad \text{for } \chi \geq N_m \end{aligned}\right\} \quad \text{Case II} \tag{4-13}$$

$$\left(\frac{\partial R}{\partial Y}\right)_{Y = -H^*} = \left[-R\left\{\left(\frac{\partial W^*}{\partial Y}\right) + \sigma N_\beta V_p - N_s + N_\eta\right\}\right]_{Y = -H^*} \tag{4-14}$$

@ $Y = 0$ (at the centerline)

($\chi > 0$)

$$\frac{\partial U}{\partial Y} = 0 \quad \text{symmetry} \tag{4-15}$$

$$V = 0 \tag{4-16}$$

@ $Y = H^*$ (at the upper wall)

($\chi > 0$)

$$w = 0$$

$$U_p = -K_{np}\left(\frac{\partial U_p}{\partial Y}\right)_{Y = H^*} \quad \text{Particle slip condition} \qquad \text{Case I}$$

$$\text{or} \begin{cases} U_p = \sigma_s(1 - \chi/N_m) - K_{np}\left(\frac{\partial U_p}{\partial Y}\right)_{Y = H^*} & \text{for } \chi < N_m \\ U_p = -K_{np}\left(\frac{\partial U_p}{\partial Y}\right)_{Y = H^*} & \text{for } \chi \geq N_m \end{cases} \qquad \text{Case II}$$

(4-17)

$$\left(\frac{\partial R}{\partial Y}\right)_{Y = H^*} = \left[-R\left\{\left(\frac{\partial W^*}{\partial Y}\right) + \sigma N_\beta V_p + N_s + N_\eta\right\}\right]_{Y = H^*} \qquad (4\text{-}18)$$

4.3 Method of Solution

Equations (3-15), (4-2), (3-17) through (3-22) in Section 3.1 can be solved together for the unknowns U, V, P, U_p, V_p, R, W* and $\dot{M}$* by the implicit finite difference technique. Since U, V and P can be solved independently from U_p, V_p, R, W* and $\dot{M}$*, a symmetrical half channel trapezoid mesh was superimposed on the flow field internal to the converging and diverging channel. However, after U, V and P are known, they are inputed into the particulate phase equations whereby a trapezoid mesh is superimposed on the entire flow field internal to both the diverging and converging channel (See Figures 4A and 4B). Thus, the fluid phase generated a matrix equation of the form,

$$A_i X_{i+1} = B_i$$

where A_i is a 20 x 20 coefficient matrix

X_{i+1} is a 20 x 1 vector to be solved

B_i is a 20 x 1 loading vector.

Note that $X_{i+1} = [U_{i+1}, V_{i+1}, P_{i+1}]^T$. The particulate phase generated a matrix equation of the form,

$$C_i Z_{i+1} = D_i$$

where C_i is a 78 x 78 coefficient matrix,

Z_{i+1} is a 78 x 1 vector to be solved,

D_i is a 78 x 1 loading vector.

Note that $Z_{i+1} = [U_{p\,i+1}, V_{p\,i+1}, R_{i+1}, W^*_{i+1}, \ldots M^*_{i+1}]^T$.

Thus, more computer time was needed to solve the converging and diverging channel since in essence a 98 x 98 matrix was solved for 140 axial positions stemming from the inlet progressing downstream. The matrix equation for the particulate phase is sparse and unsymmetric whereby the same elimination subroutines employed for the solution of the parallel-plate channel were also used for the converging and diverging channel utilizing Gaussian elimination. Again, an accuracy of 4 significant figures were realized in the computations.

4.4 Results and Discussion

In this section, the diffusive, gravitational and electric field flow characteristics of the laminar flow of suspensions in the entrance region of both a converging and diverging straight wall channel will be discussed. The fluid phase for the converging channel will be examined briefly, however the particulate phase for both the converging and diverging channel will be studied extensively. Moreover, the effect of the converging and diverging angle upon the deposition process will be investigated such that the influence of the pressure gradient on the rate of deposition can be realized. The flow characteristics for the converging channel will be discussed to a length where the plate gap width is one half the inlet width; for the diverging channel to a length where discontinuity (point of separation) occurs.

4.4.1 Fluid phase for convergent channel. Fig. (4.4) shows the axial velocity distribution of the fluid phase, U, with various angles of convergence. The selected axial positions, namely, x = 2.8, 3.8 and 7 indicate the point where the gap width is half the inlet gap width for selected angles of -10°, -7.5° and -4°, respectively. Clearly, the centerline velocity, U_c, increases with increasing convergence and the numerical value of the velocity gradient

at the wall ($\partial U/\partial Y$) increases along the x-axis.

Fig. (4.5) illustrates the vertical velocity distribution of the fluid phase, V, with various angles of convergence. As the angle of convergence increases, the magnitude of V wanes particularly downstream. All the values of V are negative which indicate that the direction of motion of the fluid particles in the normal direction is away from the wall.

Fig. (4.6) depicts the axial distribution of the fluid static pressure, p with increasing angle of convergence. The pressure drag becomes more pronounced with increasing angle of convergence since the fluid is accelerated with increasing convergence.

4.4.2 Particle phase for convergent channel - flow of suspensions with deposition due to gravity, diffusion and adhesion. Fig. (4.7) illustrates the axial distribution of particle concentration, R, with surface adhesion effect. Clearly, with an increase in surface adhesion, the concentration becomes much less near the bottom wall as in the case for the parallel-channel. The higher the adhesion, the higher the probability of complete absorption.

Fig. (4.8) shows the effect of the angle of convergence on the rate of deposition of the solid particles on

the bottom wall. The effect of gravity is large and as can be seen, the more convergent the channel, the less deposition owing to the increase of the axial particle velocity through the channel.

Fig. (4.9) illustrates the effect of the surface adhesion parameter on the rate of deposition on the bottom and top walls of a convergent channel with $\theta = -4°$. The higher the surface adhesion, the higher the inlet deposition rate as also seen in the parallel channel. Clearly, the top deposition rate becomes almost negligible when $N_s = 0.1$ and $N_\eta = 5$.

The effect of the angle of convergence when $N_\eta = 5$ on the top and bottom walls of a convergent channel is seen in Fig. (4.10). The deposition on the bottom wall becomes slightly less with increase in angle of convergence. However the top deposition rate falls slightly less rapidly for increasing angles of convergence.

4.4.3 Flow of suspensions with deposition due to gravity, surface adhesion, diffusion and electrostatic charge in a convergent channel. Fig. (4.11) shows the effect of the gravity flow parameter, N_η, on the particle concentration for an angle of convergence of $-4°$. At $x = 1$, the concentration of particles grows much larger towards the bottom wall for larger gravity flow as expected. However, at the point

when the gap width is half the inlet width, viz. at x = 7, the particle concentration is higher when $N_\eta = 1$ since more particles have been deposited in the entrance region for $N_\eta = 5$.

Fig. (4.12) illustrates the mass flux distribution of solid particles with gravitational effects in a converging channel of $\theta = -4°$. Clearly, as N_η is increased, the mass flux distribution of the solid particles drops further below the centerline with progressive downstream axial length. This effect was also seen for the parallel-channel but with different orders of magnitude.

The influence of the gravity flow parameter on the rate of deposition on both walls of a converging channel of $\theta = -7.5°$ is illustrated in Fig. (4.13). The larger the gravity flow, the larger the bottom deposition rate and the smaller the top deposition rate. This has been seen for the parallel-plate channel but the magnitude of maximum deposition rate is much less for greater convergence. Since electrostatic charge is present, one would expect a maximum bottom deposition rate for even low gravity flow.

The effect of the angle of convergence on the deposition rate for the bottom and top walls of a channel is seen in Fig. (4.14). The diffusive Peclet number is high (N_β =

10^7) and as seen before, the greater the angle of convergence, the less the deposition rate, particularly on the bottom wall.

Fig. (4.15) shows the effect of the gravity flow parameter, N_η, on the rate of deposition on both the top and bottom walls of a convergent channel where $\theta = -10°$. When compared with Fig. (4.13), the maximum bottom deposition is less for the case when $N_\eta = 5$.

Fig. (4.16) illustrates the simultaneous axial distribution of the Fraction of Deposition with the Fraction of Penetration. Both are symmetrical with respect to the centerline. At $x = 3$ for $\theta = -4°$, the mass flux of particles leaving to the mass flux of particles entering is 50 per cent suggesting that at this point, at least half of the particles have been deposited for the case when $N_\eta = 4.5$.

Fig. (4.17) shows the effect of the gravity flow parameter on the deposition rate on both the top and bottom walls of a convergent channel having $\theta = -4°$. Since electrostatic charge is present, the lower gravity flow would still achieve a peak top deposition rate as seen. Also, as previously seen in Fig. (4.13) and Fig. (4.15) the maximum deposition rate for the bottom wall for higher gravity flow shows a much greater deposition rate. As a further note, the deposition is of course higher for the

higher gravity flow on the bottom wall when $\theta = -4°$ as compared with $\theta = -7.5°$ and $-10°$ in Fig. (4.13) and Fig. (4.15), respectively.

Fig. (4.18) illustrates the axial distribution of the electrostatic charge potential, W*, for a convergent channel having $\theta = -4°$, with gravitational effects. As can be seen, the higher gravity flow causes a lesser electrostatic charge potential of the solid particles caused by the dominating influence of the gravitational force pulling the particles down towards the bottom wall of the channel.

Similarly, Fig. (4.19) illustrates the effect of the gravity flow parameter, N_η, on the electrostatic charge intensity, E*, for $\theta = -4°$. Clearly, with increasing gravitational force, the electric field intensity becomes less particularly further downstream since gravity has already pulled most of the particles towards the bottom wall causing deposition.

4.4.4 Flow of suspensions with simultaneous action of diffusion and gravity in a diverging channel. Fig. (4.20) illustrates the influence of the gravity flow parameter, N_η, on the deposition rate for the top and bottom walls where the angle of divergence is 2°. The gravitational force again pushes more particles on the bottom wall than on the top as expected, but as can be readily

discerned, there exists no single maximum point of deposition on the bottom wall since the gravitational effect is not very high.

Fig. (4.21) shows the effect of the surface adhesion parameter, N_s, on the deposition rates for the top and bottom walls of the channel. Here the angle of divergence is 2° and as can be seen the higher adhesion causes a decrease in deposition downstream from the inlet while the low adhesion simply raises the deposition on the bottom to a point where most of the particles are deposited on the bottom, thus generating a gradual decrease of particle deposition further downstream. Here, gravity is relatively high where the gravitational flow parameter assumes a value of 4.5.

Particle concentration over the inlet region of the diverging channel ($\theta = 2°$) with surface adhesion effect is seen in Fig. (4.22). With low adhesion, the concentration grows rapidly to a maximum at the bottom wall. However, for relatively high adhesion (here $N_s = 10$), the concentration maximizes at a point far below the channel centerline, particularly downstream, and then is turned suddenly in the negative x-direction towards the bottom wall.

The mass flux distribution of solid particles with significant gravitational effect is witnessed in Fig. (4.23)

where the gravity flow parameter, N_η, assumes the values of 0.5 and 4.5. Since most of the solid particles are deposited rapidly in the entrance region due to the high gravitational force, there naturally follows a smaller mass flux distribution further downstream from the inlet.

Fig. (4.24) represents the axial particle concentration, R, for a divergent channel of 2° where the gravitational effect is realized from N_η = 0.5 to 1.6. It is readily discerned that the concentration reaches a higher value the higher the gravitational pull, depending, of course, upon particle size. Furthermore, the particle concentration becomes lower at the top simply because of gravity.

Fig. (4.25) depicts the axial mass flux distribution of the solid particles with very significant gravitational influences. The mass flux for N_η = 10 becomes so infinitesimal downstream due to the fact that most of the particles have deposited early upon entrance.

Where large particles are employed, entrance effects are of extreme importance because almost all particles have dropped within a distance of one plate gap width as demonstrated by referring to Figure (4.26). This figure illustrates the deposition rate on both the top and bottom walls of the divergent channel having θ = 2°. The top deposition

is infinitesimal as compared to the bottom as expected under such a high gravitational field.

Fig. (4.27) demonstrates the effect of the surface adhesion parameter on the axial distribution of the particle concentration where the gravity flow parameter is quite high (here $N_\eta = 5$). For a typical angle of 4°, the particle concentration behaves very much the same as for gravitational flow in a parallel-plate channel.

Fig. (4.28) illustrates the effect of the surface adhesion parameter on the deposition rate for a divergent channel having $\theta = 4°$. With significant gravity effect, the deposition again wanes less further downstream from the inlet under high adhesive influences (here $N_s = 10$). However, for low adhesion (here $N_s = 0.1$), the bottom deposition rate grows to a pinnacle due to the large gravitational force and then gradually ebbs further downstream.

The divergent angle effect on the deposition rate for the bottom and top walls of the divergent channel is depicted in Fig. (4.29). Chosen angles of 2°, 4° and 7.5° clearly indicates that the larger the angle of divergence, the larger the deposition rate. A high diffusive Peclet number was utilized with significant gravity effect. As can be seen, the deposition rate goes to a very high value just before (the point of) separation takes place

indicating the predominant influence of the adverse pressure gradient upon the deposition process itself.

4.4.5 Flow of suspensions with combined action of diffusion, gravity and electric field in a diffuser. A comparison of the axial distribution of particle concentration at different surface adhesions is shown in Fig. (4.30). When $N_S = 10$, the particle concentration bulges below the centerline, particularly further downstream and then approaches complete absorption towards the bottom boundary. On the other hand, at low adhesion, $N_S = 1$, the particulate concentration simply drops towards the bottom wall.

Fig. (4.31) shows the effect of the surface adhesion parameter on the rate of deposition for the bottom and top walls of a divergent channel having $\theta = 4°$. Clearly, with low adhesion, the deposition rate on the bottom rises to a maximum and then slowly wanes further downstream, while on the top, the deposition rate simply falls to almost negligible proportions. However, for $N_S = 10$, the deposition for both walls starts from a maximum and decreases steadily downstream with again the bottom deposition rate far more predominant than the top due to gravity (here $N_\eta = 5$).

Fig. (4.32) illustrates the influence of the gravity flow parameter on the deposition rate for the bottom and top walls of the divergent channel with $\theta = 4°$ and $N_\beta =$

100. Since the adhesion is comparatively low, (here N_s = 1), the deposition rates rise to a maximum on the bottom for both gravity flows but when N_η = 5, the top deposition rate decreases from inlet while when N_η = 1, the top deposition rate rises and ebbs according to the proportionate gravity and electric field parameters.

The effect of the electrostatic charge parameter on the deposition rate with high diffusive Peclet number and N_η = 4.5 where $\theta = 4°$ is illustrated in Fig. (4.33). Clearly, when an electric field is applied, the bottom deposition increases to extreme proportions before separation occurs while with just gravity alone, the bottom deposition rises beyond proportions just before the point of separation is realized.

Fig. (4.34) depicts the effect of very high adhesion with high gravity on the deposition rate of the bottom and top walls of a divergent channel where the angles of divergence vary as $\theta = 4°$ and $\theta = 7.5°$. It is readily discernable that the higher the divergence angle the lesser the deposition downstream.

The effect of the angle of divergence on the bottom deposition rate is seen in Fig. (4.35). For an angle of 4°, the deposition behaves quite expectedly showing a maximum peak in the entrance region vicinity and then decreas-

ing downstream to separation; however, for angles of 7.5° and 9°, the deposition increases to a maximum (increasing with increasing angle), and then decreases to the neighborhood of the point of separation where the deposition suddenly rises up to the point of discontinuity.

Fig. (4.36) shows the effect of the angles of divergence (here θ = 4°, 7.5° and 9°) on the deposition rates for both the bottom and top walls of the channel where the diffusive Peclet number, N_β, is 100, and the gravity flow parameter is low (N_η = 1). The higher the angle of divergence, the higher the deposition rate particularly when the point of separation is approached for, as can be seen, the deposition rate then reaches a very high value.

Fig. (4.37) illustrates the effect of the angles of divergence (here 4°, 7.5° and 9°) on the deposition rate for the bottom and top walls where the diffusive Peclet number, N_β, is very high ($N_\beta = 10^7$) and gravity is moderately high (here N_η = 4.5). For an angle of 4°, the deposition simply grows to a relatively high value prior to separation; however, for angles of 7.5° and 9°, the deposition grows to a very high value just before separation.

The effect of the angle of divergence on the deposition rate for the bottom and top walls of a channel when N_β = 100 and N_η = 5.0 is shown in Fig. (4.38). For angle

of 4°, the deposition on the bottom behaves quite expectedly but the bottom deposition rises beyond proportions as the point of separation is approached.

Fig. (4.39) shows the effect of the electrostatic charge parameter (here N_α = 0, 1) on the rate of deposition for both the top and bottom walls of a divergent channel having θ = 4°, N_η = 5 and N_S = 10.

Since the surface adhesion is proportionately high, the deposition initiates from a maximum and drops to a gradual minimum where the deposition is much higher on the bottom than on the top. The electrical effect thus has a similar influence on the deposition as the gravitational effect.

Fig. (4.40) illustrates the gravitational influence over the axial distribution of the electric field intensity, E*, for a divergent channel having θ = 4°, and N_β = 100. For low gravity, the electric intensity remains constant in an almost linear fashion. However, when gravity becomes stronger, the electric field exhibits a nonlinear behavior particularly downstream with a definite decrease in intensity.

Fig. (4.41) shows the Fraction of Penetration and Fraction of Deposition of the solid particles when θ = 4°.

The mass flux of particles leaving the section of the channel at approximately x = 2.5 is roughly 50 per cent of the mass flux of particles entering that section. The deposition clearly grows downstream until separation occurs.

Fig. (4.42)illustrates the effect of the gravity flow parameter (here N_η = 1 and 5) on the axial distribution of the electrical potential W*when $\theta = 4°$ and $N_\beta = 100$. When gravity is not too predominant, the electrical potential expands downstream with greater magnitude as compared to the case when gravity becomes strong.

4.4.6 Deposition due to diffusive, electrical and gravitational influences with nonuniform inlet conditions. This particular case involves the situation when a straight wall parallel-plate channel is connected to a straight wall diverging channel. The parallel-plate channel of length equivalent to its width (i.e., $\chi = 2h$) is connected to a diverging channel of angle (2θ), where the selected value for 2θ is 15°. This arrangement approximates the splitter region in an actual fluidic device whereby the results of the parallel channel flow at $\chi = 2$ will be considered as the inlet conditions for the diverging channel flow.

Fig. (4.43) shows the effect of the gravity flow parameter, N_η, on the rate of deposition for both the bottom and top walls. Here, the deposition rate for the bottom

peaks higher at the higher gravity parameter and then tapers off to a minimum as seen previously from other results, but when $N_\eta = 5$, the deposition rises slightly in its immediate approach to the point of separation. The top deposition dips appreciably lower when gravity becomes high as also seen previously.

Fig. (4.44) illustrates the deposition rate on both the top and bottom walls when gravity is very high (here $N_\eta = 10$) and the surface adhesion is proportionately high (here $N_S = 7$). Again, the maximum deposition rate on the bottom occurs within one channel length and then steeps to a minimum; for the top, the maximum occurs at the inlet and decreases to a minimal (almost infinitesimal) value.

From this analysis dealing with nonuniform inlet conditions, it was found that the conclusions drawn from the results with uniform inlet conditions are nearly the same as with nonuniform inlet conditions for the situations studied. High gravity causes greater deposition in the entrance region and for higher angles of divergence causes extreme deposition.

CONCLUSIONS

From this investigation, the conclusions reached for the parallel-plate, converging and diverging channel flows are given as follows:

(1) An increase of the gravity flow parameter causes greater deposition rate on the bottom wall and much less deposition rate on the top wall. This can be seen, for example, by referring to Fig.(3.4) which indicates an increase deposition rate from 0.002 to 0.009.

(2) An increase of electrostatic charge on the solid particles causes a greater deposition rate on both walls of the channels as seen from Fig.(3.14) which shows an increase of deposition rate from 0.075 to 0.16 on the bottom wall, and from 0.045 to 0.12 on the top wall.

(3) Surface adhesion can also cause an increase of deposition rate particularly upon inlet as seen by referring to Fig.(3.8) which indicates an inlet deposition rate of 0.125 for $N_s = 5.0$, and 0.0125 for $N_s = 0.5$.

(4) The diffusive Peclet number exhibits a maximum bottom deposition rate only at low N_β (e.g., $N_\beta = 40.$) for the parallel and diffuser channel flows. However, for the converging channel flow, there exists

a maximum deposition close to the inlet for both low and high N_β.

Furthermore, it was found that the angle of divergence has a considerable effect on the rate of deposition when gravity and electrostatic charge are taken into account. Since increasing the diffuser angle causes a higher adverse pressure gradient, the flow is impeded near the wall allowing both the gravitational and electrostatic force to cause a large deposit on the walls, especially on the bottom wall due to gravity. At larger angles of divergence, the deposition rate increases very rapidly on the bottom wall especially near the point of separation.

However, it was also found that the angle of convergence has a considerable effect on the rate of deposition when gravity and electrostatic charge are considered. By increasing the angle of convergence, the flow field increases its velocity development thereby the pressure itself is decreasing rapidly in the downstream direction causing much less deposition rate especially on the bottom wall.

RECOMMENDATIONS FOR FUTURE STUDY

The subject of multiphase flow can be applied in numerous applications and situations. Since gravity is of great significance in various problems, the lift force per unit mass, f_L, could be treated as a function of space variables, along with the variation of gravity with elevation. The fluid phase medium could furthermore be treated as a phase transporting particles of different species such as particles of different diameters and densities. Also, a transport medium, such as air, could be used to transfer a radioactive gas through the entrance of varying size channels and ducts. This type of analysis is of extreme importance especially when treating the problem of radioactive leakage from powerplants or atomic wastes.

The exhaust system of a car could be handled as a series of cylindrical tubes containing many phases in a multi phase flow system. The muffler itself acts as a fluidic device with contamination effects particularly due to solid particle velocities and build-up.

In this investigation, the situation of two phase flow in a two dimensional channel, i.e., a parallel, converging and diverging channel, was considered whereby all configurations were assumed horizontal. Attempts should be made

to further this study for any inclination of the channel with the direction of gravity. Moreover, an investigation of the deposition rate in the entrance region of pipes for any inclination of the pipe with the direction of gravity should also be formulated.

Although many studies have been concerned with two-phase flow, a matter of further interest would be to investigate systems concerned with three or four phase flow for cases such as an air compressor whereby air, solid particles and oil would constitute the three phases. With the advent of the rocket age, increased interest of rocket nozzle exhausts of solid-liquid propellants lend analysis to many multi-phase flow situations. Special interest could also lie in the particle or particulate temperature profile enabling the availability of heat rate information and other thermal properties of significance for design.

REFERENCES

1. Abramowitz, M., "On Backflow of a Viscous Fluid in a Diverging Channel," Journal of Math. Phys., Vol. 28, 1949, pp. 1-21.

2. Berezin, J. S. and Zhidkov, N. P., Computing Methods, Pergamon Press, London, Vol. II, 1965, pp. 534-544.

3. Blasius, H., "Laminare Strömung in Kanälen Wechselnder Breite," F. Math. und Physik., Vol. 58, 1910, p. 225.

4. Bodoia,J. R., "The Finite Difference Analysis of Confined Viscous Flows," Doctor of Philosophy Thesis - Carnegie Institute of Technology, New York, New York, 1959.

5. Carleson, J. J., Johnstown, J. P., "The Ratio of Terminal Velocity to Minimum Fluidizing Velocity for Spherical Particles," Can. J. Chem. Eng., Vol. 46, 1968, pp. 325-328.

6. Chen, R. Y., "Diffusive Deposition of Particles in a Short Channel," Powder Technology, Vol. 16, pp. 131-135, 1977.

7. Chen, R. Y. and Comparin, R. A., "Deposition of Aerosols in the Entrance of a Tube," J. Aerosol Sci., Vol. 7, pp. 335-341, 1976.

8. Chua, J. H. and Wang, C. S., "Deposition of Submicron Particles from Steady Flows in a Branched Tube," J. Res. Assoc. Powder Tech., Vol. 9, 1972, pp. 37-45.

9. Comparin, R. A., Moses, H. L. and Powell, E. E., III, "Contamination Effects in a Laminar Proportional Amplifier," Fluidics,State of-the-Art Symposium, Sep. 30-Oct. 3., Vol. 1, 1974, pp. 247-259, U. S. Army (H.D.L.) Material Command.

10. Corn, M., "The Adhesion of Solid Particles to Solid Surfaces," J. Air Pollution Control Assoc., Vol. 11 (1), 1961, pp. 523-528 and Vol. 11 (12), 1961, pp. 566-576, 584.

11. Davies, C. N., Aerosol Science, Academic Press, London and New York, 1966, Chapter XII.

12. Eldighidy, S. M., Chen, R. Y., and Comparin, R. A., "Deposition of Suspensions in the Entrance of a Channel," presented at ASME Winter Annual Meeting, New York, 1976. 76-WA/F 1 Cs-13, J. of Fluids Engrg., Trans. ASME Vol. 99, June 1977, pp. 365-370.

13. Friedlander, S. K. and Johnstone, H. F. "Deposition of Suspended Particles from Turbulent Gas Streams," Ind. and Eng. Chem., Vol. 49, No. 7, 1957, pp. 1151-1156.

14. Fröberg, C.E., Introduction to Numerical Analysis, Addison-Wesley Publishing Company, Second Edition, 1968, Chapters 4 and 15.

15. Fuchs, N., Mechanics of Aerosols, Pergamon Press, 1964.

16. Ingham, D. B., "Diffusion and Sedimentation of Aerosol Particles from Poiseuille Flow in Rectangular Tubes," J. Aerosol Sci., Vol. 7, pp. 13-20, 1976.

17. Ingham, D. B., "Simultaneous Diffusion and Sedimentation of Aerosol Particles in Rectangular Tubes," J. Aerosol Sci., Vol. 7, pp. 373-380, 1976.

18. John, J. E., Gas Dynamics, Allyn and Bacon, Inc., Fourth printing, 1973, Chapter 16.

19. Kunkel, W. B., "The Static Electrification of Dust Particles on Dispersion into a Cloud," J. Appl. Phys., Vol. 21, 1950.

20. Michael, D. H., "The Steady Motion of a Sphere in a Dusty Gas," J. Fluid Mech. Vol. 31, Part 1, 1968, pp. 175-192.

21. Murray, J. D., "On the Mathematics of Fluidization," J. Fluid Mech., Vol. 21, 1965, p. 465, Vol. 22, 1965, P. 57.

22. Pai, S. I. and Hsieh, T., "Interaction Terms in Gas-Solid Two-Phase Flows," Z. Flugwiss. 21, 1973, Heft 12, pp. 442-445.

23. Peddieson, J., Jr., "Flow Induced in a Solid-Fluid Suspension by Impulsive Motion of an Infinite Flat Plate," - presented at Ninth Annual Meeting of Society of Engineering Science, 1971.

24. Peddieson, J., Jr., "The Hydrodynamics of Dust Collection," - Proceedings of the 18th Annual Technical Meeting of the Institute of Environmental Sciences, 1972.

25. Peddieson, J., Jr., "Dust Collection at Moderate Void Fractions," - Proceedings of the Annual Technical Meeting of the Institute of Environmental Sciences, 1973.

26. Quarmby, A., "A Finite Difference Analysis of Developing Slip Flow," Appl. Sci. Res., Vol. 19, 1968, pp. 18-33.

27. Savilonis, B. J., Fu. S. E. and Lee, J. S., "Charged Aerosol Deposition in Straight and Curved Conducting Tubes," 1977 Biomechanics Symposium AM D- Vol. 23, ASME Publication, pp. 29-31.

28. Schlichting, H., Boundary Layer Theory, McGraw-Hill Book Co., 6th Edition, 1968, Chapters 4 and 7.

29. Soo, S. L., Fluid Dynamics of Multiphase Systems, Blaisdell Publishing Co., 1976, Chapters 6 and 8.

30. Soo, S. L., "Pipe Flow of Suspensions," Appl. Sci. Res., Vol. 21, 1969, pp. 68-84.

31. Soo, S. L., "Effect of Diffusion on Collection and Impaction of Sphere," Powder Technology, Vol. 7, 1973, pp. 267-269.

32. Soo, S. L. and Rodgers, L. W., "Further Studies on the Electro-Aerodynamic Precipitator," Powder Technology, Vol. 5, 1971, pp. 43-50.

33. Soo, S. L. and Tung, S. K., "Pipe Flow of Suspensions in Turbulent Fluid, Electrostatic and Gravity Effects," Appl. Sci. Res., Vol. 24, 1971, pp. 83-97.

34. Soo, S. L. and Tung, S. K., "Deposition and Entrainment in Pipe Flow of Suspension," Powder Technology, Vol. 6, 1972, pp. 283-294.

35. Stukel, J. J. and Soo, S. L., "Turbulent Flow of a Suspension into a Channel," Powder Technology, Vol. 2, 1968/1969, pp. 278-289.

36. Tan, C. W. and Hsu, C. J., "Diffusion of Aerosols in Laminar Flow in a Cylindrical Tube," J. of Aerosol Sci., Vol. 2, 1971, pp. 117-124.

37. Wilson, I. B., "The Deposition of Charged Particles in Tubes, with Reference to the Retention of Therapeutic Aerosols in the Human Lung," J. of Colloid Sci., Vol. 2, No. 2, April 1947, pp. 271-276, Refereed by Savilomis et al. (16).

38. Yang, Y. C. and Peddieson, J., Jr., "Some Parallel Flows of Solid-Fluid Suspension," - presented at Ninth Annual Meeting of Society of Engineering Science, 1971.

39. Zagainov, V. A., Sutugin, A. G., Petrianov-Sokolov, I. V. and Lusknikov, A. A., "On the Sticking Probability of Molecular Clusters to Solid Surfaces," J. Aerosol Sci., Vol. 7, pp. 389-395, 1976.

APPENDIX A

SIMPLIFICATION OF THE MOMENTUM EQUATIONS FOR BOTH THE FLUID AND PARTICULATE PHASES

The equation of motion of the fluid phase alone was given by Soo [29] as,

$$\rho\{\frac{\partial U_i}{\partial t} + U_j \frac{\partial}{\partial X_j}(U_i)\} = -[1 - K_m \frac{\rho_p}{\overline{\rho}_p}] \frac{\partial P}{\partial X_i} + \frac{\partial}{\partial X_j}[\mu_f \Delta_{ij} + \mu_{f2} \Omega_f \delta_{ij}]$$

$$+ \rho f_i - \frac{1}{2}\overline{\rho} K_m \frac{\rho_p}{\overline{\rho}_p}[\frac{\partial}{\partial t}(U_i - U_{pi}) + U_{pj} \frac{\partial}{\partial X_j}(U_i - U_{pi})]$$

$$- \frac{9}{2\sqrt{\pi}} \sqrt{\mu\rho}\, K_m \frac{\rho_p}{\overline{\rho}_p} \int_{t_o}^{t_p} [\frac{d}{d\tau}(U_i - U_{pi})](t_p - \tau)^{-1/2} d\tau$$

$$- K_m \rho_p F (U_i - U_{pi}) \qquad \text{eq. (A-1)}$$

For a dilute suspension, $K_m \equiv 0$. If we neglect body forces for the fluid phase alone, we have,

$$\rho\{\frac{\partial U_i}{\partial t} + U_j \frac{\partial}{\partial X_j}(U_i)\} = -\frac{\partial P}{\partial X_i} + \frac{\partial}{\partial X_j}[\mu_f \Delta_{ij} + \mu_{f2} \Omega_f \delta_{ij}] \quad \text{(A-2)}$$

Here, $j = 1, 2$ and $i = 1, 2$ where 1 corresponds to the axial component and 2 corresponds to the vertical component.

Since steady flow was assumed, $\partial/\partial t \equiv 0$. Also, since

$$\Delta_{ij} = \frac{\partial U_j}{\partial X_i} + \frac{\partial U_i}{\partial X_j}$$

and

$$\Omega_f = \frac{\partial U_i}{\partial X_i},$$

eq. (A-2) becomes,

$$\rho[u\frac{\partial u}{\partial X} + v\frac{\partial u}{\partial y}] = -\frac{\partial P}{\partial X} + \frac{\partial}{\partial X}[\mu_f(2\frac{\partial u}{\partial X})] + \frac{\partial}{\partial y}[\mu_f(\frac{\partial u}{\partial y} + \frac{\partial v}{\partial X})]$$

$$+ \frac{\partial}{\partial X}(\mu_{f2}(\frac{\partial u}{\partial X}) \qquad \text{eq. (A-3)}$$

$$\rho[u\frac{\partial v}{\partial x} + v\frac{\partial v}{\partial y}] = -\frac{\partial p}{\partial y} + \frac{\partial}{\partial X}[\mu_f(\frac{\partial u}{\partial y} + \frac{\partial v}{\partial X})] + \frac{\partial}{\partial y}[2\mu_f\frac{\partial v}{\partial y}]$$

$$+ \frac{\partial}{\partial y}(\mu_{f2}\frac{\partial v}{\partial y}) \qquad \text{eq. (A-4)}$$

However, in accordance with the boundary layer simplifications by Schlichting[28], the equation for the normal component eq. (A-4), reduces simply to $\partial P/\partial y = 0$, and eq. (A-3) becomes eq. (3-7), i.e.,

$$\rho[u\frac{\partial u}{\partial X} + v\frac{\partial u}{\partial y}] = -\frac{dP}{dX} + \mu_f\frac{\partial^2 u}{\partial y^2} \qquad (3\text{-}7)$$

The momentum equation of the particulate phase was also given by Soo [29] as,

$$\rho_p[\frac{\partial}{\partial t}(U_{pi}) + U_{pj}\frac{\partial}{\partial X_j}(U_{pi})] = \frac{\partial}{\partial X_j}[\mu_p(\Delta_p)_{ij} + \mu_{p2}\Omega_p\delta_{ij}]$$

$$+ \rho_p f_{pi} + \rho_p F(U_i - U_{pi}) \qquad (A\text{-}5)$$

Here, i = 1, 2 and j = 1, 2 where 1 refers to the axial component and 2 refers to the vertical component.

Since steady flow was assumed, $\partial/\partial t \equiv 0$. Also, since,

$$(\Delta_p)_{ij} = \frac{\partial U_{pj}}{\partial X_i} + \frac{\partial U_{pi}}{\partial X_j}$$

and

$$\Omega_p = \frac{\partial U_{pi}}{\partial X_i} ,$$

eq. (A-5) becomes,

$$\rho_p [u_p \frac{\partial u_p}{\partial X} + v_p \frac{\partial u_p}{\partial y}] = \frac{\partial}{\partial X} [2\mu_p \frac{\partial u_p}{\partial X}] + \frac{\partial}{\partial y} [\mu_p (\frac{\partial u_p}{\partial y} + \frac{\partial v_p}{\partial X})]$$

$$+ \frac{\partial}{\partial X} [\mu_{p2} \frac{\partial u_p}{\partial X}] + \rho_p f_{px} + \rho_p F (u - u_p) \qquad \text{eq. (A-6)}$$

$$\rho_p [u_p \frac{\partial v_p}{\partial X} + v_p \frac{\partial v_p}{\partial y}] = \frac{\partial}{\partial X} [\mu_p (\frac{\partial u_p}{\partial y} + \frac{\partial v_p}{\partial X})] + \frac{\partial}{\partial y} [2\mu_p \frac{\partial v_p}{\partial y}]$$

$$+ \frac{\partial}{\partial y} [\mu_{p2} \frac{\partial v}{\partial y}] + \rho_p f_{py} + \rho_p F (v - v_p) \qquad \text{eq. (A-7)}$$

The body force in the x direction, f_{px} is assumed negligible; however, the body force in the y direction is,

$$f_{py} = -(\frac{q}{mp}) \frac{\partial w}{\partial y} - g \qquad \text{(A-8)}$$

If we assume that the suspension is dilute, then $\nu_p \sim D_p$ such that $\mu_p = \rho_p D_p$ where D_p is the particle diffusivity (assumed constant).

If we neglect higher order terms associated with the axial variation of the particle velocity in the streamwise direction, eq. (A-6) becomes eq. (3-9), i.e.,

$$\rho_p [u_p \frac{\partial u_p}{\partial x} + v_p \frac{\partial u_p}{\partial y}] = \rho_p F (u - u_p) + D_p \frac{\partial}{\partial y} (\rho_p \frac{\partial u_p}{\partial y}) \quad (3\text{-}9)$$

In treating the momentum equation for the normal component of the particle velocity, the viscous forces are negligible in comparison to the inertial forces, thus eq. (A-7) becomes eq. (3-10), i.e.,

$$\rho_p [u_p \frac{\partial v_p}{\partial x} + v_p \frac{\partial v_p}{\partial y}] = \rho_p F (v - v_p) + \rho_p f_{py} \quad (3\text{-}10)$$

where f_{py} is given by eq. (A-8).

APPENDIX B

DIMENSIONLESS QUANTITIES AND PARAMETERS

PHYSICAL MEANING

(1) Dimensionless Quantities and Parameters

$\chi = x/h$

$Y = y/h$

$Y^* = Y/(1 + \chi \text{ Tan } \theta)$

$H^* = h(x)/h$

$U = u/u_o$

$V = v/u_o$

$U_p = u_p/u_o$

$V_p = v_p/u_o$

$P = (p - p_o)/(\rho u_o^2)$

$N_{DF} = (D_p/Fh^2)^{1/2}$

$N_{ED} = (\rho_{po}/4\varepsilon_o)(q/m_p)(h^2/D_p)$

$N_m = u_o/hF$

$N_R = u_o h/\nu$

$K_{np} = L_p/h$

$M^* = \dot{m}/(\rho_{po} u_o)$

$W^* = (q/m_p) w/D_p F$

$R = \rho_p/\rho_{po}$

$N_\alpha = (N_{ED} N_{DF})^2 = (\rho_{po}/4\varepsilon_o)(q/m_p)^2 (h^2/FD_p)$

$N_\beta = N_m/N_{DF}^2 = u_o h/D_p$

$N_{Fr} = u_o/\sqrt{gh}$

$E^* = \partial W^*/\partial Y = (q/m_p) hE/D_p F$

$$N_\eta = N_m^2/(N_{Fr}^2 N_{DF}^2) = N_\beta N_m/N_{Fr}^2$$

$$N_\gamma = N_m/(N_{Fr}^2 N_{DF}^2) = N_\eta/N_m$$

$$N_\lambda = hfw/FD_p$$

$$N_s = \sigma_w N_\lambda$$

$$N_{scp} = \nu/D_p$$

(2) Physical Meaning

$N_{DF} = (D_p/Fh^2)^{1/2}$ Diffusion response number

which is the square root of the ratio of the relaxation time (1/F) to the diffusion time (h^2/D_p).

$N_{ED} = (\rho_{po}/4\varepsilon_o)^{1/2}(q/m_p)(h^2/D_p)$ Electro-diffusion number

which is the ratio of the displacement by the electrostatic repulsion to that by diffusion

$N_m = u_o/hF$ Momentum-transfer number

which is the ratio of the relaxation time (1/F) to the transport time (h/u_o).

$N_R = u_o/h\nu$ Reynolds number (based on half channel width)

which is the ratio of inertial forces to viscous forces.

$N_{scp} = \nu/D_p$ Schmidt particle number

which is the ratio of viscous forces to particle diffusive forces (analagous to the Prandtl number in heat transfer).

$K_{np} = L_p/h$ particle Knudsen number

which is the ratio of particle-fluid interaction length (L_p) to half the channel width (h). This number governs the particle slip condition at the wall.

$$N_\alpha = (N_{ED}N_{DF})^2 = (\rho_{po}/4\varepsilon_o)(q/m_p)^2(h^2/FD_p)$$

Electrostatic-charge parameter

which characterizes the electrostatic charge of the solid particles.

$$N_\beta = (N_m/N_{DF}^2) = N_{scp}N_R = u_o h/D_p$$

Diffusive Peclet number

which is the ratio of inertial forces to diffusive forces. This number is a momentum-diffusion parameter.

$N_{FR} = u_o/\sqrt{gh}$ Froude number

which is the ratio of the inertial forces to the gravity force.

$N_\eta = N_m^2/N_{Fr}^2N_{DF}^2) = hg/D_pF$ Gravity flow parameter

which is the ratio of the gravity force to the diffusive forces of particles.

$N_\lambda = hfw/FD_p$ Adhesive-force parameter

which is the ratio of the wall adhesive forces to the diffusive forces of particles. Note that $N_s = \sigma_w N_\lambda$ was used

as a surface adhesion parameter.

$\dot{M}^* = \dot{m}/\rho_{po}u_o$ Dimensionless rate of deposition of particles

which is the ratio of the rate of deposition of the particles to the mass flow rate of the particles at inlet.

(3) Order of Magnitude

An actual fluidic device can have a half channel width of h = 0.05 cm. For air as a fluid phase with a pressure of 1 atm and a temperature of 20°C, by using the relation by John [18]

$$L_p = 3\nu/\sqrt{8/\pi\ g_c R/T}\ ,$$

it follows that the particle Knudsen number is $K_{np} = 0.00013$.

A range of (0.0001-0.1) was considered for K_{np}. Assuming a uniform inlet velocity of $u_o = 3000$ cm/sec, the Reynolds number can be found based upon half the channel width such that,

$$N_R \cong 1000.$$

The momentum transfer number, N_m, contains the inverse relaxation time such that,

$$F = 9\bar{\mu}/2a^2\bar{\rho}_p$$

in the Stokes regime.

For a suspension of 0.4 volume fraction solid of 1 micron MgO in air at room conditions gives

$\bar{\mu} = 0[10^{-7}]$ Kg/cm sec

Let $\bar{\mu} = 2.0 \times 10^{-7}$ Kg/cm sec

$\rho = 0.001204$ g/cm^3

$\bar{\rho}_p \cong 4 \times 10^{-3}$ Kg/cm^3

Considering various particle radii, the inverse relaxation time can be calculated; consequently, the momentum transfer number can be realized.

Thus, for a particle radius, a, of:

$0.05\mu \rightarrow F = 9.0 \times 10^{6}$ sec^{-1}

$0.1\mu \rightarrow F = 2.25 \times 10^{6}$ sec^{-1}

$0.2\mu \rightarrow F = 5.6 \times 10^{5}$ sec^{-1}

$1\mu \rightarrow F = 2.25 \times 10^{4}$ sec^{-1}

Consequently,

$N_m = 6.67 \times 10^{-3}$ for particles of 0.1μ diameter

$N_m = 2.67 \times 10^{-2}$ for particles of 0.2μ diameter

$N_m = 0.107$ for particles of 0.4μ diameter

and $N_m = 2.67$ for particles of 2μ diameter

The particle density at inlet can be assumed to be on the order $0[10^{-6}]$ g/cm^3 (e.g., 4×10^{-6} g/cm^3). According to Davies [11], the coefficient of diffusion, D_p, can vary as:

$D_p = 6.8 \times 10^{-6}$ cm^2/sec for particles of 0.1μ diameter

$D_p = 2.2 \times 10^{-6}$ cm^2/sec for particles of 0.2μ diameter

$D_p = 8.4 \times 10^{-7}$ cm^2/sec for particles of 0.4μ diameter

and $D_p = 1.3 \times 10^{-7}$ cm^2/sec for particles of 2μ diameter

Hence, the diffusive Peclet number, N_β, can be calculated such as,

$N_\beta = 2.2 \times 10^7$ for particles of 0.1μ diameter

$N_\beta = 6.82 \times 10^7$ for particles of 0.2μ diameter

$N_\beta = 1.76 \times 10^8$ for particles of 0.4μ diameter

and $N_\beta = 1.15 \times 10^9$ for particles of 2μ diameter

The gravity flow parameter, N_η, can be calculated if the local acceleration of gravity, g, can be assumed a certain value. Hence, g = 980.6 cm/sec^2 at sea level (standard gravity). Thus, an order of magnitude analysis can be performed indicating a possible range of N_η depending of course on particle size.

Based upon a half channel width of 0.05 cm, N_η can be calculated as,

$N_\eta = 0.024$ for particles of 0.04μ diameter

$N_\eta = 0.8$ for particles of 0.1μ diameter

$N_\eta = 10$ for particles of 0.2μ diameter

and $N_\eta = 104$ for particles of 0.4μ diameter

A range of $N_\eta \in \{0.05, 1, 1.6, 4.5, 5, 10, 100\}$ was considered in the analysis.

The electrostatic charge parameter,

$$N_\alpha = (\rho_{po}/4\varepsilon_o)(q/m_p)^2(h^2/FD_p)$$

where $\varepsilon_o = 8.854 \times 10^{-12}$ coul^2/N-m^2 (permitivity of free space)

can also be varied with due respect to particle size. As previously used by Eldighidy et al. [12], for an air velocity of 35 m/sec ($\tilde{}$ 30 m/sec);

$$(q/m_p) = 1.633 \times 10^{-3} \text{ coul/Kg};$$

which is the electrostatic charge to mass ratio needed for the determination of N_α.

Hence,

$N_\alpha = 2.0 \times 10^{-3}$ for particles of 0.04μ diameter

$N_\alpha = 6.65 \times 10^{-2}$ for particles of 0.1μ diameter

$N_\alpha = 0.82$ for particles of 0.2μ diameter

and $N_\alpha = 8.65$ for particles of 0.4μ diameter

(Note: $N_\alpha = 139$ if 2μ diameter spherical particles were considered.)

The surface adhesion parameter, $N_s = \sigma_w N_\lambda$, can also be calculated for illustrative purposes when particle size information is provided. Since σ and σ_w are both probabili-

stic quantities (sticking probabilities), they were assigned a range from (0.5-1.0). However, since $N_\lambda = hfw/FD_p$, particle size information is not sufficient for the adhesive force at the immediate vicinity of the wall, fw, must be known.

Thus, for convenience, the surface adhesion parameter will be varied such that a range of $N_s \in \{0.1, 1, 10, 20, 1000\}$ was considered.

Hence, as a practical illustration, consider a suspension of 0.4 volume fraction solid of 0.2 micron diameter magnesia oxide in air flowing through a brass parallel channel having a half channel width of h = 0.05 centimeter, under ambient room conditions. The flow parameters would thus be realized as : $N_\eta = 10$, $N_\alpha = 1$, $N_\beta = 10^7$, $N_m = 0.03$, $N_R = 1000$, $N_s = 1$, $K_{np} = 0.0001$.

APPENDIX C

NUMERICAL PROCEDURES FOR SOLVING THE EQUATIONS DERIVED IN CHAPTERS 3 AND 4

The governing equations (3-15), (4-2), (3-17) to (3-21) can be written in the implicit finite difference form as follows:

$$\frac{U_{i+1,\ell} - U_{i,\ell}}{\Delta X} + \frac{V_{i+1,\ell+1} - V_{i+1,\ell}}{\Delta Y} = 0 \qquad \text{(C-1)}$$

$$U_{i+1,2} + 4\sum_{K=1}^{m} U_{i+1,2K+1} + 2\sum_{K=1}^{m-1} U_{i+1,2(K+1)} = 3.0/\Delta Y \qquad (m = 10) \qquad \text{(C-2)}$$

$$U_{i,\ell}\left(\frac{U_{i+1,\ell} - U_{i,\ell}}{\Delta X}\right) + V_{i,\ell}\left(\frac{U_{i+1,+1} - U_{i+1,j-1}}{2\Delta Y}\right)$$

$$= -\left(\frac{P_{i+1} - P_i}{\Delta X}\right) + \left(\frac{U_{i+1,\ell+1} - 2U_{i+1,\ell} + U_{i+1,\ell-1}}{N_R(\Delta Y)^2}\right) \qquad \text{(C-3)}$$

$$U_{Pi,j}\left(\frac{U_{Pi+1,j} - U_{Pi,j}}{\Delta X}\right) + V_{Pi,j}\left(\frac{U_{Pi+1,j+1} - U_{Pi+1,j-1}}{2\Delta Y}\right)$$

$$= \left(\frac{U_{i+1,j} - U_{Pi+1,j}}{N_m}\right) + \left(\frac{U_{Pi+1,j+1} - 2U_{Pi+1,j} + U_{Pi+1,j-1}}{N_\beta(\Delta Y)^2}\right)$$

$$+ \frac{(R_{i,j+1} - R_{i,j-1})(U_{Pi+1,j+1} - U_{Pi+1,j-1})}{4N_\beta(\Delta Y)^2 R_{i,j}} \qquad \text{(C-4)}$$

$$U_{Pi,j}\left(\frac{V_{Pi+1,j} - V_{Pi,j}}{\Delta X}\right) + V_{Pi,j}\left(\frac{V_{Pi+1,j+1} - V_{Pi+1,j}}{\Delta Y}\right)$$

$$= \left(\frac{V_{i+1,j} - V_{Pi+1,j}}{N_m}\right) - \left(\frac{W_{i+1,j+1} - W_{i+1,j-1}}{2\Delta Y N_\beta N_m}\right)$$

$$- N_\eta / N_\beta N_m \qquad \text{(C-5)}$$

$$U_{i+1,j}\left(\frac{R_{i+1,j} - R_{i,j}}{\Delta X}\right) + V_{i+1,j}\left(\frac{R_{i+1,j+1} - R_{i+1,j-1}}{2\Delta Y}\right)$$

$$= \frac{R_{i+1,j+1} - 2R_{i+1,j} + R_{i+1,j-1}}{N_\beta (\Delta Y)^2}$$

$$+ \frac{(R_{i+1,j+1} - R_{i+1,j-1})(W_{i,j+1} - W_{i,j-1})}{4N_\beta (\Delta Y)^2}$$

$$- \frac{4N_\alpha R_{i,j} R_{i+1,j}}{N_\beta} + \frac{N_\eta}{N_\beta}\left(\frac{R_{i+1,j+1} - R_{i+1,j-1}}{2\Delta Y}\right)$$

(C-6)

$$- \frac{W_{i+1,j+1} - 2W_{i+1,j} + W_{i+1,j-1}}{(\Delta Y)^2} = 4N_\alpha R_{i+1,j}$$

(C-7)

Since symmetrical flow was considered only for the fluid phase, the boundary conditions for the fluid phase alone take the form,

@ i = 2 (Inlet)

$(2 \leq \ell \leq N - 8)$

$U_{2,\ell} = 1.0$ (uniform)

$V_{2,\ell} = 0$

$P_{2,\ell} = 0$

@ $\ell = 2(\mathfrak{L})$ $i > 2$ [at Centerline]

$U_{i+1,3} = U_{i+1,1}$ Symmetry

$V_{i+1,2} = 0$

@ $\ell = N - 8$ (top wall)

$U_{i+1,N-8} = V_{i+1,N-8} = 0$ No slip fluid phase

For the parallel channel flow, $\Delta Y = 0.1$; $\Delta X = 0.001$, 0.01, 0.1, 0.2 and 0.3. But, for converging and diverging channel flow, $\Delta X = 0.001$, 0.01, 0.1, 0.2 and 0.3 while ΔY varies according to the converging or diverging angle (2θ). Different values for θ were chosen, in particular $\theta = 2°$, 4°, 5°, 7.5°, 9° and 10° for the diverging channel; $\theta =$ -4°, -7.5° and -10° for the converging channel. For an actual fluidic device, the diffuser angle in the splitter region is about 15°, i.e., $\theta = 7.5°$.

The width of the converging or diverging channel is a function of axial position such that,

$$WP_{i+1} = WP_i + \Delta X \mathrm{Tan}\theta$$

Thus, $\Delta Y_{i+1} = WP_{i+1}/N$ where $N = 10$, $WP_1 = 1.0$ and $\Delta Y_1 = 0.1$.

For all the channels under consideration,

$i = 2$ to m where m is taken up to 141

$j = 3$ to $N + 1$ where $N = 20$.

The equations of the boundary conditions (3-33) to (3-39); (4-12) to (4-18) can be written in the approximate form,

@ i = 2 (at inlet, corresponding to X = 0)

$(2 \leq j \leq N + 2)$

$U_{P2,j} = R_{2,j} = 1.0$ (uniform)

$V_{P2,j} = W_{2,j} = 0$

These uniform inlet boundary conditions are applied for parallel, convergent or divergent channel flows only when there is no connection among them.

@ j = 2 for $(i > 2)$ [at the channel bottom wall corresponding to $Y = -(1 + X\text{Tan}\theta)$]

$$W_{i+1,2} = 0$$

$$U_{Pi+1,2} = \frac{K_{np}/\Delta Y}{(1 + K_{np}/\Delta Y)} U_{Pi+1,3} \quad \text{(slip-particle phase)} \quad \text{(Case I)}$$

or

$$U_{Pi+1,2} = \sigma_s\left(\frac{1 - \Delta X(i-2)/N_m}{(1 + K_{np}/\Delta Y)} + \frac{K_{np}/\Delta Y}{(1 + K_{np}/\Delta Y)} U_{Pi+1,3}\right) \quad \text{for } i < (N_m/\Delta X) + 2$$

$$U_{Pi+1,2} = \frac{K_{np}/\Delta Y}{(1 + K_{np}/\Delta Y)} U_{Pi+1,3} \quad \text{for } i \geq (N_m/\Delta X) + 2 \quad \text{(Case II)}$$

$$R_{i+1,2} = R_{i+1,3}/[1 - \Delta Y(W^*_{i,3}/\Delta Y + \sigma N_\beta V_{Pi,2} - N_s + N_\eta)]$$

@ j = N + 2 [at the top wall, corresponding to $Y = (1 + X\text{Tan}\theta)$]

$(i > 2)$

$$W_{i+1,N+2} = 0$$

$$U_{Pi+1,N+2} = \frac{K_{np}/\Delta Y}{1 + K_{np}/\Delta Y} U_{Pi+1,N+1} \quad \text{slip-particle phase}$$

(Case I)

or

$$\left.\begin{aligned} U_{Pi+1,N+2} &= \sigma_s\left(\frac{1 - \Delta X(i-2)/N_m}{1 + K_{np}/\Delta Y}\right) \\ &+ \frac{K_{np}/\Delta Y}{(1 + K_{np}/\Delta Y)} U_{Pi+1,N+1} \quad \text{for } i < (N_m/\Delta X) + 2 \end{aligned}\right\}$$

$$\left.\begin{aligned} U_{Pi+1,N+2} &= \frac{K_{np}/\Delta Y}{1 + K_{np}/\Delta Y} U_{Pi+1,N+1} \\ &\text{for } i \geq (N_m/\Delta X) + 2 \end{aligned}\right\} \quad \text{(Case II)}$$

$$R_{i+1,N+2} = R_{i+1,N+1}/[1 + \Delta Y(\sigma N_\beta V_{Pi,N+2} - W^*_{i,N+1}/\Delta Y + N_s + N_\eta)]$$

Also, equation (3-22) can be written in approximate form as,

$$DPRT_{i+1} = R_{i+1,N+2}[\sigma V_{Pi+1,N+2} + N_s/N_\beta] + R_{i+1,2}[N_s/N_\beta - \sigma V_{Pi+1,2}] \qquad \text{(C-8)}$$

Let

$$\alpha 1_{i,\ell} = -\left(\frac{V_{i,\ell}}{2\Delta Y} + \frac{1}{(\Delta Y)^2 N_R}\right)$$

$$\alpha 2_{i,\ell} = -\left(\frac{V_{i,\ell}}{2\Delta Y} + \frac{1}{(\Delta Y)^2 N_R}\right)$$

$$\alpha 3_{i,\ell} = \frac{V_{i,\ell}}{2\Delta Y} - \frac{1}{(\Delta Y)^2 N_R}$$

$$\beta 1_{i,j} = \left[\frac{R_{i,j+1} - R_{i,j-1}}{4N_\beta (\Delta Y)^2 R_{i,j}} - \frac{1}{N_\beta (\Delta Y)^2} - \frac{V_{Pi,j}}{2\Delta Y}\right]$$

$$\beta 2_{i,j} = \frac{U_{Pi,j}}{\Delta X} + \frac{1}{N_m} + \frac{2}{N_\beta (\Delta Y)^2}$$

$$\beta 3_{i,j} = \frac{V_{Pi,j}}{2\Delta Y} - \frac{1}{N_\beta (\Delta Y)^2} - \frac{R_{i,j+1} - R_{i,j-1}}{4N_\beta (\Delta Y)^2 R_{i,j}}$$

$$\gamma 1_{i,j} = \frac{U_{pi,j}}{\Delta X} - \frac{V_{pi,j}}{\Delta Y} + \frac{1}{N_m}$$

$$\gamma 2_{i,j} = \frac{V_{Pi,j}}{\Delta Y}$$

$$\zeta 1_{i,j} = -\left[\frac{V_{i+1,j}}{2\Delta Y} + \frac{1}{N_\beta (\Delta Y)^2} - \frac{N_\eta}{2N_\beta \Delta Y} - \frac{W^*_{i,j+1} - W^*_{i,j-1}}{4N_\beta (\Delta Y)^2}\right.$$

$$\zeta 2_{i,j} = \frac{U_{i+1,j}}{\Delta X} + \frac{2}{N_\beta (\Delta Y)^2} + \frac{4N_\alpha}{N_\beta} R_{i,j}$$

$$\zeta 3_{i,j} = \frac{V_{i+1,j}}{2\Delta Y} - \frac{1}{N_\beta (\Delta Y)^2} - \frac{N_\eta}{2N_\beta \Delta Y} - \frac{W^*_{i,j+1} - W^*_{i,j-1}}{4N_\beta (\Delta Y)^2}$$

$$F1_{i,\ell} = \frac{U^2_{i,\ell} + P_i}{\Delta X}$$

$$F2_{i,\ell} = \xi\, U_{i,\ell}$$

$$\phi 1_{i,j} = \frac{U^2_{Pi,j}}{\Delta X} + \frac{U_{i+1,j}}{N_m}$$

$$\phi 2_{i,j} = \frac{U_{Pi,j} V_{Pi,j}}{\Delta X} + \frac{V_{i+1,j}}{N_m} - \frac{N_\eta}{N_\beta N_m}$$

$$\phi 3_{i,j} = \frac{U_{i+1,j} R_{i,j}}{\Delta X}$$

$$\tau 1 = 1/(2.0 N_\beta N_m \Delta Y)$$

$$\tau 2 = 1/(N_\beta N_m \Delta Y)$$

$$\psi = 4 N_\alpha (\Delta Y)^2$$

$$\xi = \frac{\Delta Y}{\Delta X}$$

$$CK = (K_{np}/\Delta Y)/(1 + K_{np}/\Delta Y)$$

Then equations (C-1) to (C-7) and equation (C-8) can be written in simplified form (neglecting the second term on the left-hand side of equation (C-5) since it is small compared with the other terms),

$$\alpha 1_{i,\ell} U_{i+1,\ell-1} + \alpha 2_{i,\ell} U_{i+1,\ell} + \alpha 3_{i,\ell} U_{i+1,\ell+1} + P_{i+1}/\Delta X = F1_{i,\ell} \qquad \text{(C-9)}$$

$$U_{i+1,C+L} + 4 \sum_{K=1}^{r} U_{i+1,2K+1} + 2 \sum_{K=1}^{r-1} U_{i+1,2(K+1)} = 3.0/\Delta Y \qquad (r = 10) \qquad \text{(C-10)}$$

$$V_{i+1,\ell+1} - V_{i+1,\ell} + \xi U_{i+1,\ell} = F2_{i,\ell} \qquad \text{(C-11)}$$

$$\beta 1_{i,j} U_{Pi+1,j-1} + \beta 2_{i,j} U_{Pi+1,j} + \beta 3_{i,j} U_{Pi+1,j+1} = \phi 1_{i,j} \qquad \text{(C-12)}$$

$$\gamma 1_{i,j} V_{Pi+1,j} - \tau 2 W_{i+1,j} + \tau 2 W_{i+1,j+1} = \phi 2_{i,j} \qquad \text{(C-13)}$$

$$\zeta 1_{i,j} R_{i+1,j-1} + \zeta 2_{i,j} R_{i+1,j} + \zeta 3_{i,j} R_{i+1,j+1} = \phi 3_{i,j} \qquad \text{(C-14)}$$

$$W_{i+1,j-1} - 2W_{i+1,j} + W_{i+1,j+1} + \psi R_{i+1,j} = 0 \qquad \text{(C-15)}$$

$$DPRT_{i+1} = R_{i+1,N+2}[\sigma V_{Pi+1,N+2} + N_s/N_\beta] + R_{i+1,2}[N_s/N_\beta - \sigma V_{Pi+1,2}] \qquad \text{(C-16)}$$

where i = 2 to m for all equations and j = 3 to N + 1 for equations (C-12 (C-14) and (C-15); j = 2 to N + 2 for equation (C-13); ℓ = 2 to N1 + 1 for equation (C-9) and (C-11). Note that N1 = 10.

Hence, equations (C-9) to (C-16) can be expanded to give (5N — 1) equations for a fixed value of i and different values of j and ℓ. Using the boundary conditions with these equations, the unknowns will be as follows:

Phase	Unknowns	No. of Unknowns
Fluid Phase	$U_{i+1,2}, U_{i+1,3}, \ldots, U_{i+1,N1+1}$	N-10
	P_{i+1}	1
	$V_{i+1,3}, \ldots, V_{i+1,N+1}$	N-11
Particle Phase	$U_{Pi+1,3}, U_{Pi+1,4}, \ldots, U_{Pi+1,N+1}$	N-1
	$V_{Pi+1,2}, V_{Pi+1,3} \ldots, V_{Pi+1,N+2}$	N+1
	$R_{i+1,3}, R_{i+1,4}, \ldots, R_{i+1,N+1}$	N-1
	$W^*_{i+1,3}, W^*_{i+1,4}, \ldots, W^*_{i+1,N+1}$	N-1
	$\dot{M}^*_{i+1}$	1
	Total =	5N-1

Hence, the number of equations is equal to the number of unknowns, therefore the system of equations can be solved.

APPENDIX D

COMPUTER PROGRAM VARIABLES

Symbol	Explanation
M,N	number of grid steps in the X- and Y-directions, respectively
HP,SP	Step sizes in the X- and Y-directions, respectively for the Particle Phase
HF,SF	Step sizes in the X- and Y-directions, respectively for the Fluid Phase.
WP	h, half the channel width
AKNP	K_{np}, particle Knudsen number
THETA	θ, half the converging or diverging angle
ANM	N_m, momentum transfer number
ANR	N_R, Reynolds number
ETA	N_η, gravity flow parameter
ALPHA	N_α, electrostatic charge parameter
BETA	N_β, diffusive Peclet number
SIGMA	σ, sticking probability accounting for electroviscous forces
SIGMAW	σ_w, sticking probability accounting for adhesive forces at the wall
ANS	$\sigma_w N_\lambda$, surface adhesion parameter
SIGMAS	σ_s, slip velocity factor

ALPHA1(I,L)	$\alpha 1_{i,\ell}$, given in Appendix C
ALPHA2(I,L)	$\alpha 2_{i,\ell}$, given in Appendix C
ALPHA3(I,L)	$\alpha 3_{i,\ell}$, given in Appendix C
ALPHA13	$\alpha 13 = \alpha 1_{i,2} + \alpha 3_{i,2}$
F1(I,L)	$F1_{i,\ell}$, given in Appendix C
F2(I,L)	$F2_{i,\ell}$, given in Appendix C
BETA1(I,J)	$\beta 1_{i,j}$, given in Appendix C
BETA2(I,J)	$\beta 2_{i,j}$, given in Appendix C
BETA3(I,J)	$\beta 3_{i,j}$, given in Appendix C
BETA12	$\beta 12 = \beta 1_{i,3} \cdot CK + \beta 2_{i,3}$
BETA23	$\beta 23 = \beta 2_{i,N+1} + \beta_{i,N+1} \cdot CK$
GAMA1(I,J)	$\gamma 1_{i,j}$, given in Appendix C
GAMA2(I,J)	$\gamma 2_{i,j}$, given in Appendix C
ZETA1(I,J)	$\zeta 1_{i,j}$, given in Appendix C
ZETA2(I,J)	$\zeta 2_{i,j}$, given in Appendix C
ZETA3(I,J)	$\zeta 3_{i,j}$, given in Appendix C
ZETA4	$\zeta 4 = 1.0/[1.0-\Delta Y(W_{i,3}/\Delta Y+\sigma N_\beta V_{Pi,2}-N_s+N_\eta)]$
ZETA5	$\zeta 5 = 1.0/[1.0+\Delta Y(\sigma N_\beta V_{Pi,N+2}-N_s+N_\eta)]$
PHI1(I,J)	$\phi 1_{i,j}$, given in Appendix C
PHI2(I,J)	$\phi 2_{i,j}$, given in Appendix C
PHI3(I,J)	$\phi 3_{i,j}$, given in Appendix C
TAU1	$\tau 1 = 1.0/(2.0)(ANM)(BETA)$
TAU2	$\tau 2 = 1.0/(ANM)(BETA)$
PSI	ψ, given in Appendix C
A(II,JJ)	A, matrix of coefficients } of matrix equation AX=B for fluid phase
B(JJ)	B, column vector } of matrix equation AX=B for fluid phase

C(II,JJ)	C, matrix of coefficients } of matrix equation
D(JJ)	D, column vector } CX=D for particle phase
U(IB,J)	$U_{i+1,j}$, axial velocity of fluid phase
P(IB)	P_{i+1}, fluid static pressure
V(IB,J)	$V_{i+1,j}$, normal velocity of fluid phase
UP(IB,J)	$U_{Pi+1,j}$, axial velocity of particle phase
VP(IB,J)	$V_{Pi+1,j}$, normal velocity of particle phase
R(IB,J)	$R_{i+1,j}$, particle concentration
RHOU(IB,J)	$R_{i+1,j}U_{Pi+1,j}$, mass flux of particles in the X direction
RHOV(IB,J)	$R_{i+1,j}V_{Pi+1,j}$, mass flux of particles in the Y direction
W(IB,J)	$W_{i+1,j}$, Electric field potential
E(IB,J)	$E_{i+1,j}$, Electric field intensity
PENET(IB)	$PEN\cdot_{i+1}$, fraction of penetration
DPR1	$\dot{M}1^{*}_{i+1}$, deposition rate of particles on bottom wall
DPR2	$\dot{M}2^{*}_{i+1}$, deposition rate of particles on top wall
DPRT	$\dot{M}^{*}_{i+1} = \dot{M}T^{*}_{i+1}$, total deposition rate

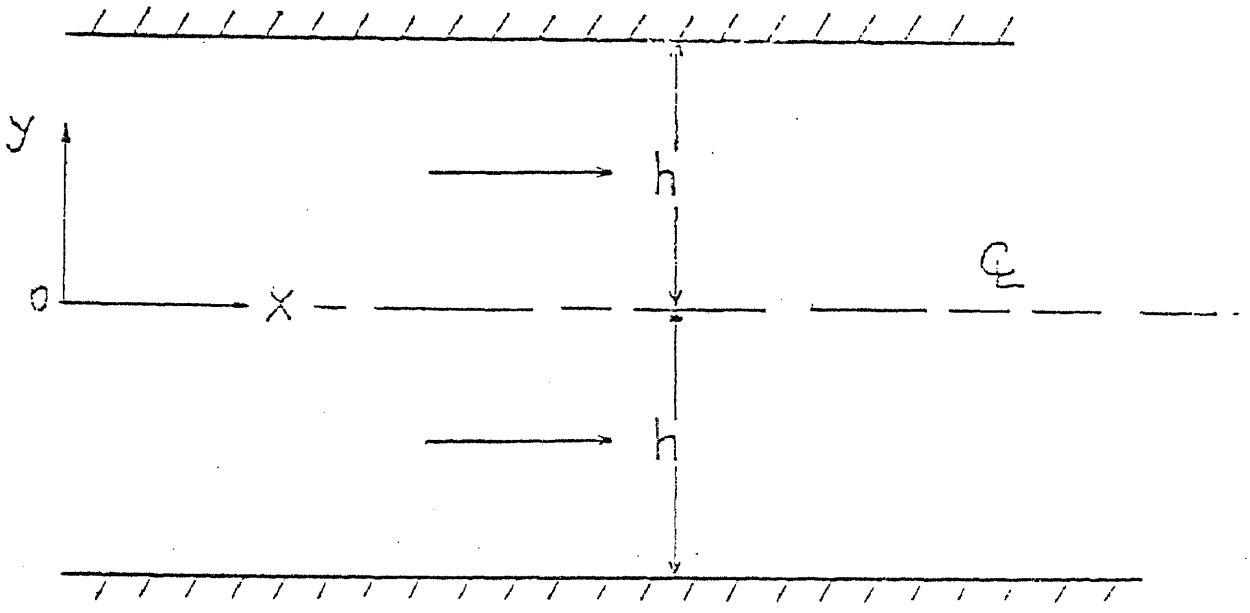

FIG. 3.1 PARALLEL CHANNEL CONFIGURATION

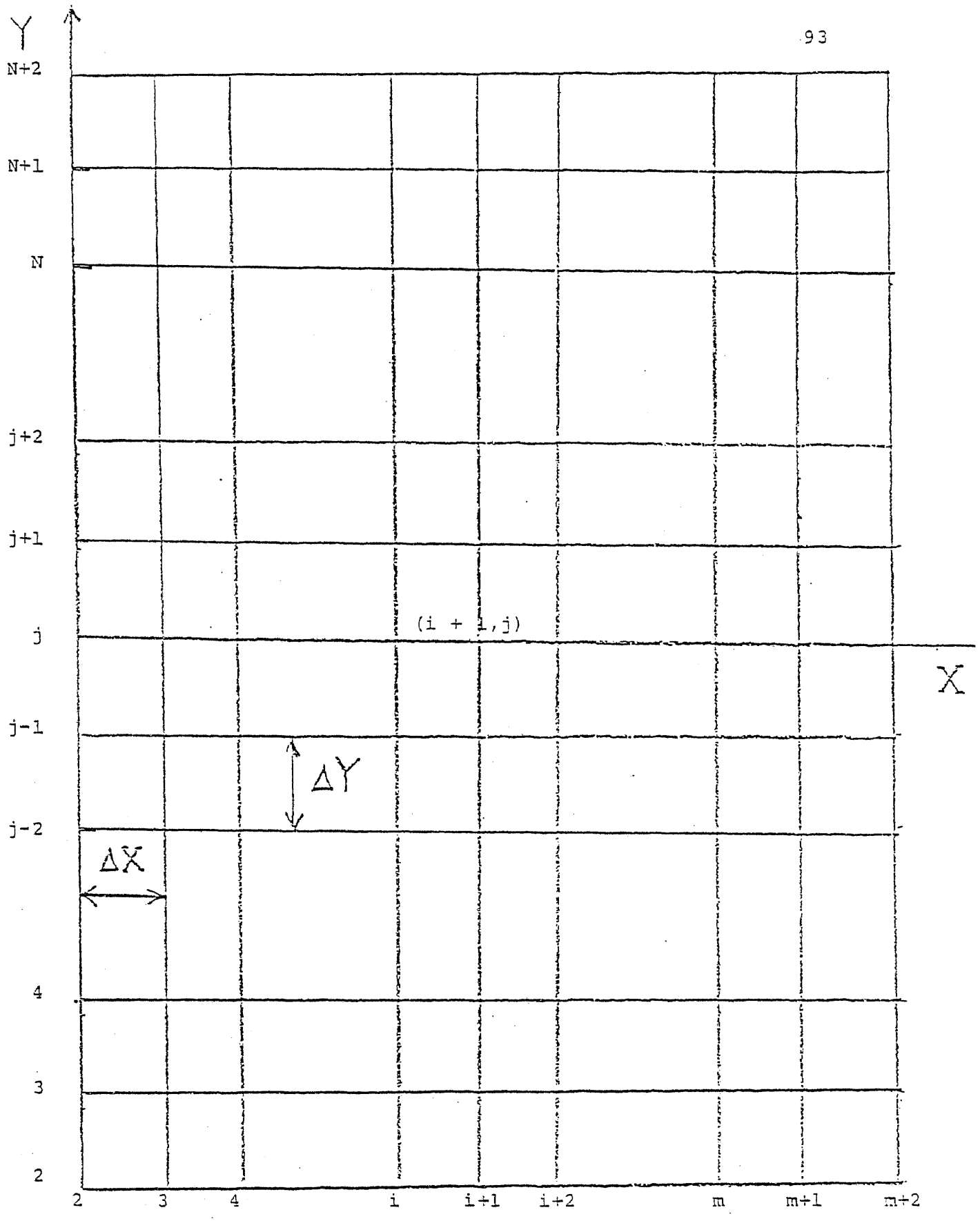

FIG. 3.A FINITE DIFFERENCE GRID SUPERIMPOSED ON PARALLEL CHANNEL FLOW FIELD

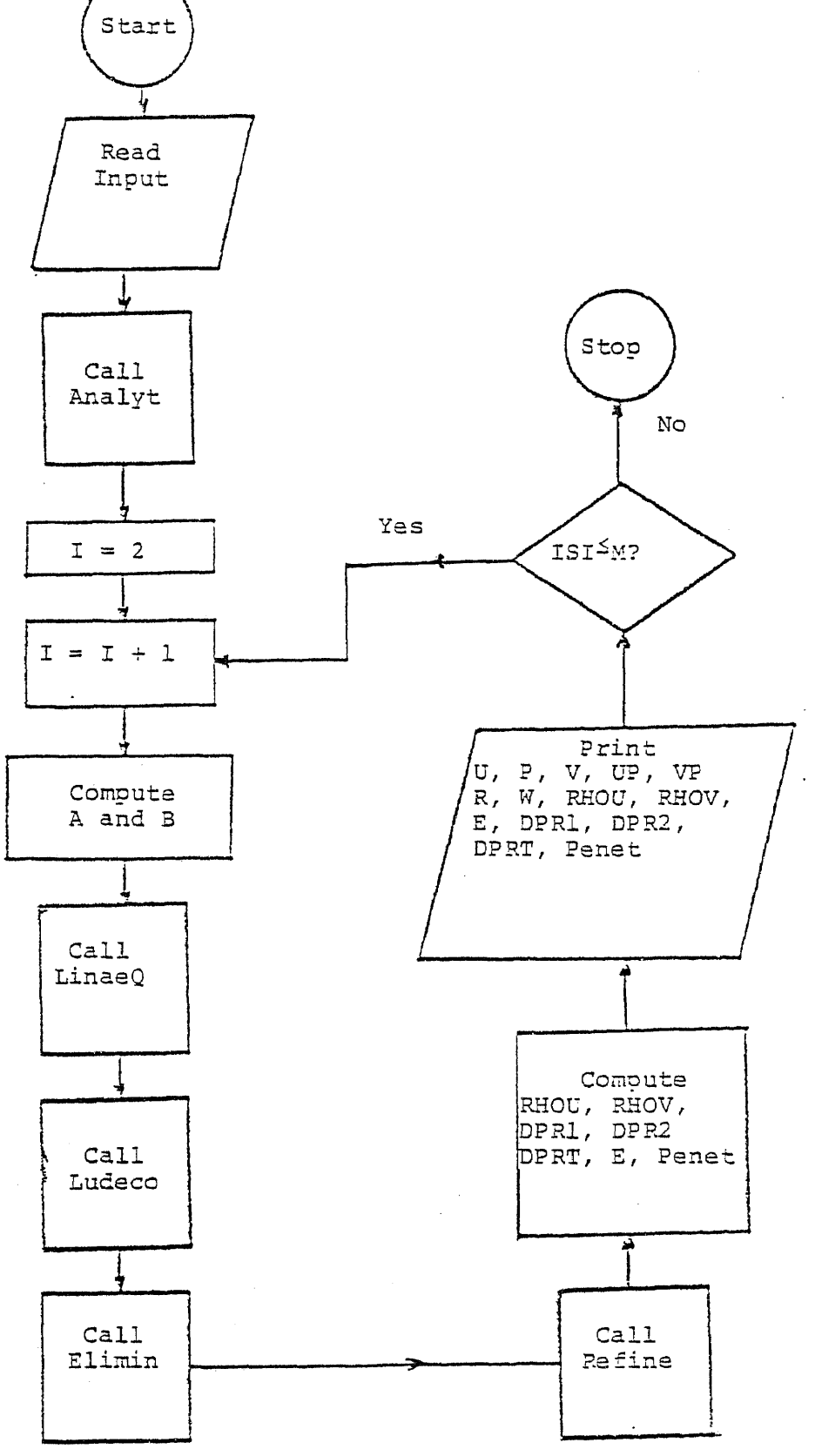

FIG. 3.2 COMPUTER FLOW CHART FOR PARALLEL CHANNEL FLOW

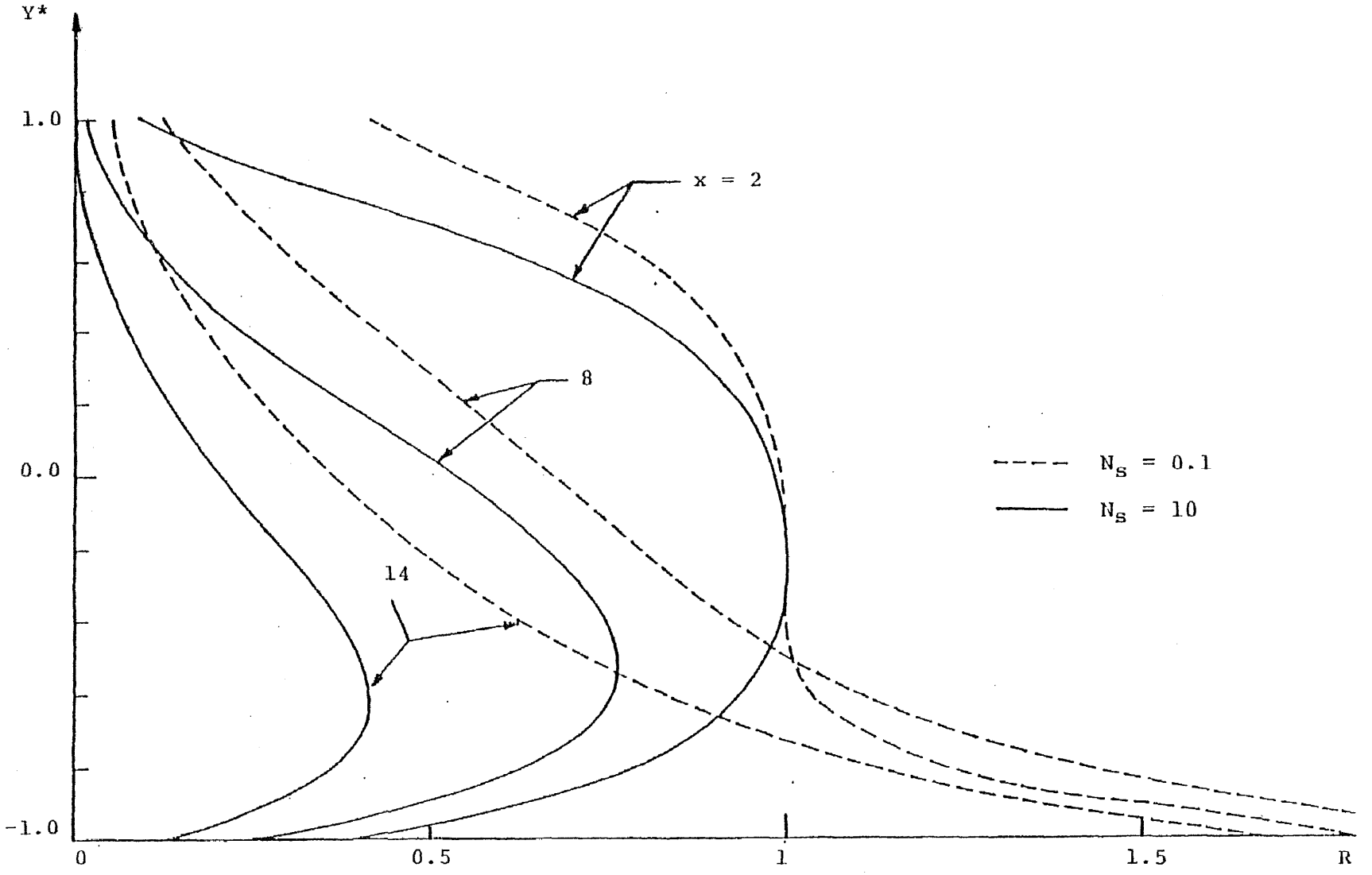

FIG. 3.3 EFFECT OF SURFACE ADHESION ON CONCENTRATION DISTRIBUTION IN A PARALLEL CHANNEL FLOW (K_{np} = 0.0001, N_α = 0, N_η = 4.5, N_β =40, N_m = 2, N_R = 1000, σ = 0.5)

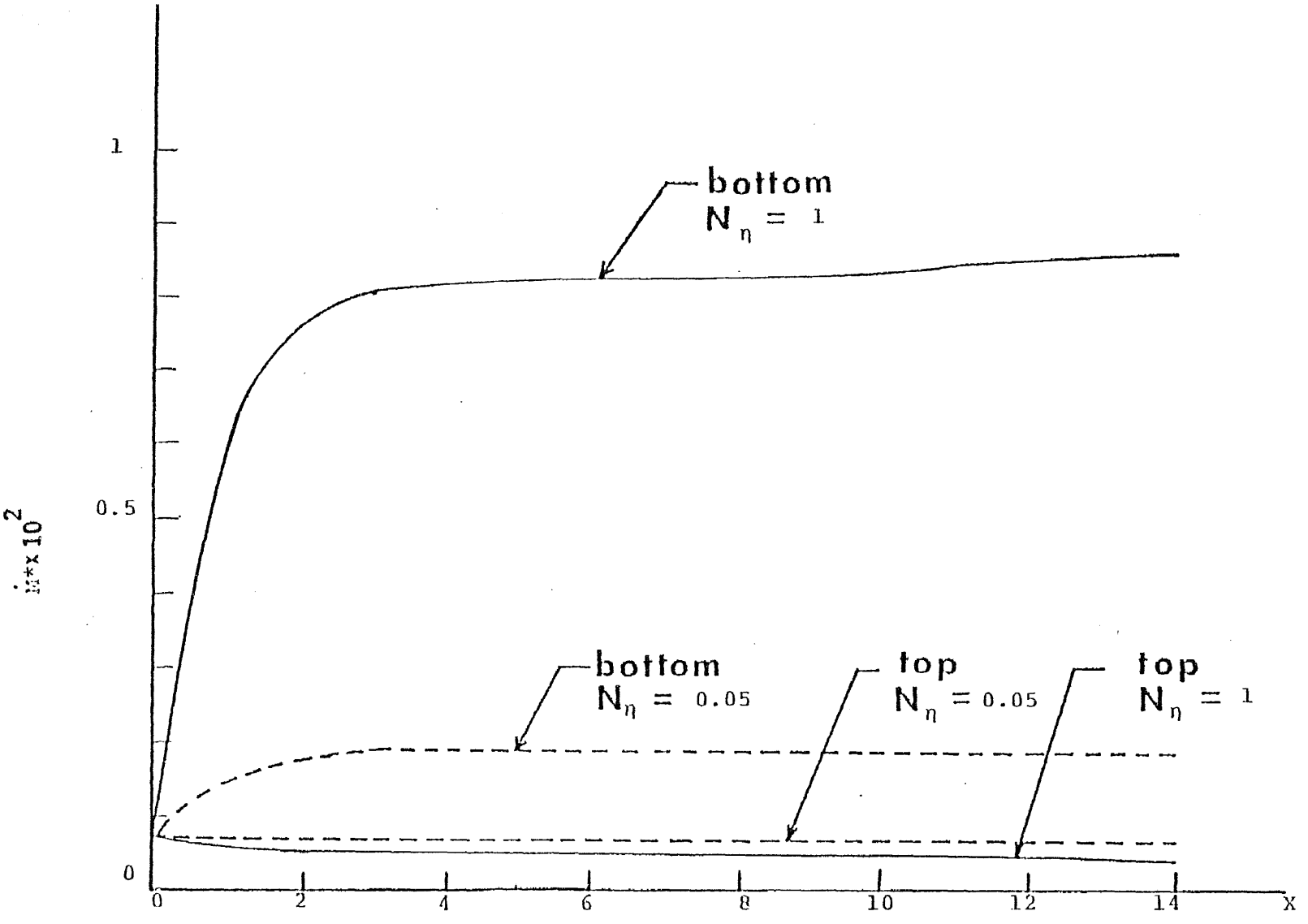

FIG. 3.4 INFLUENCE OF GRAVITY FLOW PARAMETER WITH LOW ADHESION ON DEPOSITION RATE IN A PARALLEL CHANNEL FLOW ($K_{np} = 0.0001$, $N_\alpha = 0$, $N_\beta = 40$, $N_m = 2$, $N_s = 0.05$, $N_R = 1000$, $\sigma = 0.5$)

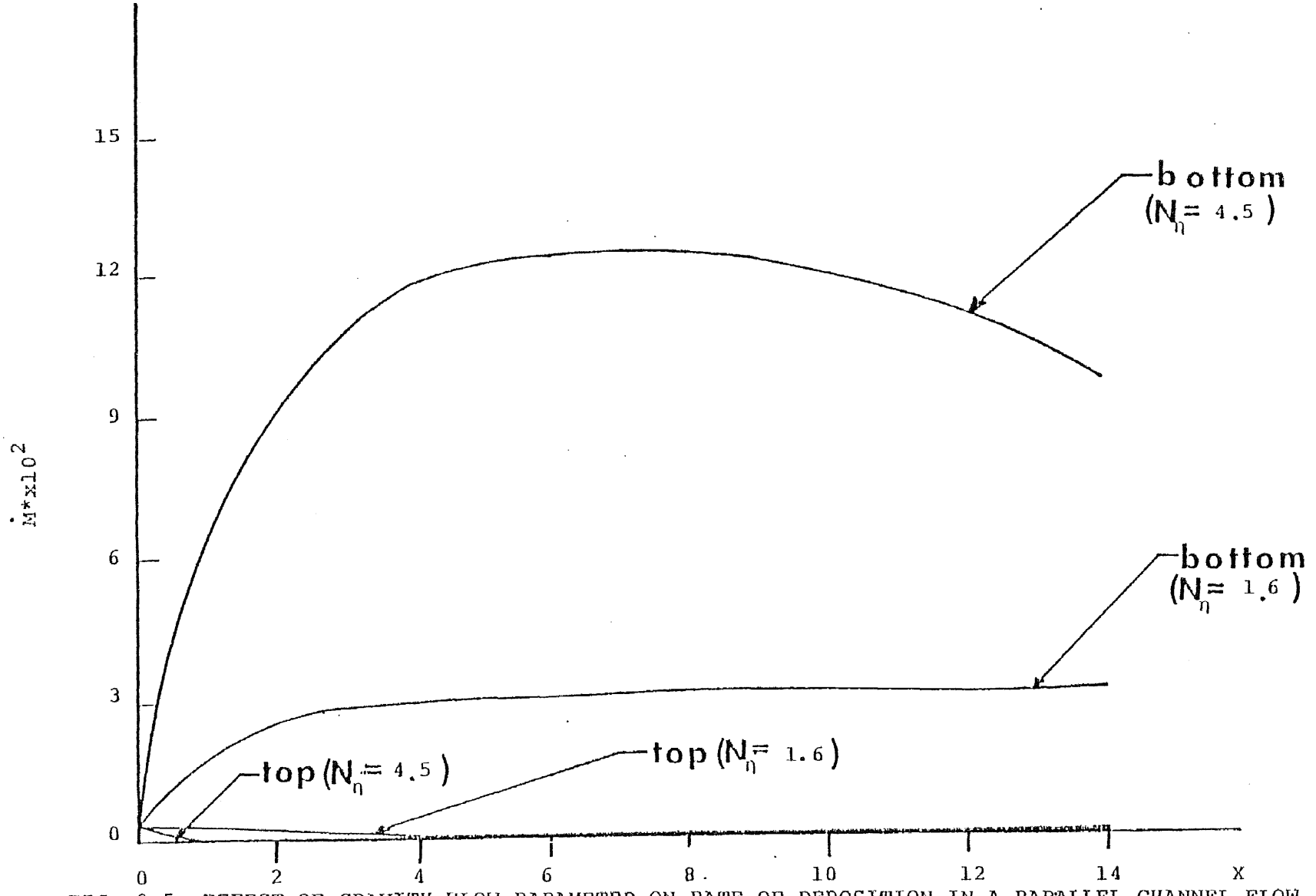

FIG. 3.5 EFFECT OF GRAVITY FLOW PARAMETER ON RATE OF DEPOSITION IN A PARALLEL CHANNEL FLOW

(K_{np} = 0.0001, N_α = 0, N_β = 40, N_m = 2, N_S = 0.1, N_R = 1000, δ = 0.5)

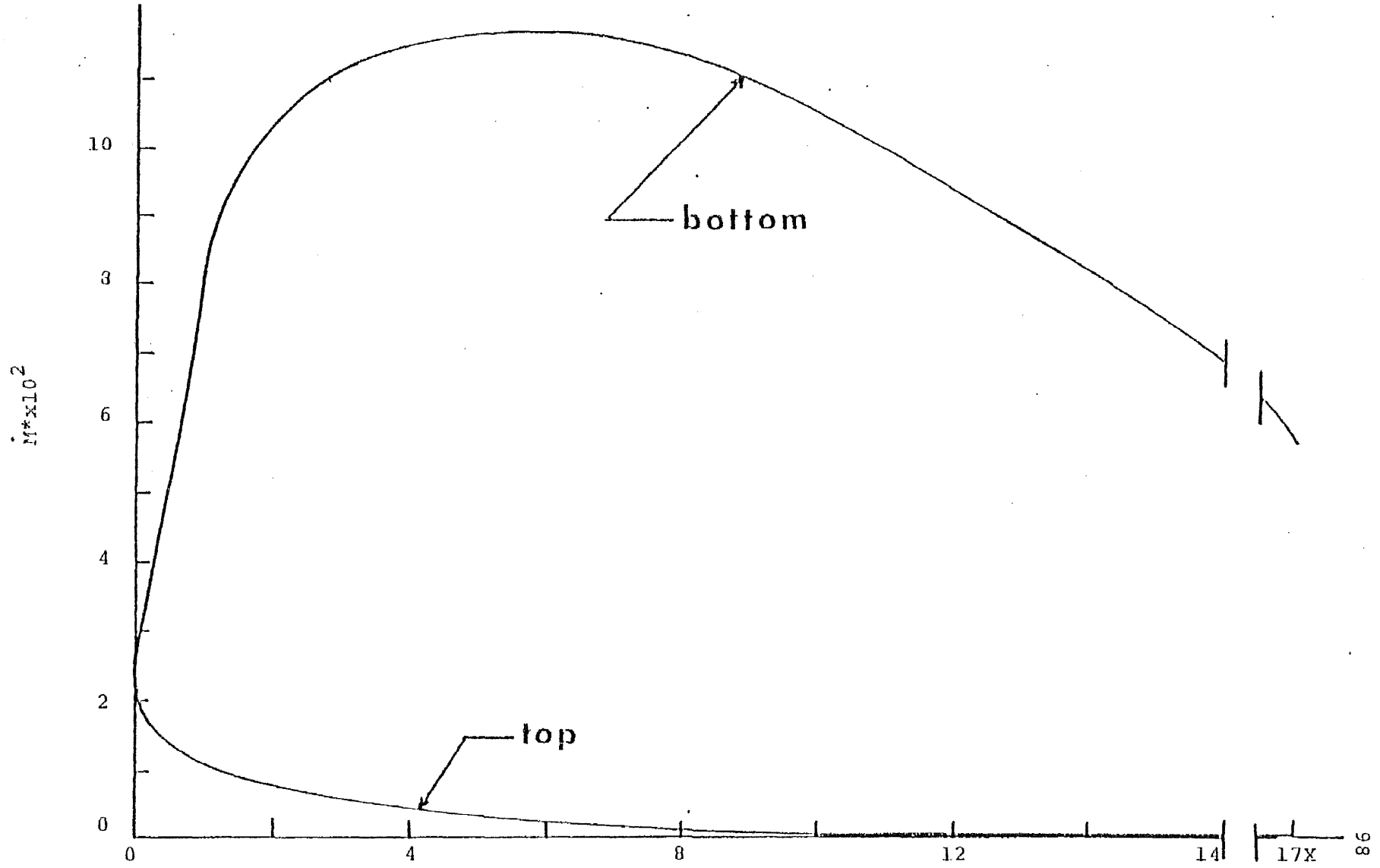

FIG. 3.6 AXIAL DISTRIBUTION OF RATE OF DEPOSITION WITH K_{np} = 0.1 IN A PARALLEL CHANNEL FLOW

(N_α = 0, N_η = 4.5, N_β = 40, N_m = 2, N_s = 1, N_R = 1000, σ = 0.5)

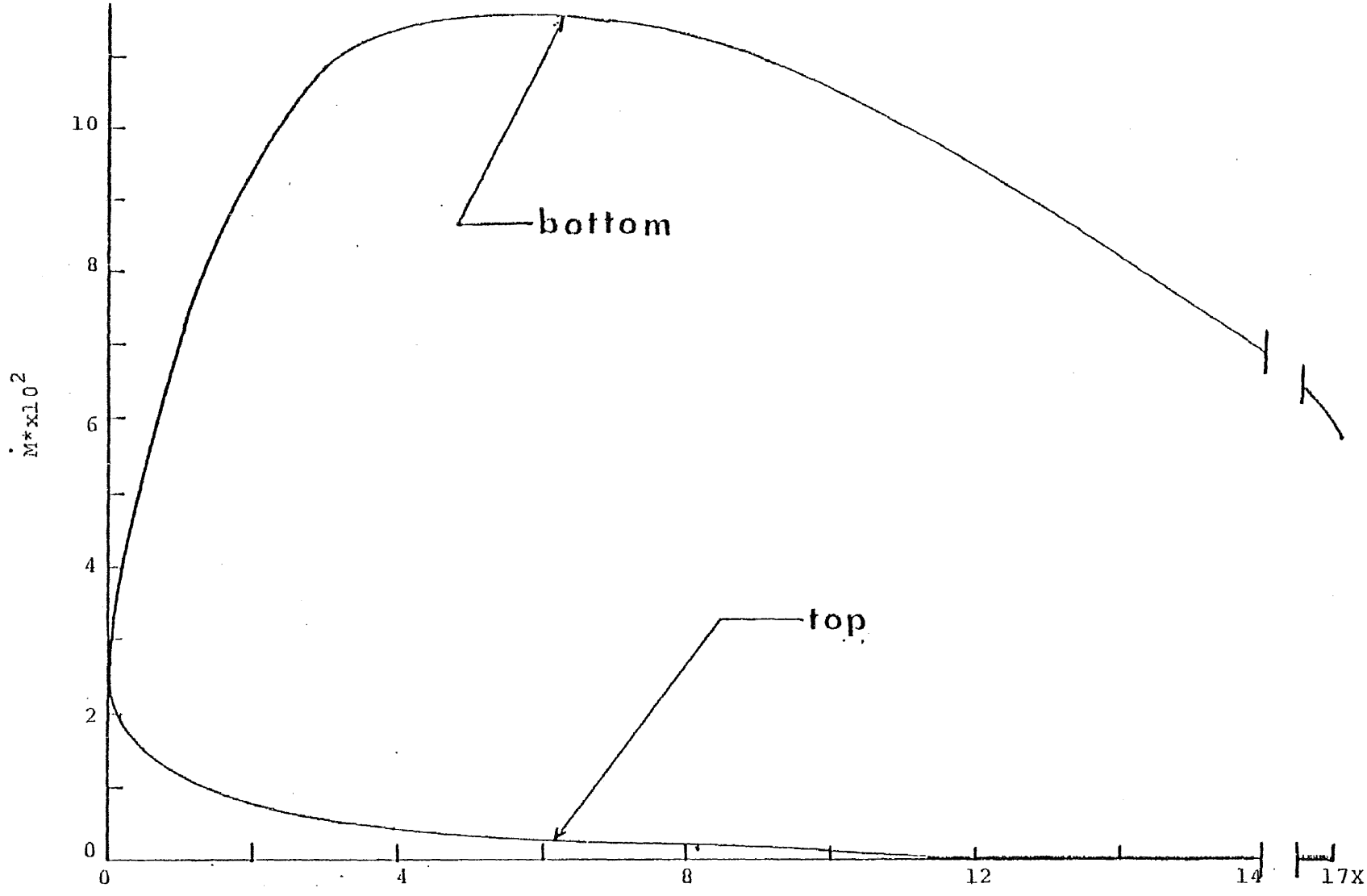

FIG. 3.7 AXIAL DISTRIBUTION OF RATE OF DEPOSITION WITH K_{np} = 0.2 IN A PARALLEL CHANNEL FLOW (N_α = 0, N_η = 4.5, N_β = 40, N_m = 2, N_s = 1, N_R = 1000, σ = 0.5)

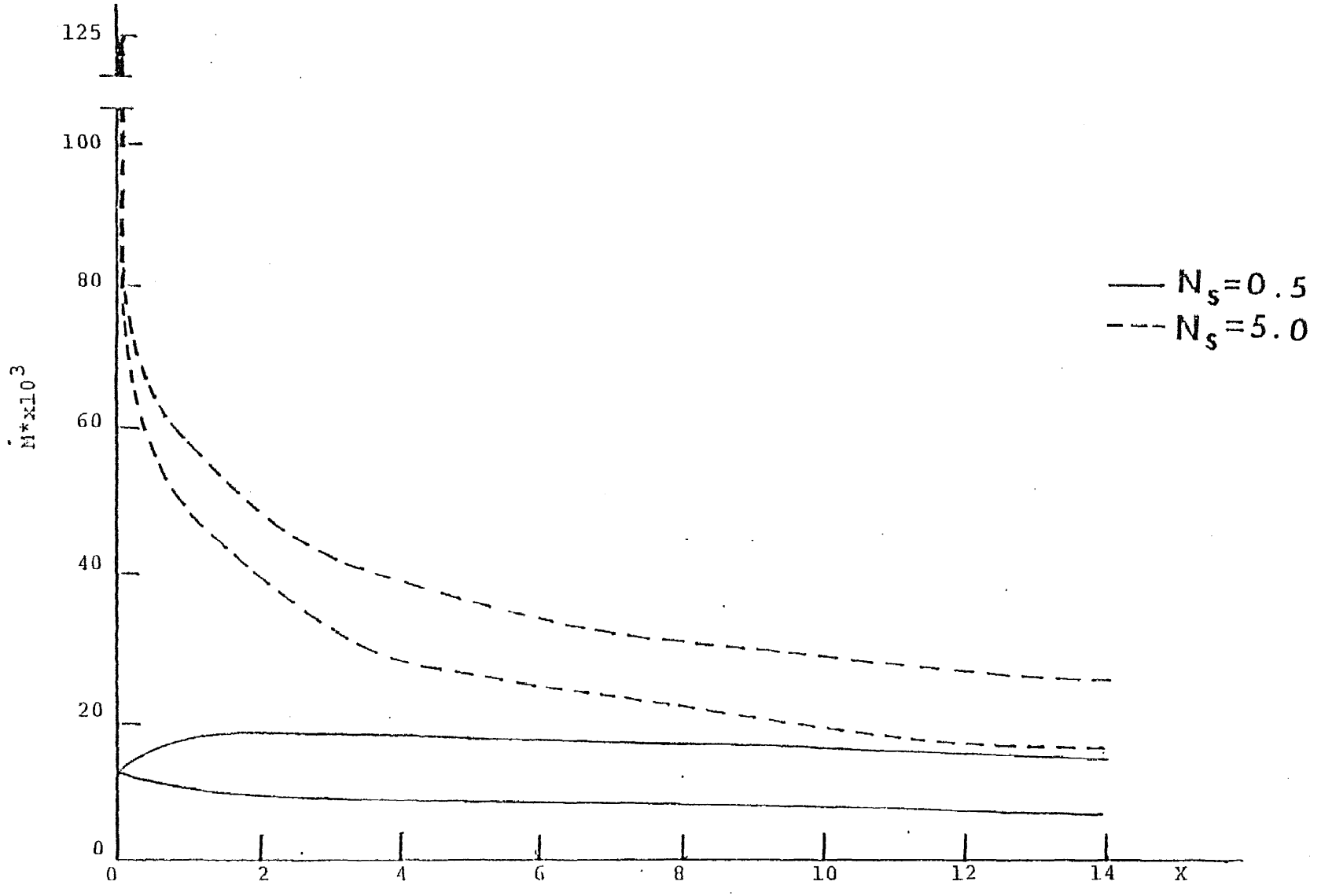

FIG. 3.8 INFLUENCE OF SURFACE ADHESION ON DEPOSITION RATE IN A PARALLEL CHANNEL FLOW

(K_{np} = 0.0001, N_α = 0, N_η = 1, N_β = 40, N_m = 2, N_R = 1000, σ = 0.5)

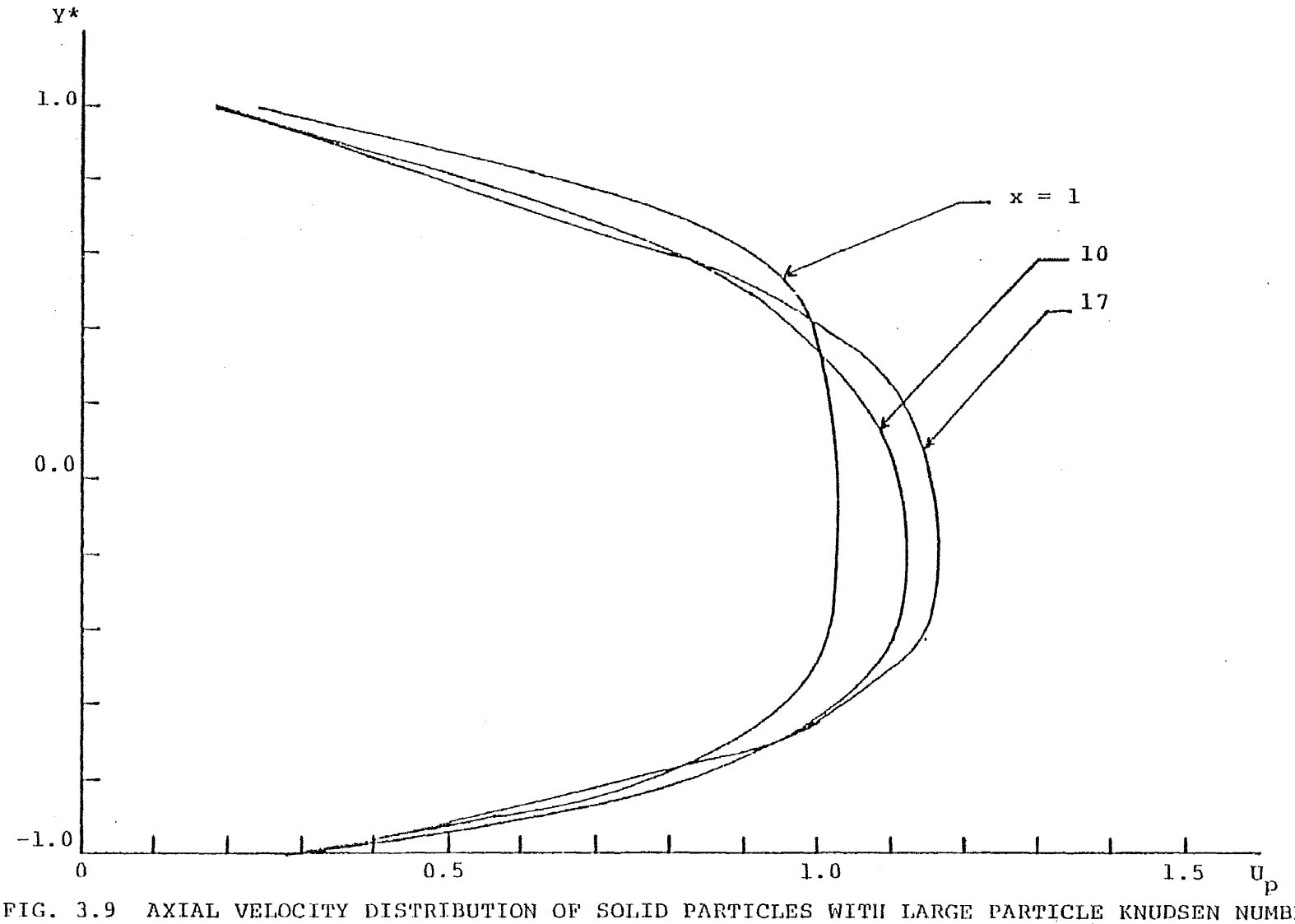

FIG. 3.9 AXIAL VELOCITY DISTRIBUTION OF SOLID PARTICLES WITH LARGE PARTICLE KNUDSEN NUMBER IN A PARALLEL CHANNEL FLOW (K_{np} = 0.1, N_α = 0, N_η = 4.5, N_β = 40, N_s = 1, N_m = 2, N_R = 1000, σ = 0.5)

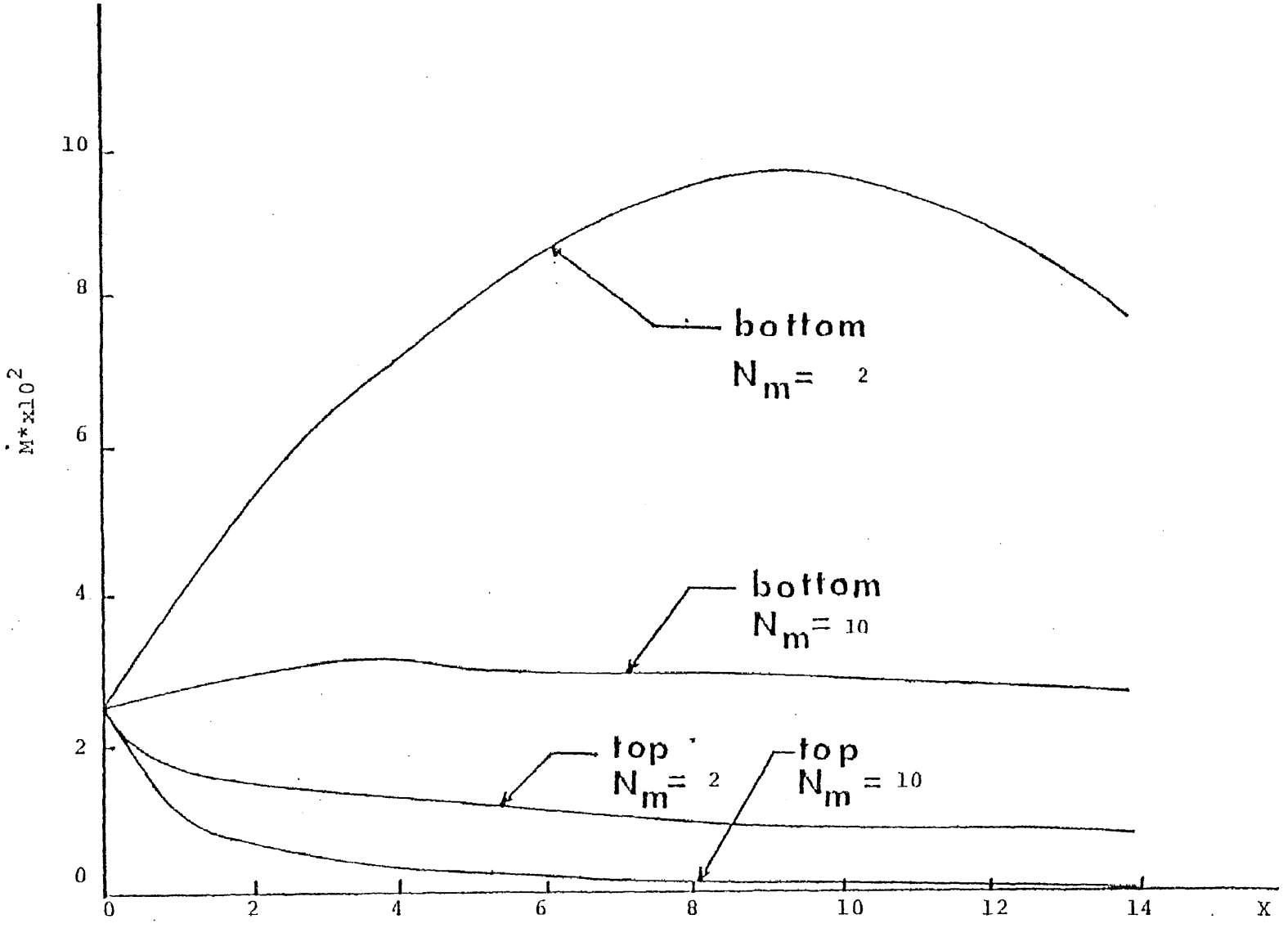

FIG. 3.10 EFFECT OF MOMENTUM TRANSFER NUMBER ON RATE OF DEPOSITION IN A PARALLEL CHANNEL FLOW (K_{np} = 0.0001, N_α = 0, N_η = 1, N_β = 40, N_S = 1, N_R = 1000, σ = 0.5)

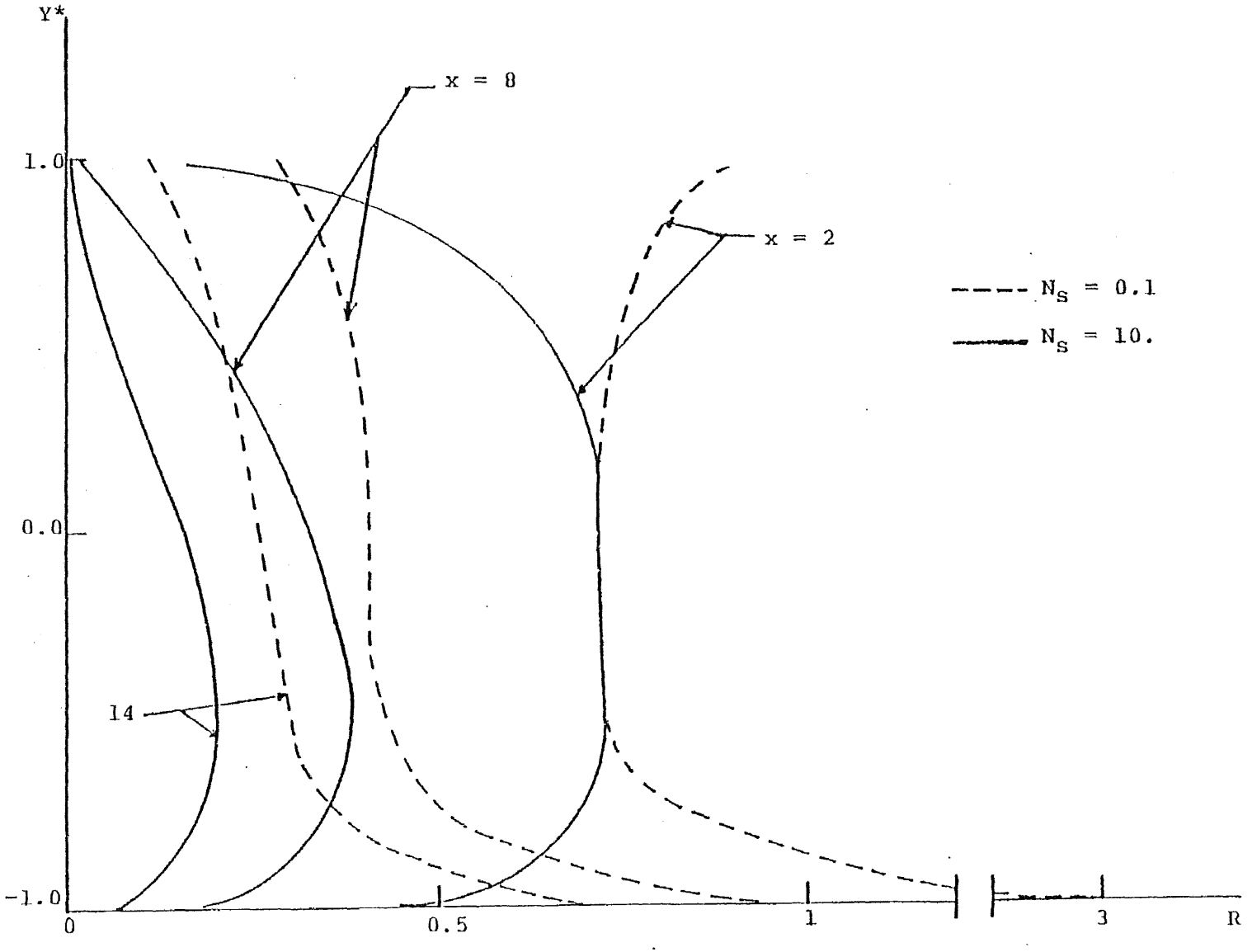

FIG. 3.11 AXIAL DISTRIBUTION OF PARTICLE CONCENTRATION WITH SURFACE ADHESION EFFECT IN A PARALLEL CHANNEL FLOW (K_{np} = 0.0001, N_α = 2, N_η = 4.5, N_β = 40, N_m = 2, N_R = 1000, σ = 0.5)

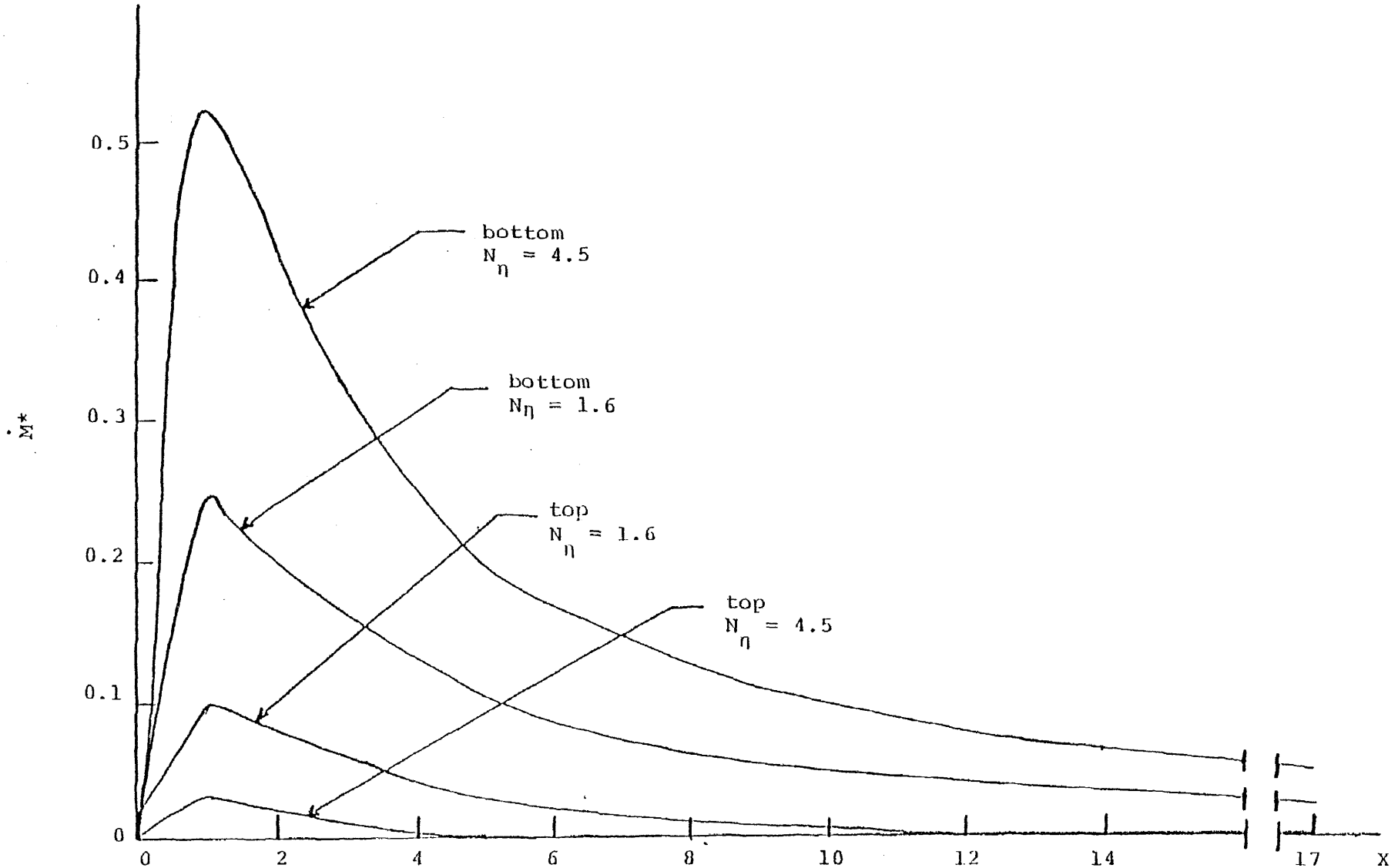

FIG. 3.12 AXIAL DISTRIBUTION OF RATE OF DEPOSITION WITH GRAVITY EFFECT IN A PARALLEL CHANNEL FLOW ($K_{np} = 0.0001$, $N_\alpha = 2$, $N_\beta = 40$, $N_m = 2$, $N_s = 0.1$, $N_R = 1000$, $\sigma = 0.5$)

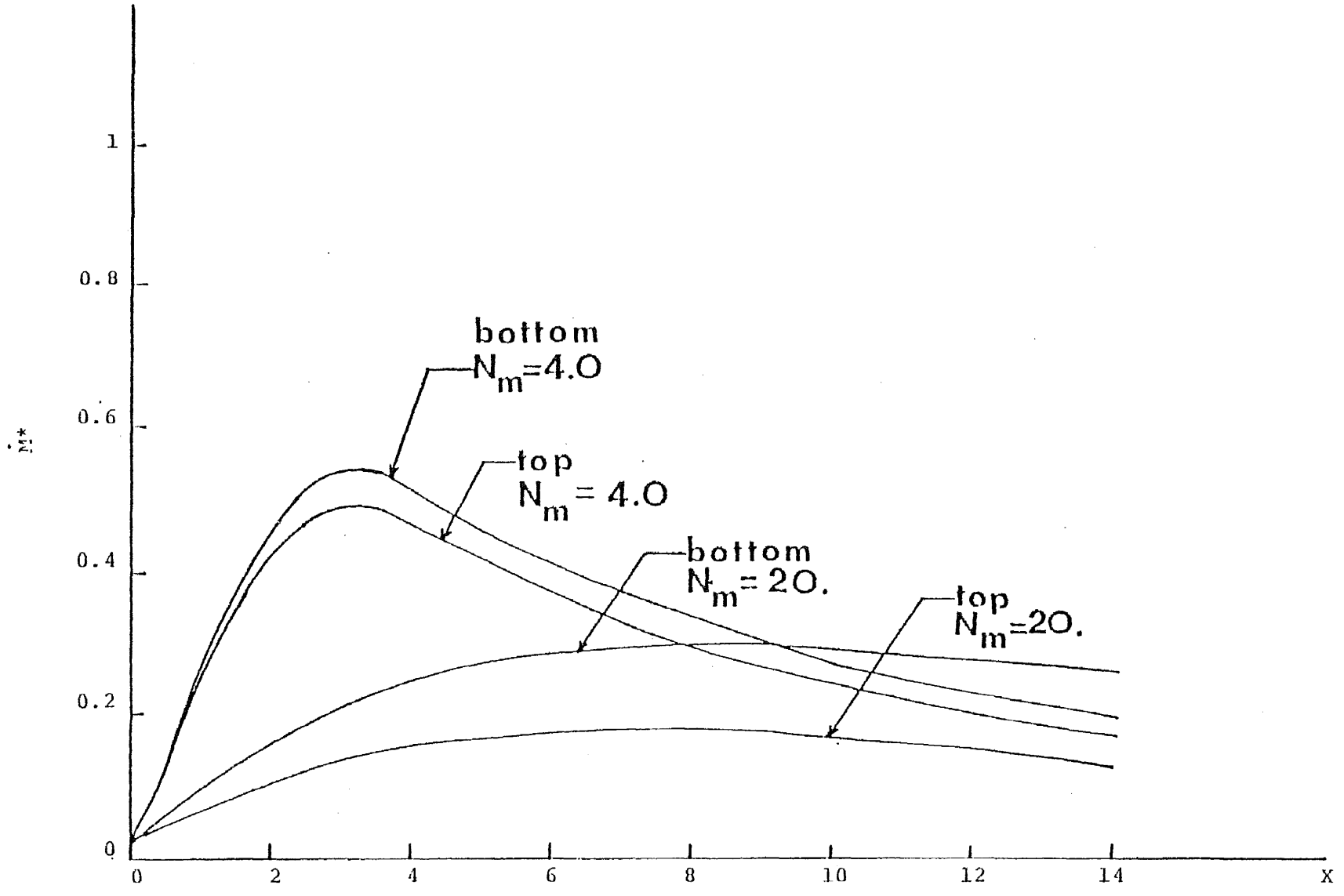

FIG. 3.13 INFLUENCE OF MOMENTUM TRANSFER NUMBER ON DEPOSITION RATE IN A PARALLEL CHANNEL FLOW (K_{np} = 0.0001, N_α = 1, N_η = 0.05, N_β = 40, N_S = 0.1, N_R = 1000, σ = 0.5)

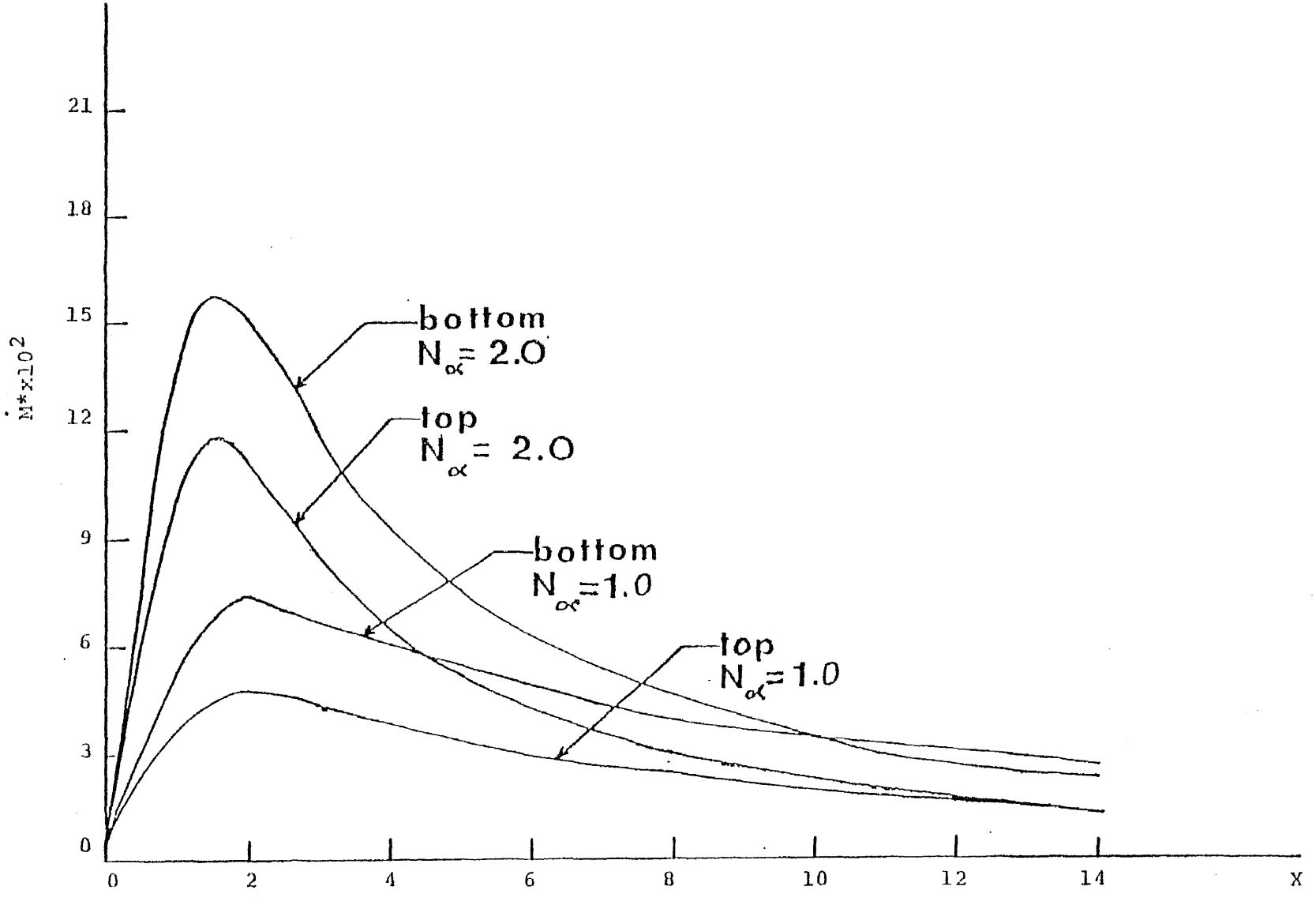

FIG. 3.14 EFFECT OF ELECTROSTATIC CHARGE PARAMETER ON DEPOSITION RATE IN A PARALLEL CHANNEL FLOW (K_{np} = 0.0001, N_η = 1, N_β = 40, N_m = 2, N_s = 0.1, N_R = 1000, σ = 0.5)

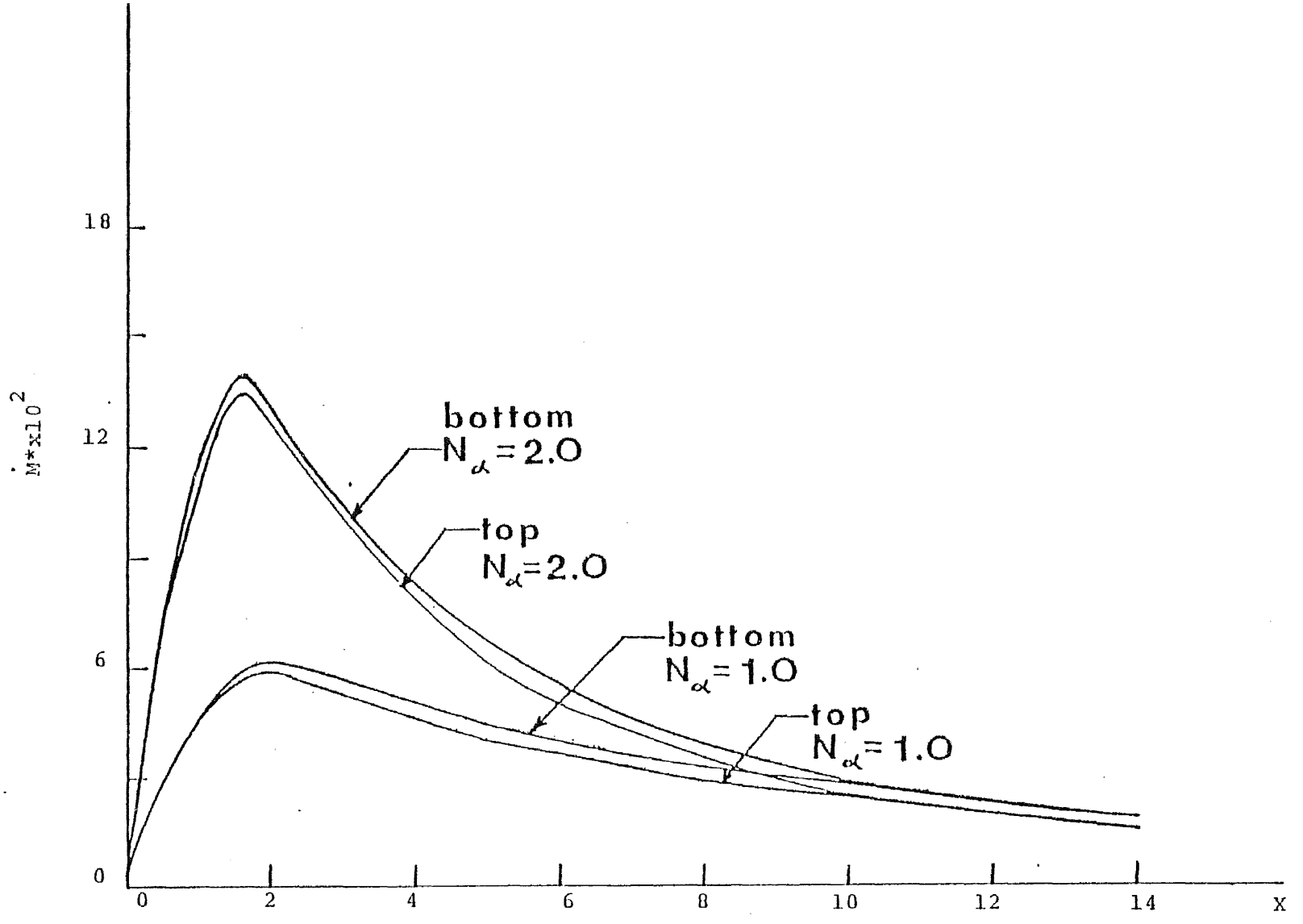

FIG. 3.15 EFFECT OF ELECTROSTATIC CHARGE PARAMETER ON DEPOSITION RATE WITH LOW GRAVITY IN A PARALLEL CHANNEL FLOW (K_{np} = 0.0001, N_η = 0.05, N_β = 40, N_m = 2, N_s = 0.1, N_R = 1000, σ = 0.5)

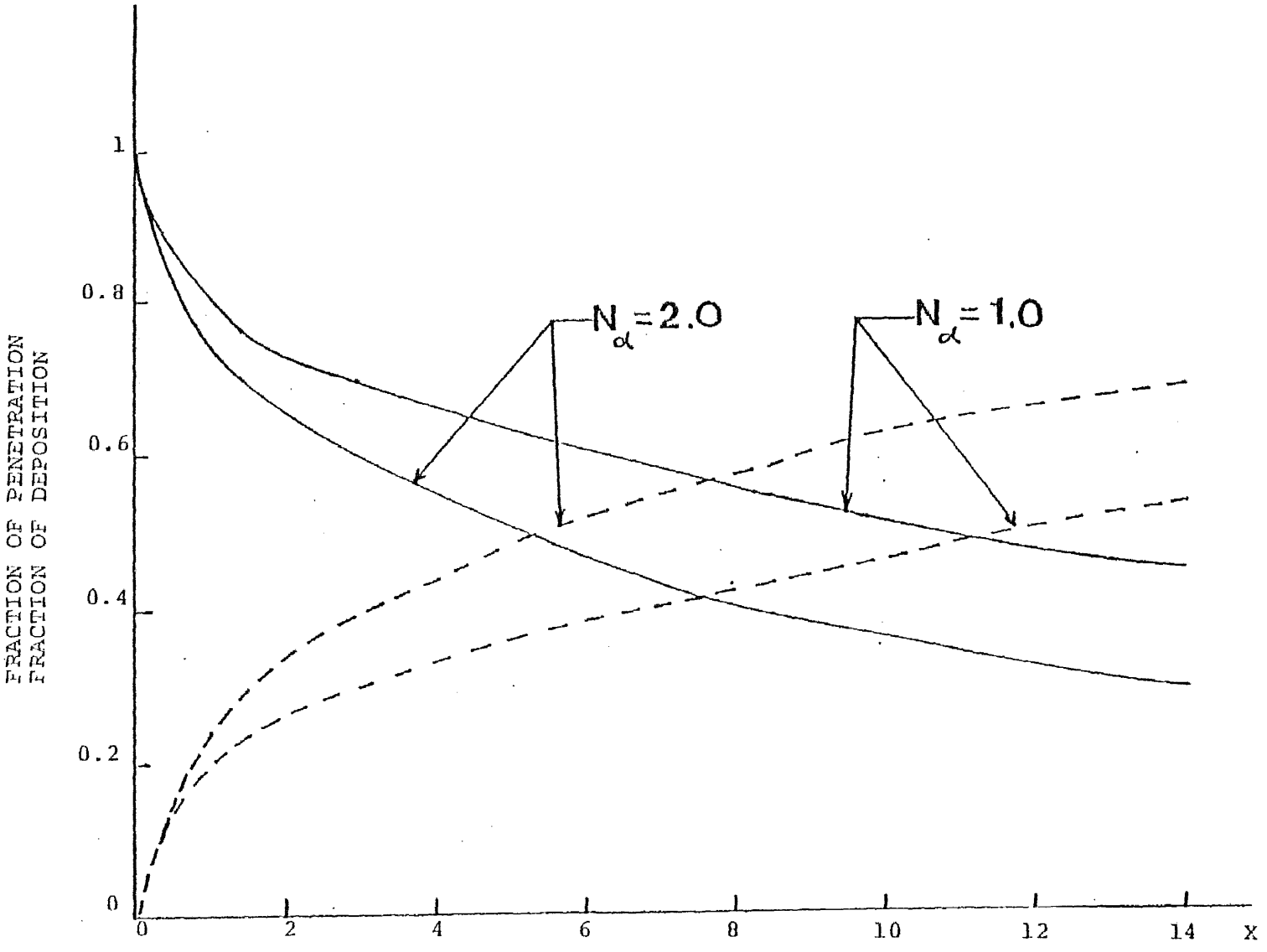

FIG. 3.16 EFFECT OF ELECTROSTATIC CHARGE PARAMETER ON FRACTION OF PENETRATION AND DEPOSITION IN A PARALLEL CHANNEL FLOW (K_{np} = 0.0001, N_η = 1, N_β = 40, N_m = 2, N_S = 0.1, N_R = 1000, σ = 0.5)

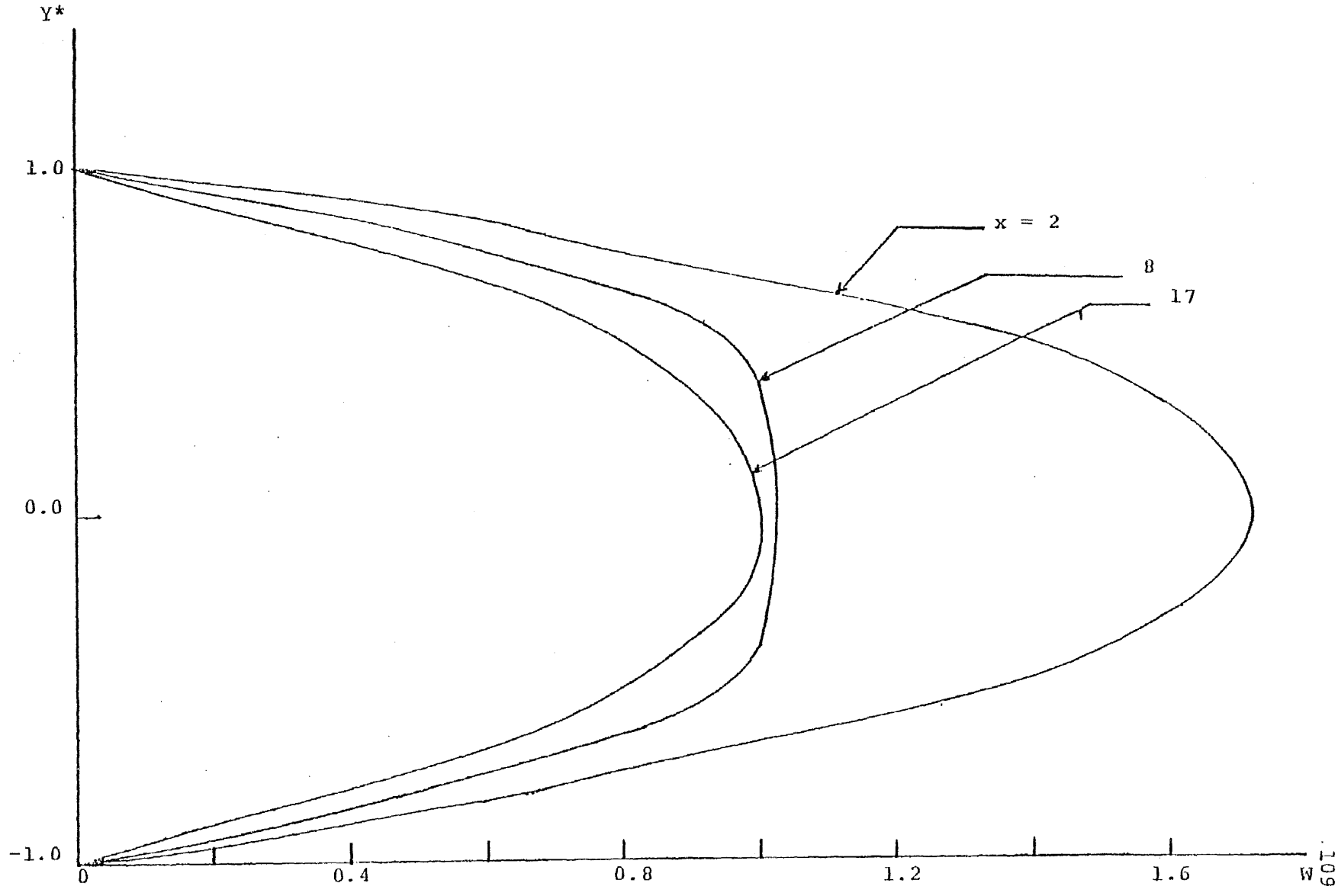

FIG. 3.17 AXIAL DISTRIBUTION OF ELECTROSTATIC POTENTIAL WHEN $N_\alpha = 1$ IN A PARALLEL CHANNEL FLOW ($K_{np} = 0.0001$, $N_\eta = 1$, $N_\beta = 40$, $N_m = 2$, $N_s = 0.1$, $N_R = 1000$, $\sigma = 0.5$)

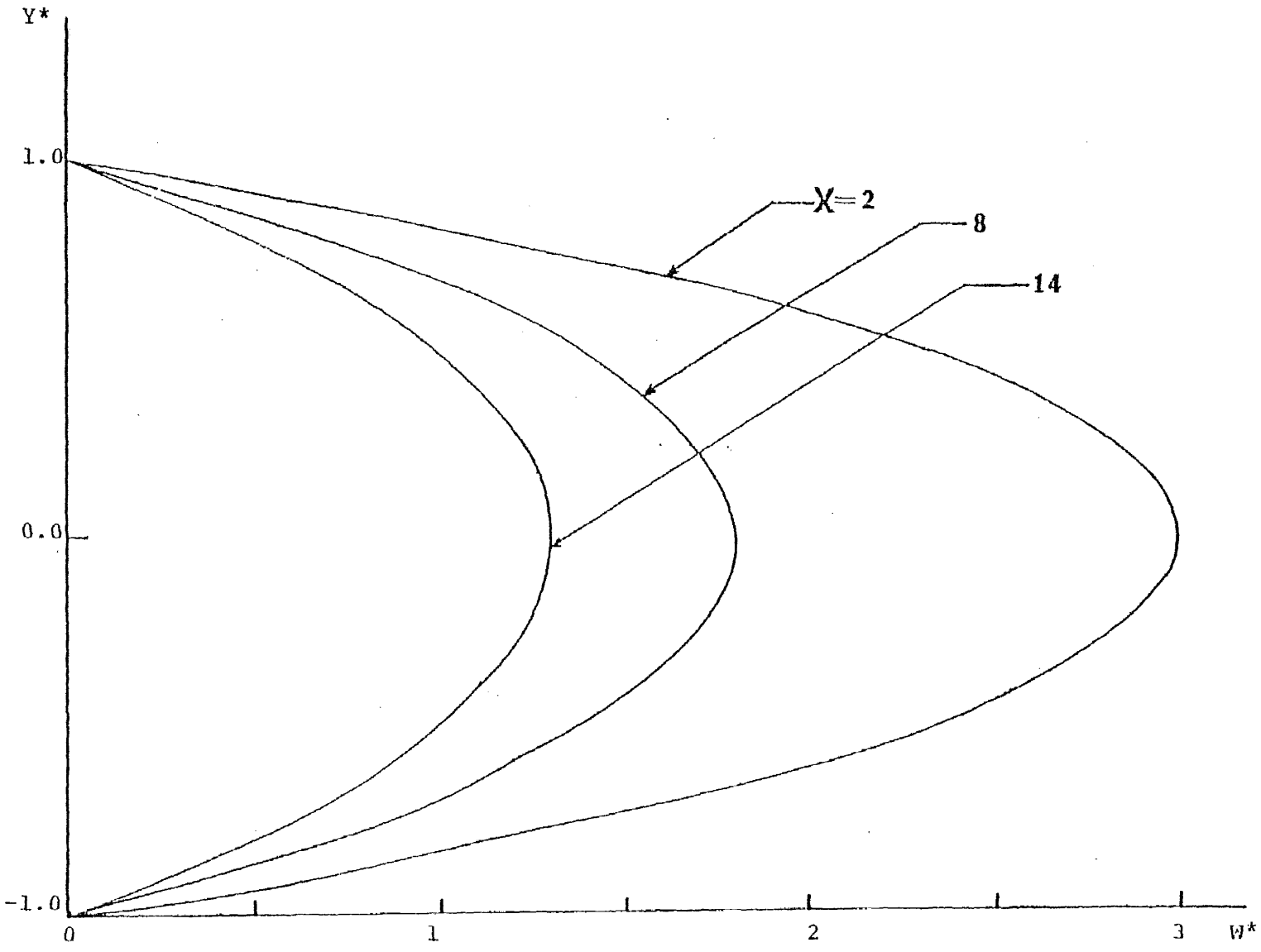

FIG. 3.18 AXIAL DISTRIBUTION OF ELECTROSTATIC POTENTIAL WITH N_α = 2 IN A PARALLEL CHANNEL FLOW (N_η = 1, N_β = 40, N_m = 2, N_s = 0.1, N_R = 1000, σ = 0.5, K_{np} = 0.0001)

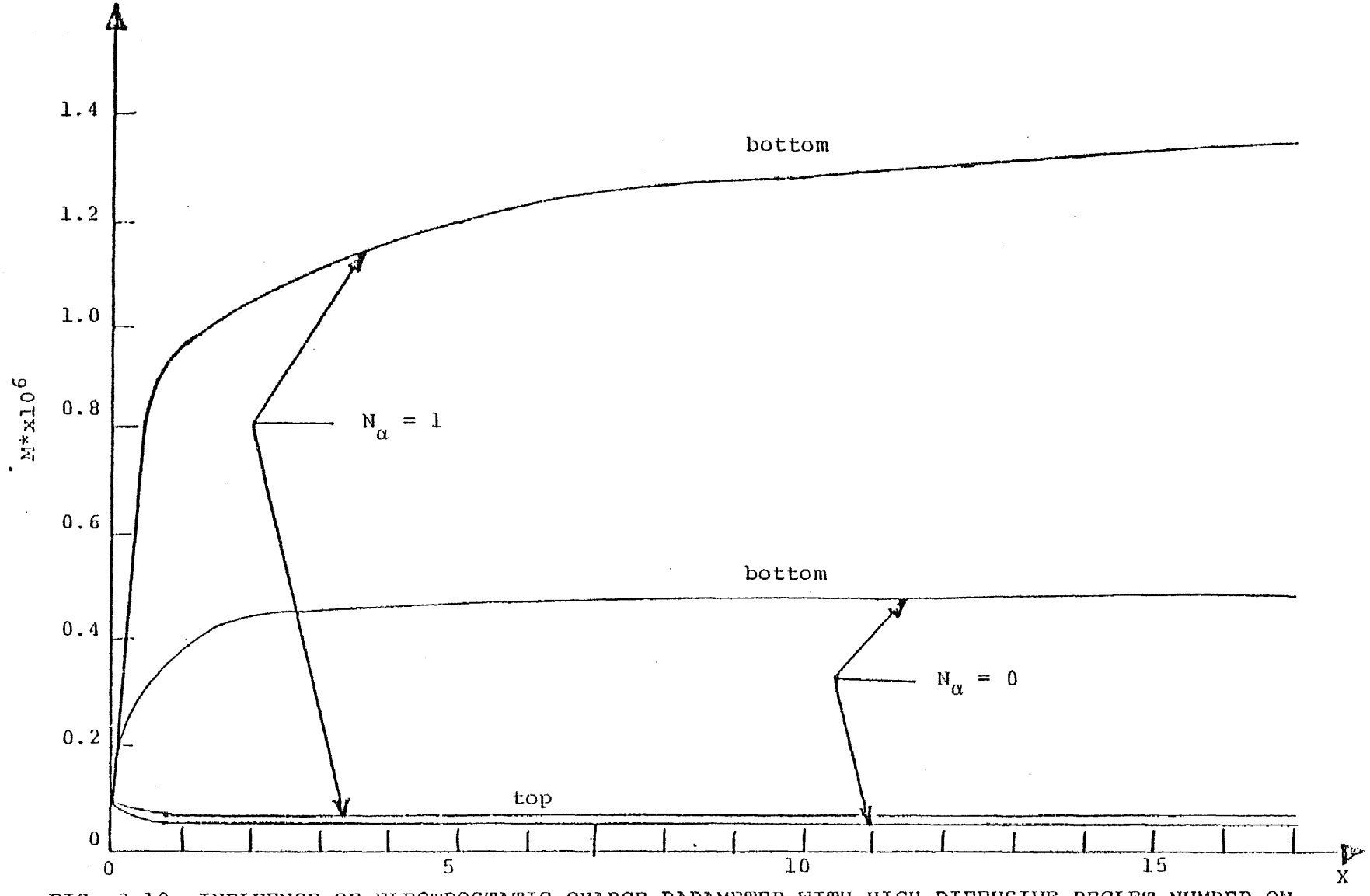

FIG. 3.19 INFLUENCE OF ELECTROSTATIC CHARGE PARAMETER WITH HIGH DIFFUSIVE PECLET NUMBER ON DEPOSITION RATE IN A PARALLEL CHANNEL FLOW ($K_{np} = 0.0001$, $N_\eta = 5$, $N_\beta = 10^7$, $N_m = N_s = 1$, $N_R = 1000$, $\sigma = 0.5$)

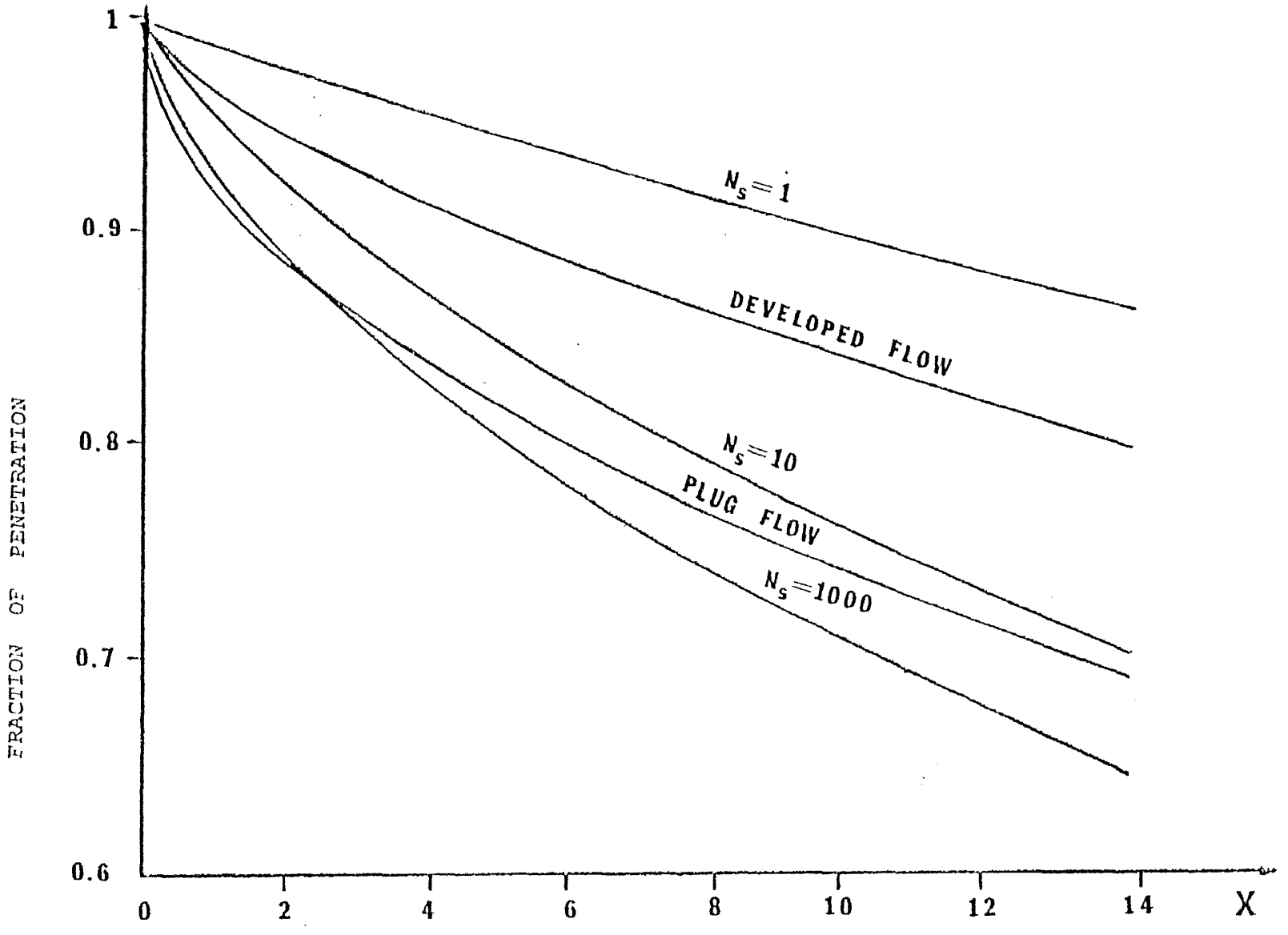

FIG. 3.20 AXIAL DISTRIBUTION OF THE FRACTION OF PENETRATION IN COMPARISON WITH FULLY DEVELOPED AND PLUG FLOWS IN A PARALLEL CHANNEL (N_η =], N_β = 100, N_α = 0, K_{np} = 0.0001, σ = 0.5)

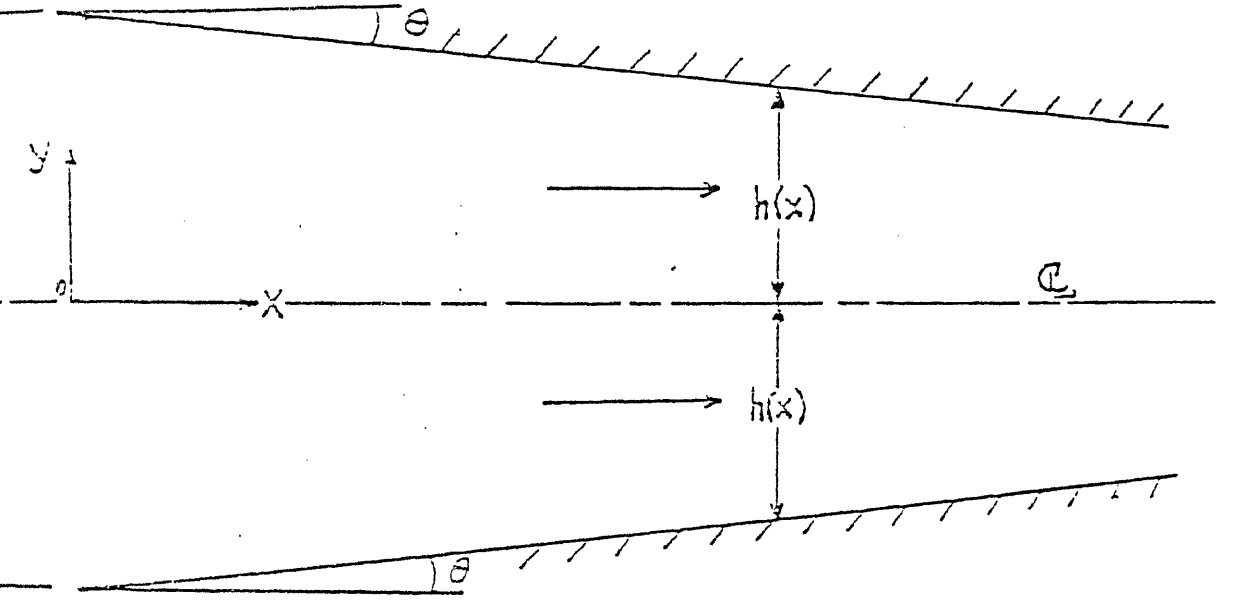

FIG. 4.1 CONVERGING CHANNEL CONFIGURATION

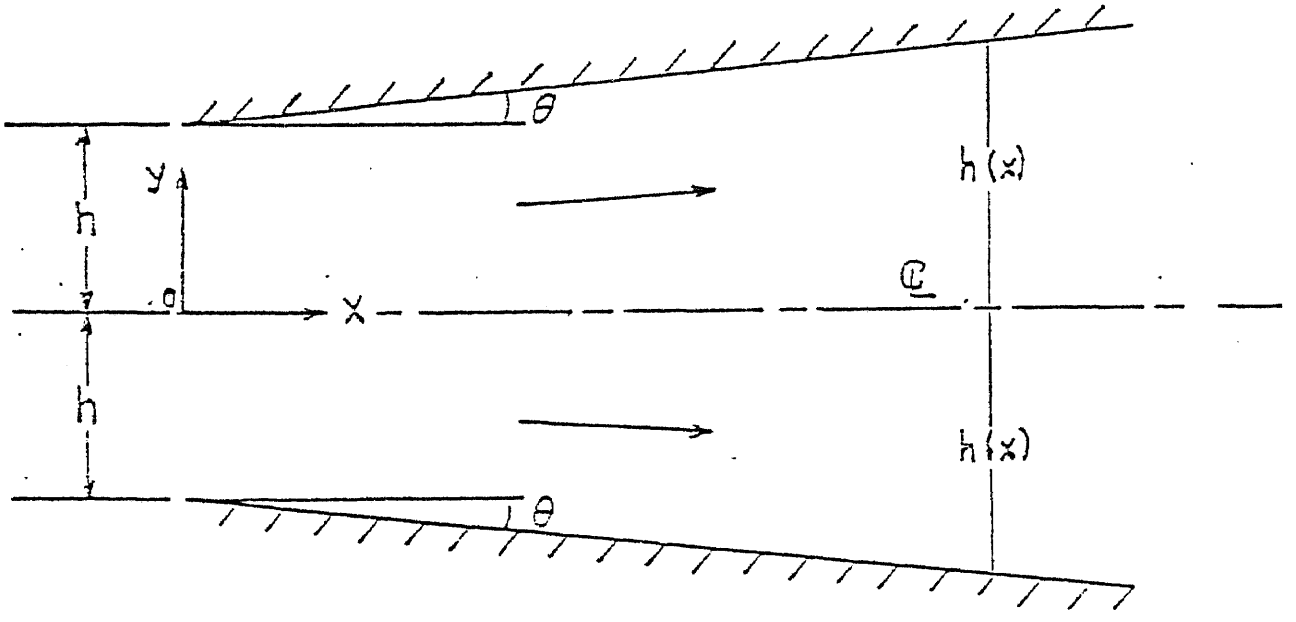

FIG. 4.2 DIVERGING CHANNEL CONFIGURATION

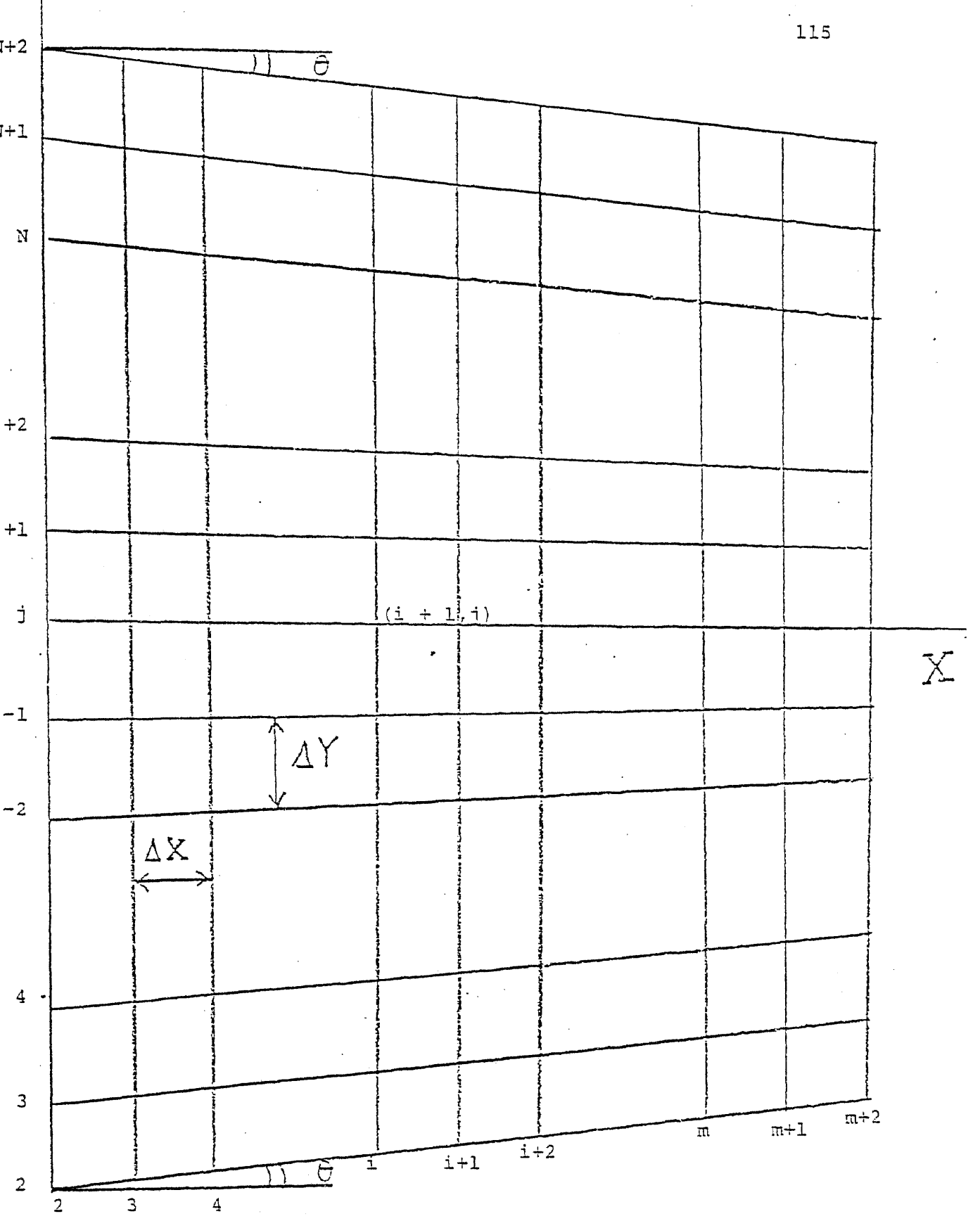

FIG. 4.A FINITE DIFFERENCE GRID SUPERIMPOSED ON CONVERGING CHANNEL FLOW FIELD

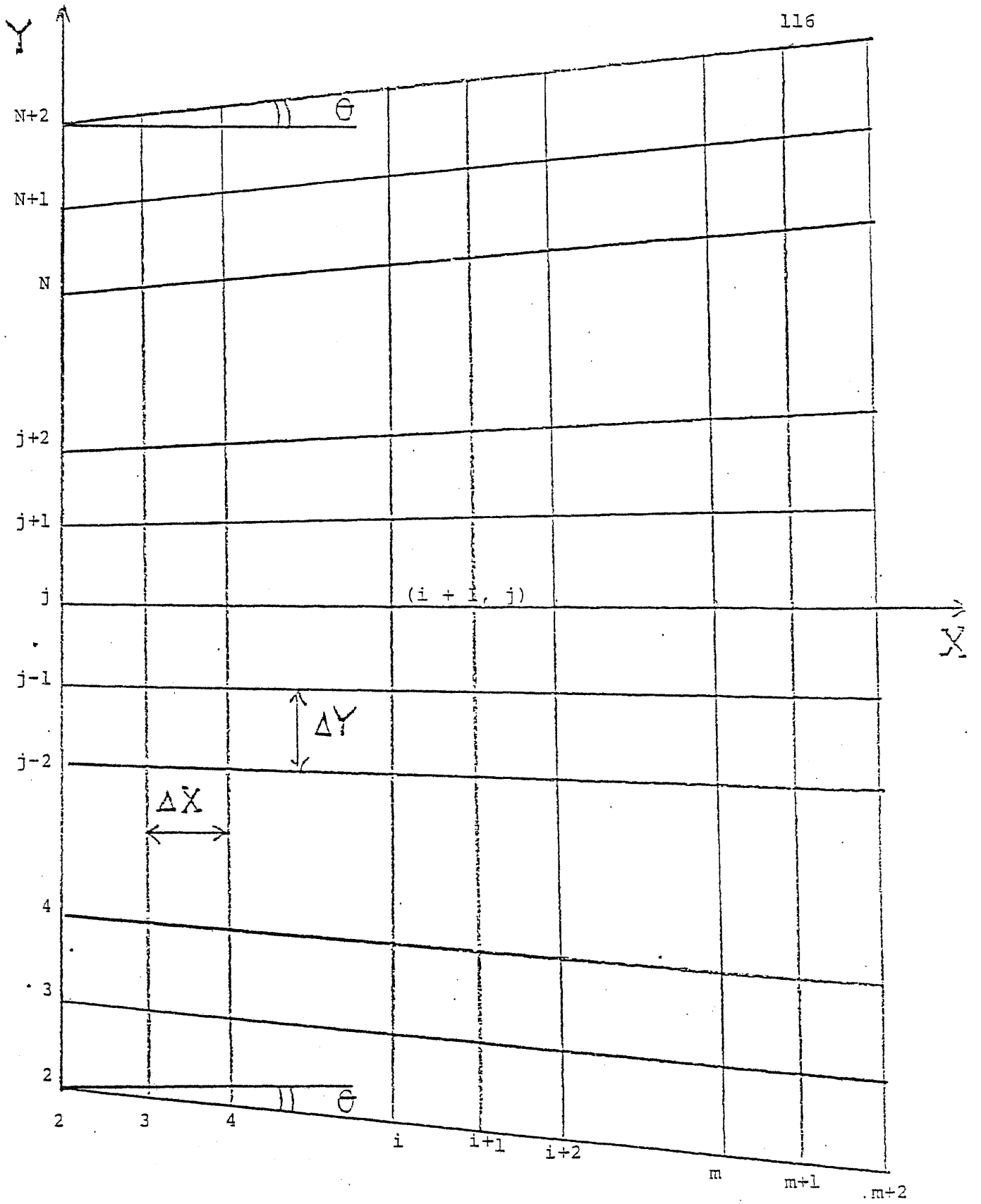

FIG. 4.B FINITE DIFFERENCE GRID SUPERIMPOSED ON DIVERGING CHANNEL FLOW FIELD

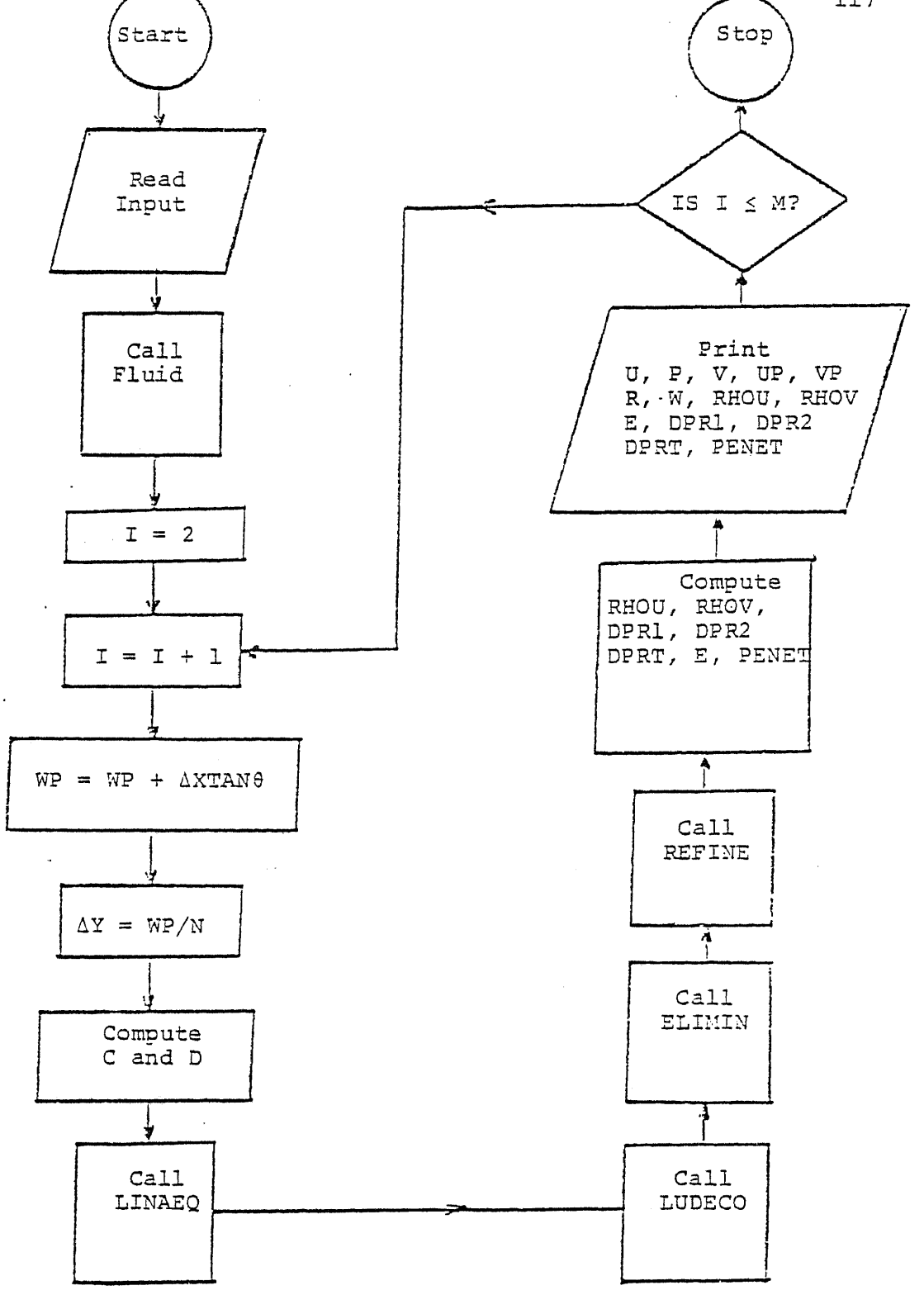

FIG. 4.3 COMPUTER FLOW CHART FOR CONVERGING AND DIVERGING CHANNEL

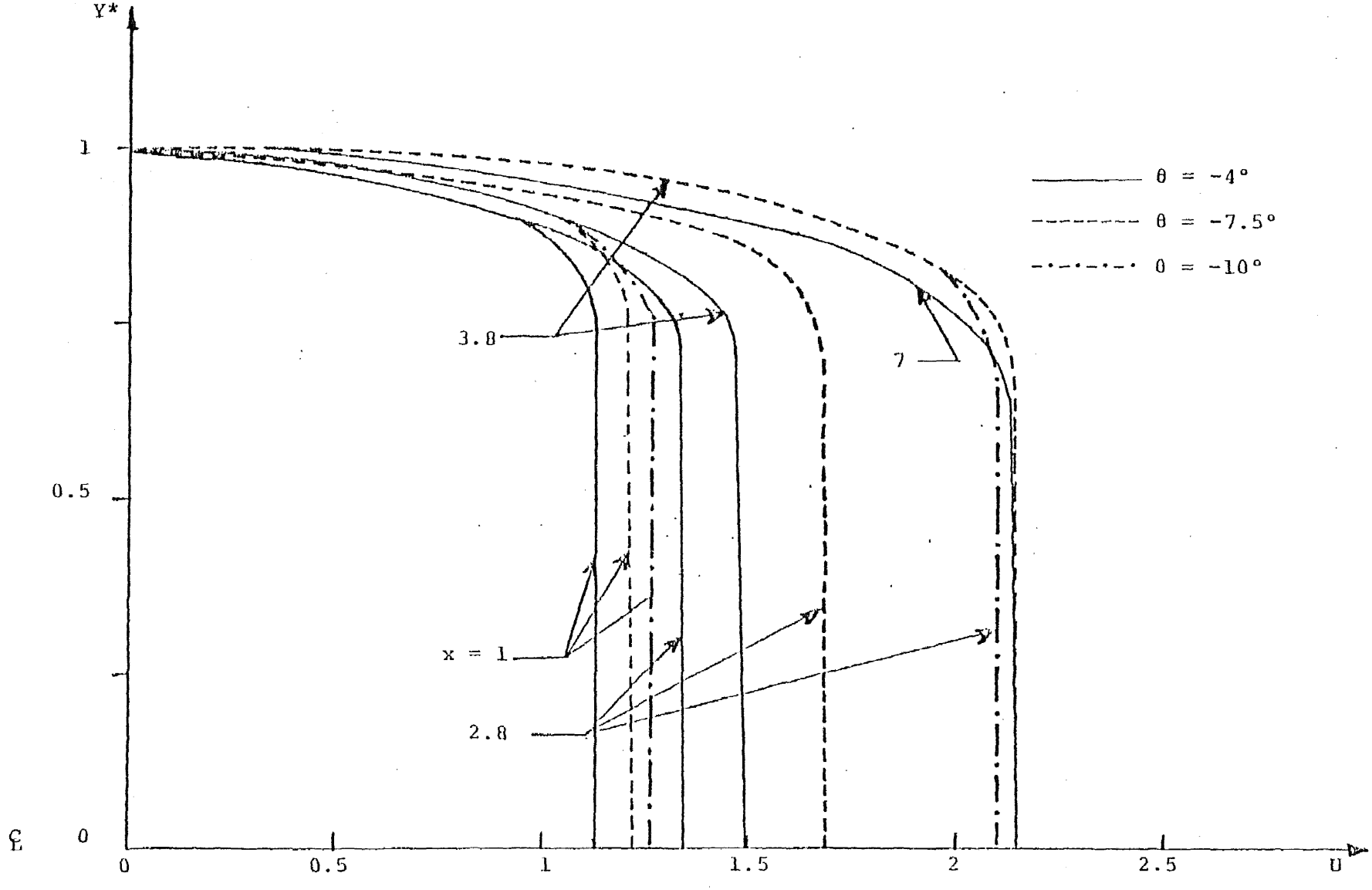

FIG. 4.4 AXIAL VELOCITY DISTRIBUTION OF THE FLUID PHASE WITH VARYING ANGLES OF CONVERGENCE ($\theta = -4°, -7.5°$ and $-10°$)

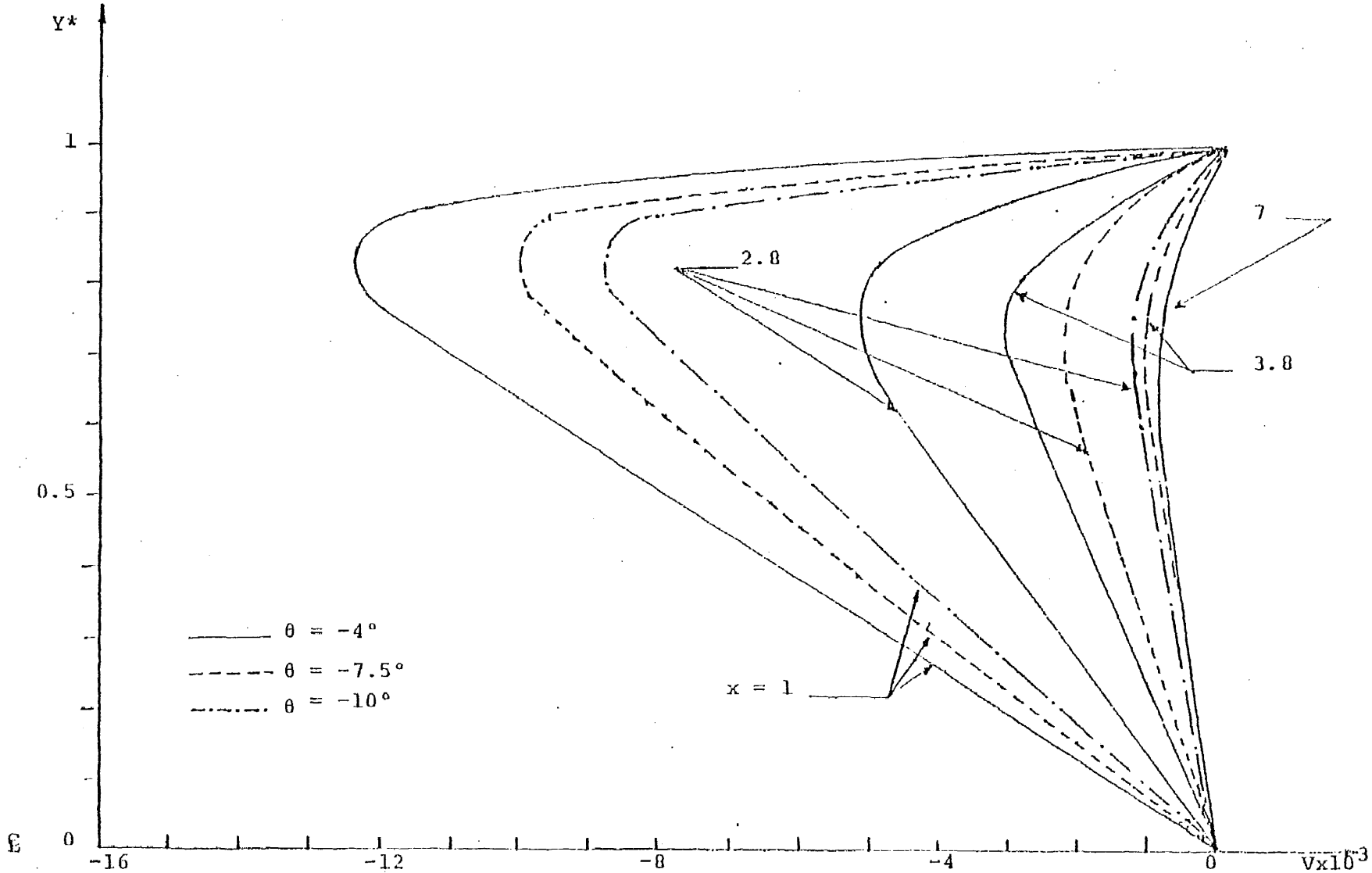

FIG. 4.5 VERTICAL VELOCITY DISTRIBUTION OF THE FLUID PHASE WITH VARYING ANGLES OF CONVERGENCE (θ = -4°, -7.5° and -10°)

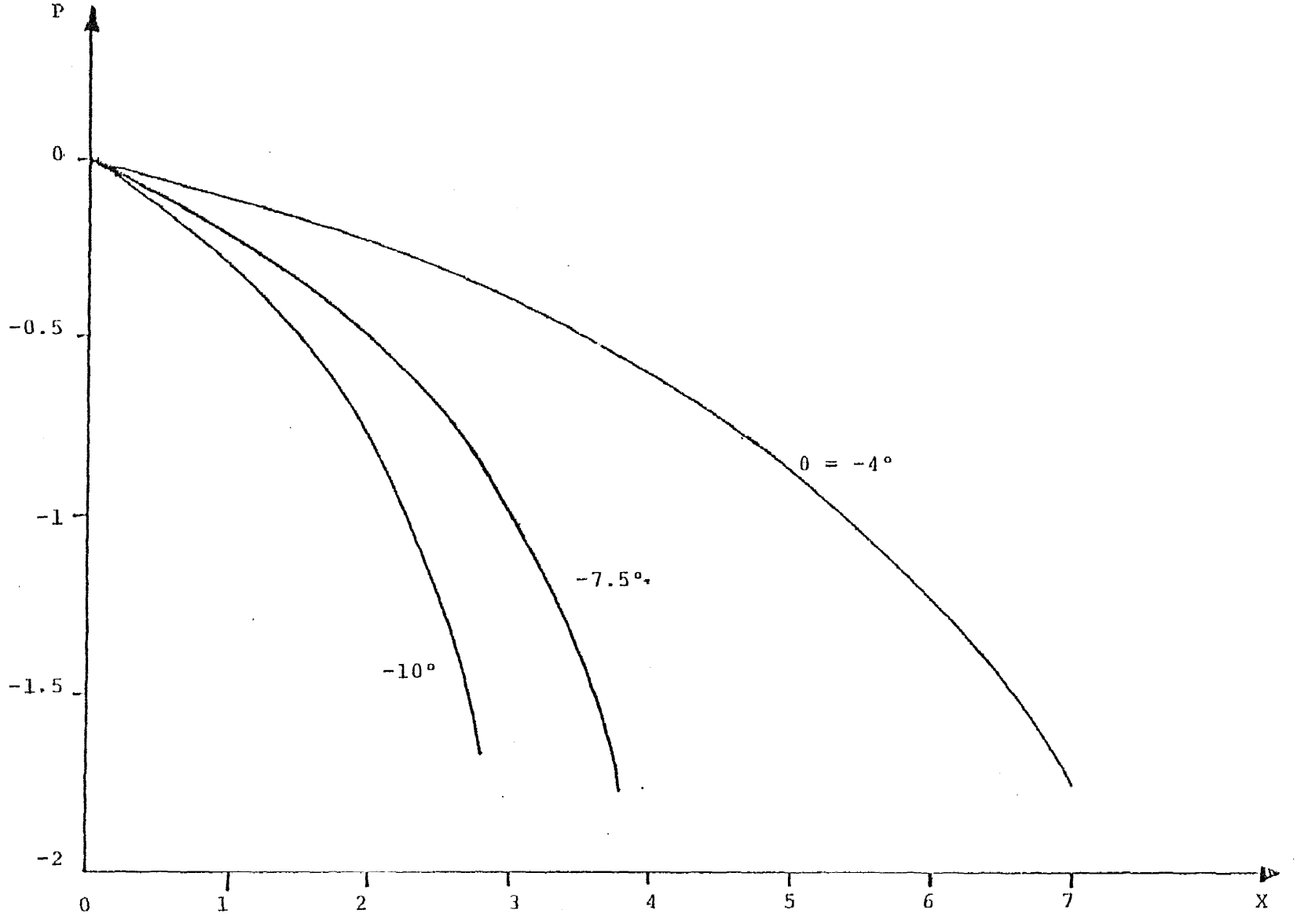

FIG. 4.6 AXIAL DISTRIBUTION OF THE FLUID STATIC PRESSURE, P, WITH INCREASING ANGLES OF CONVERGENCE (θ = -4°, -7.5° and -10°)

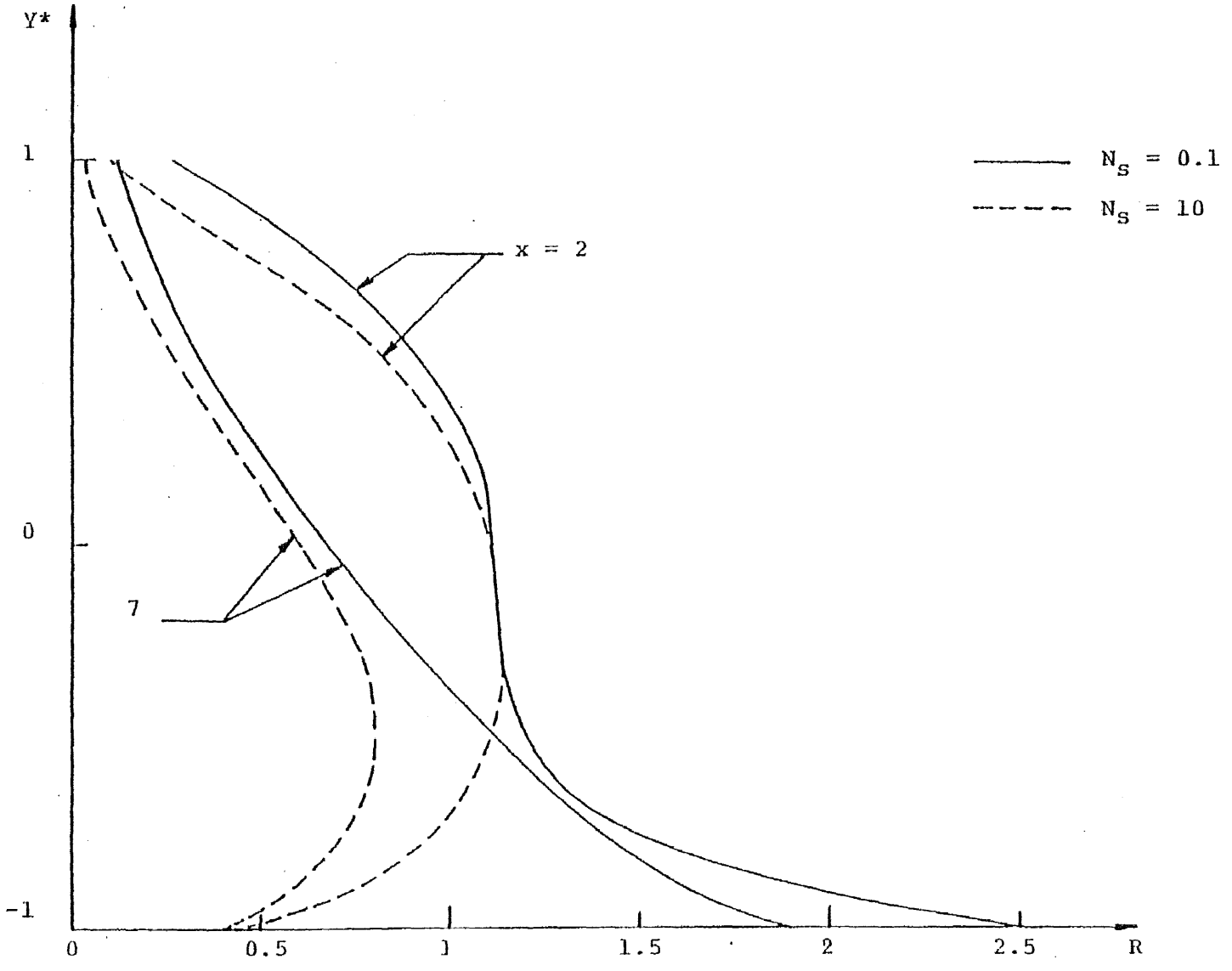

FIG. 4.7 AXIAL DISTRIBUTION OF PARTICLE CONCENTRATION WITH SURFACE ADHESION EFFECT IN A CONVERGENT CHANNEL (K_{np} = 0.0001, θ = -4°, N_α = 0, N_η = 5, N_β = 40, N_m = 2, N_R = 1000, σ = 0.5)

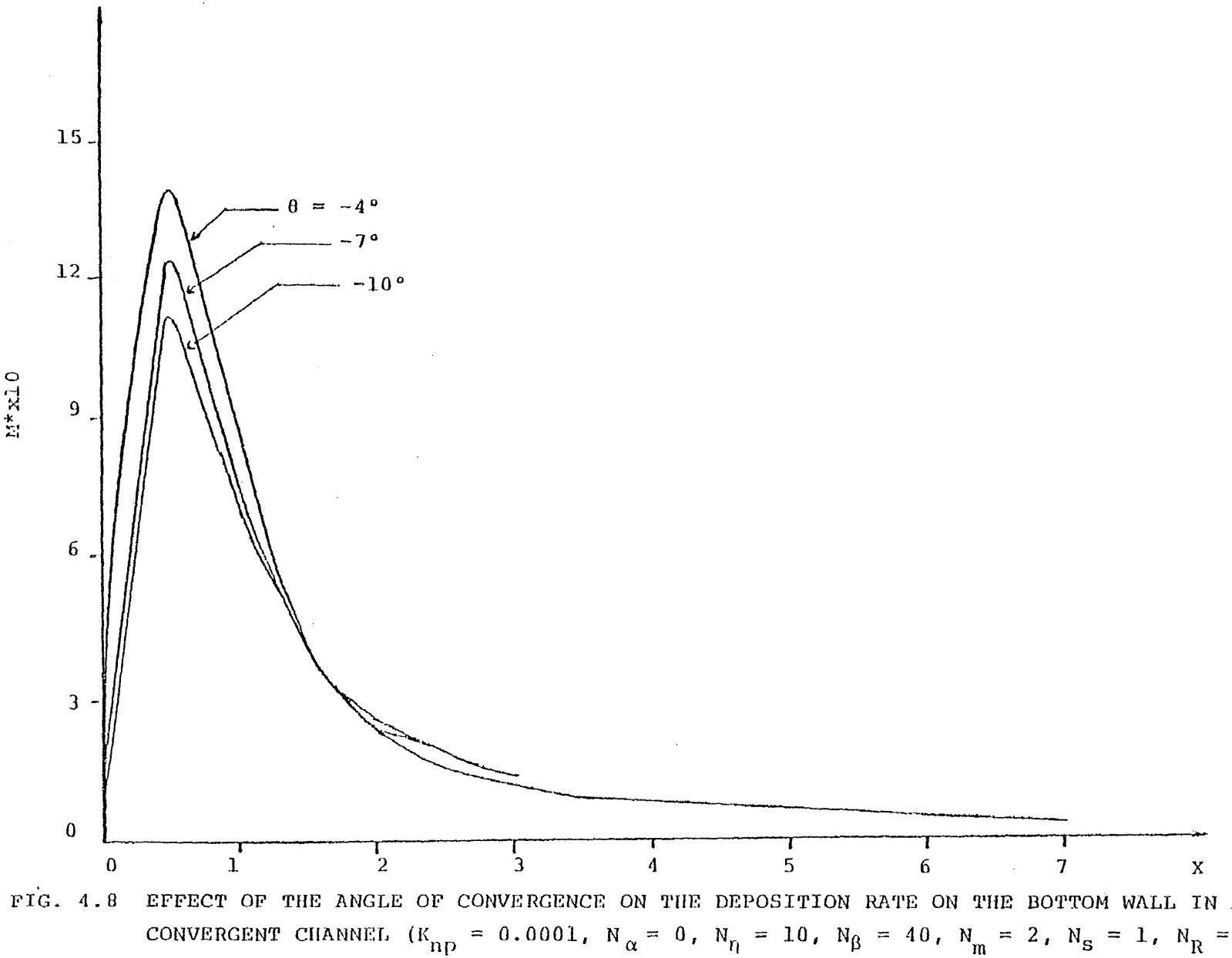

FIG. 4.8 EFFECT OF THE ANGLE OF CONVERGENCE ON THE DEPOSITION RATE ON THE BOTTOM WALL IN A CONVERGENT CHANNEL (K_{np} = 0.0001, N_α = 0, N_η = 10, N_β = 40, N_m = 2, N_s = 1, N_R = 1000, σ = 0.5)

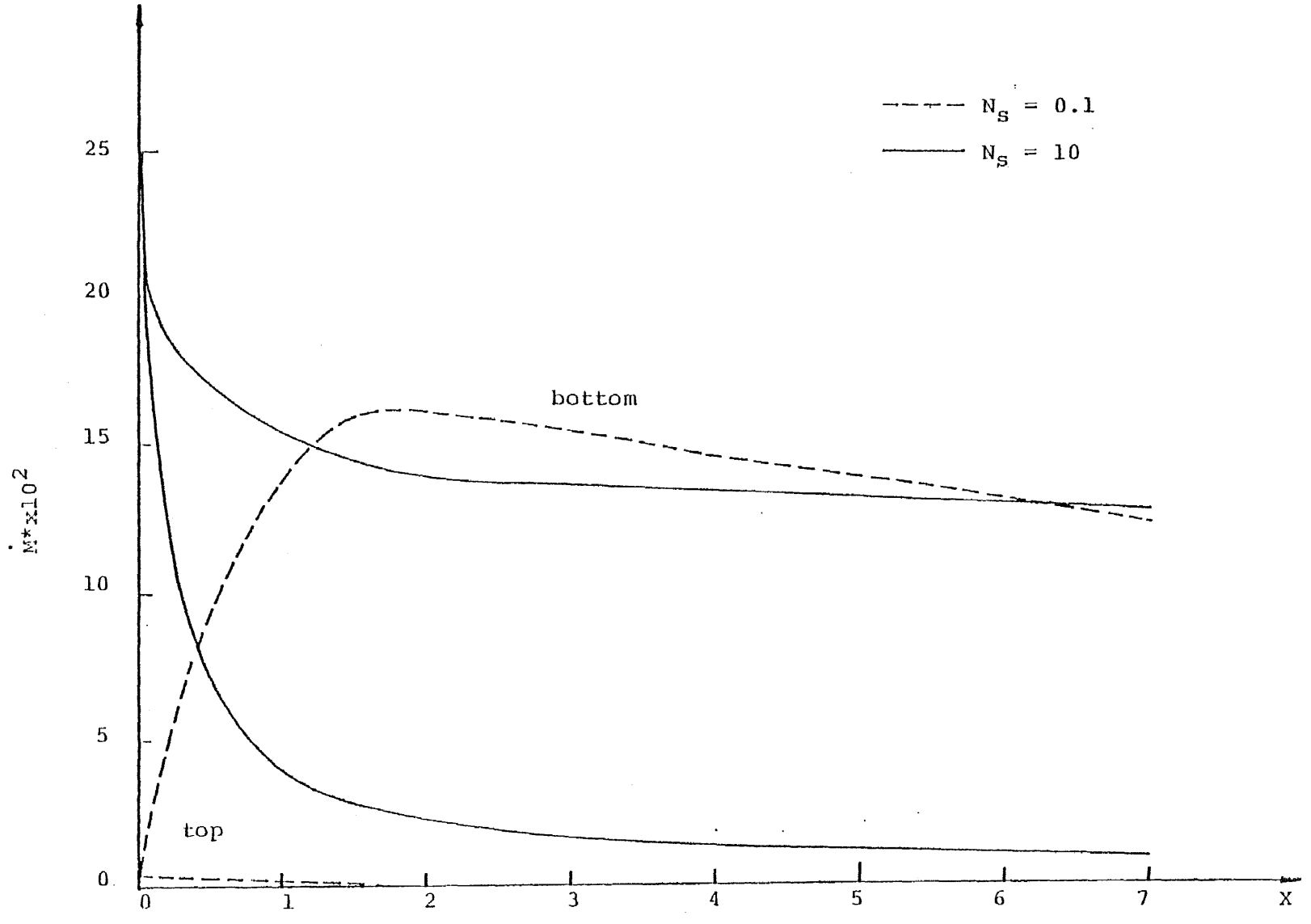

FIG. 4.9 EFFECT OF SURFACE ADHESION PARAMETER ON RATE OF DEPOSITION IN A CONVERGENT CHANNEL

(K_{np} = 0.0001, N_α = 0, N_η = 5,0 = -4°, N_β = 40, N_m = 2, N_R = 1000, σ = 0.5)

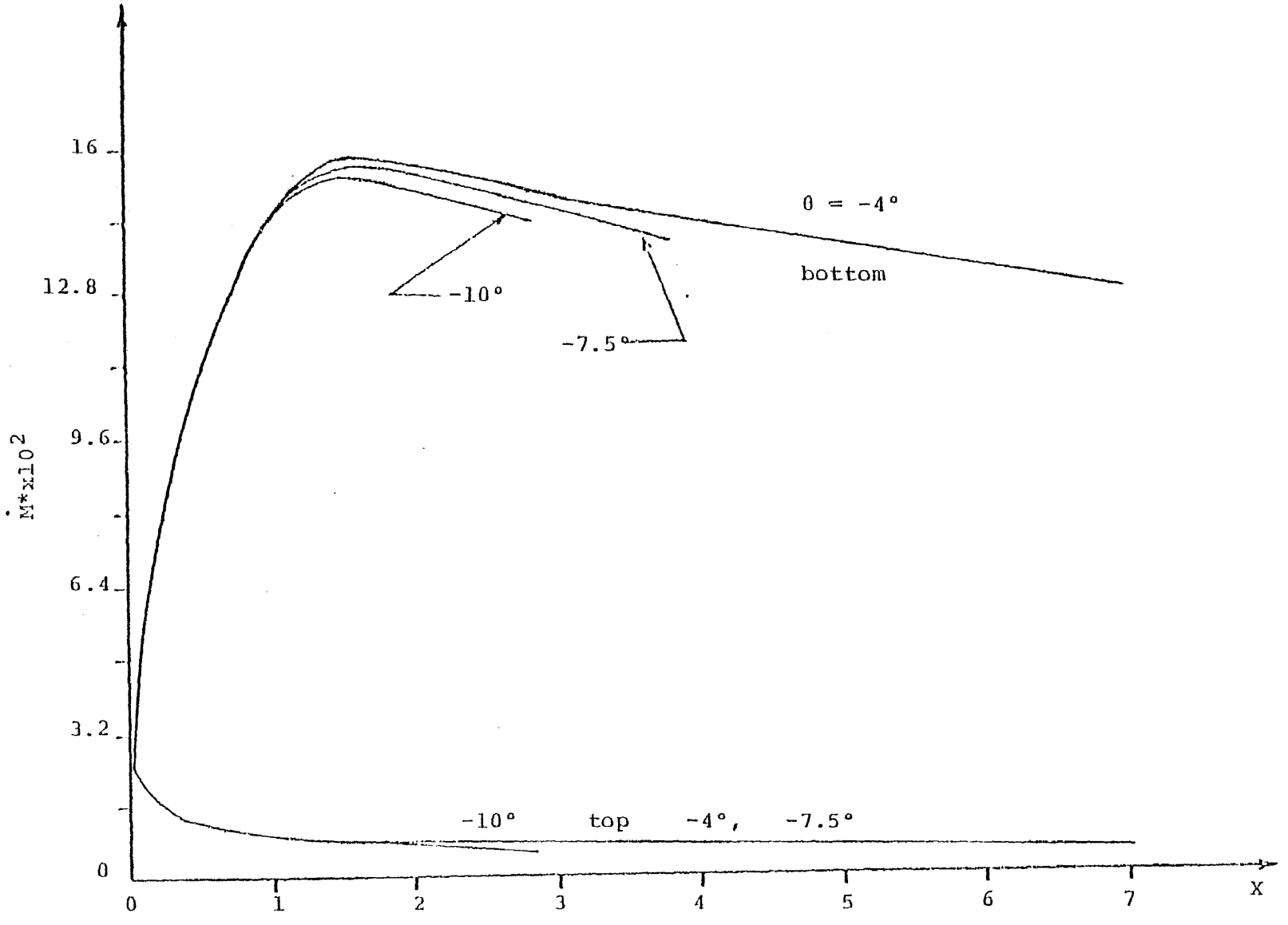

FIG. 4.10 EFFECT OF THE ANGLE OF CONVERGENCE IN A CONVERGENT CHANNEL (K_{np} = 0.0001, N_α = 0, N_η = 5, N_β = 40, N_m = 2, N_S = 1, N_R = 1000, σ = 0.5)

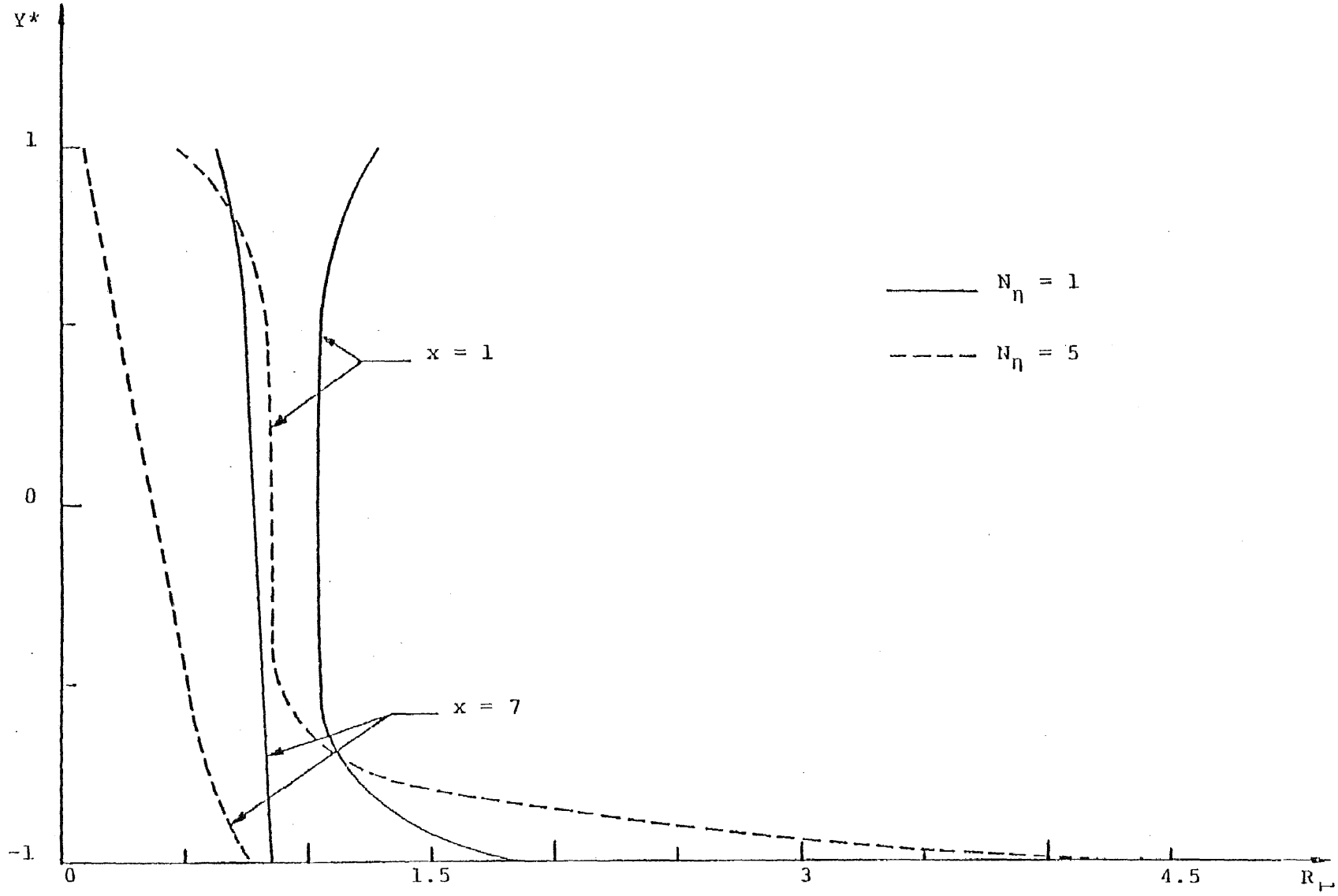

FIG. 4.11 EFFECT OF THE GRAVITY FLOW PARAMETER ON THE PARTICLE CONCENTRATION IN A CONVERGENT CHANNEL (K_{np} = 0.0001, N_α = 1, θ = -4°, N_β = 40, N_m = 2, N_s = 1 N_R = 1000, σ = 0.5)

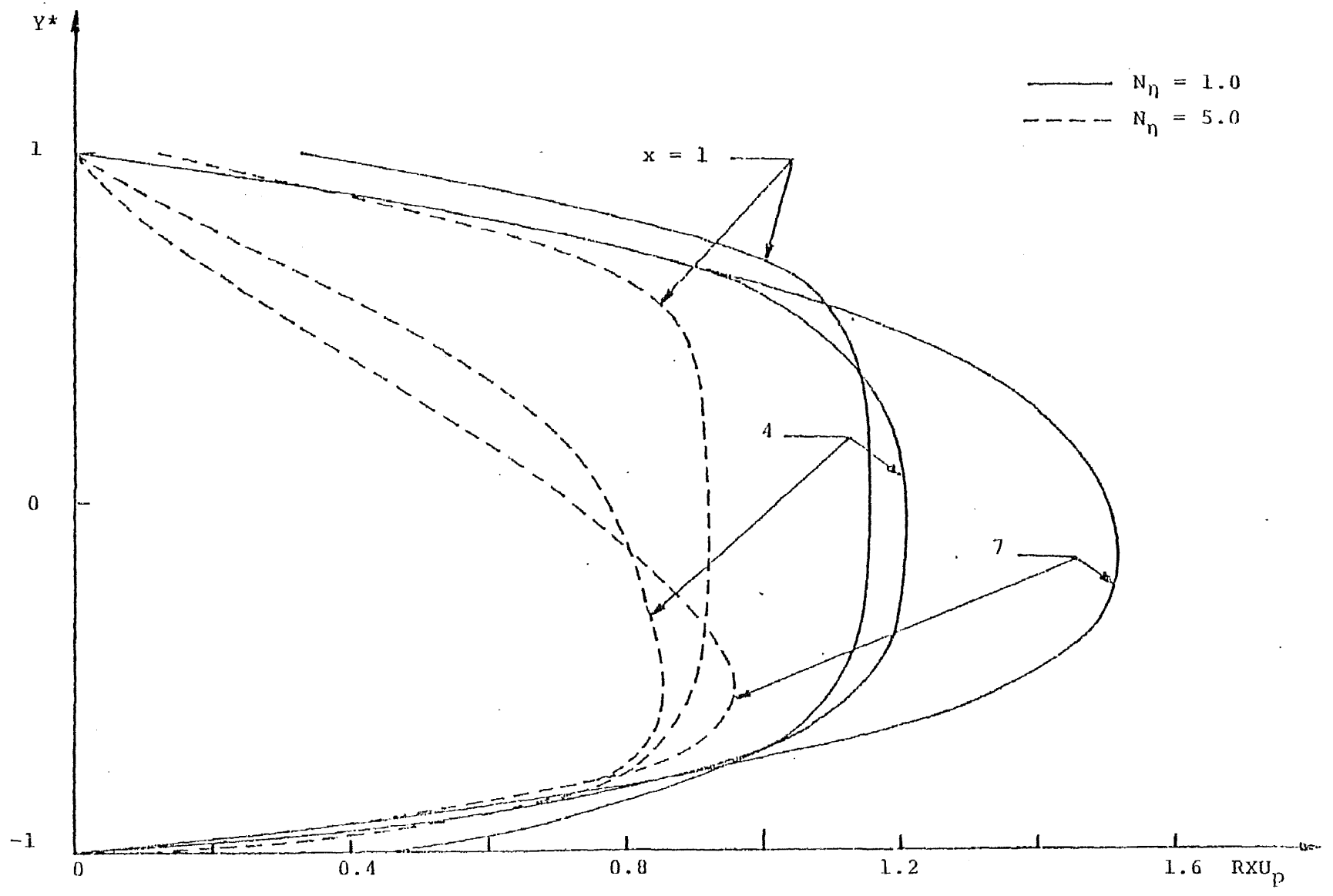

FIG. 4.12 MASS FLUX DISTRIBUTION OF SOLID PARTICLES WITH GRAVITATIONAL EFFECTS IN A CONVERGENT CHANNEL (K_{np} = 0.0001, N_α = 1, θ = -4°, N_β = 40, N_m = 2, N_s = 1, N_R = 1000, σ = 0.5)

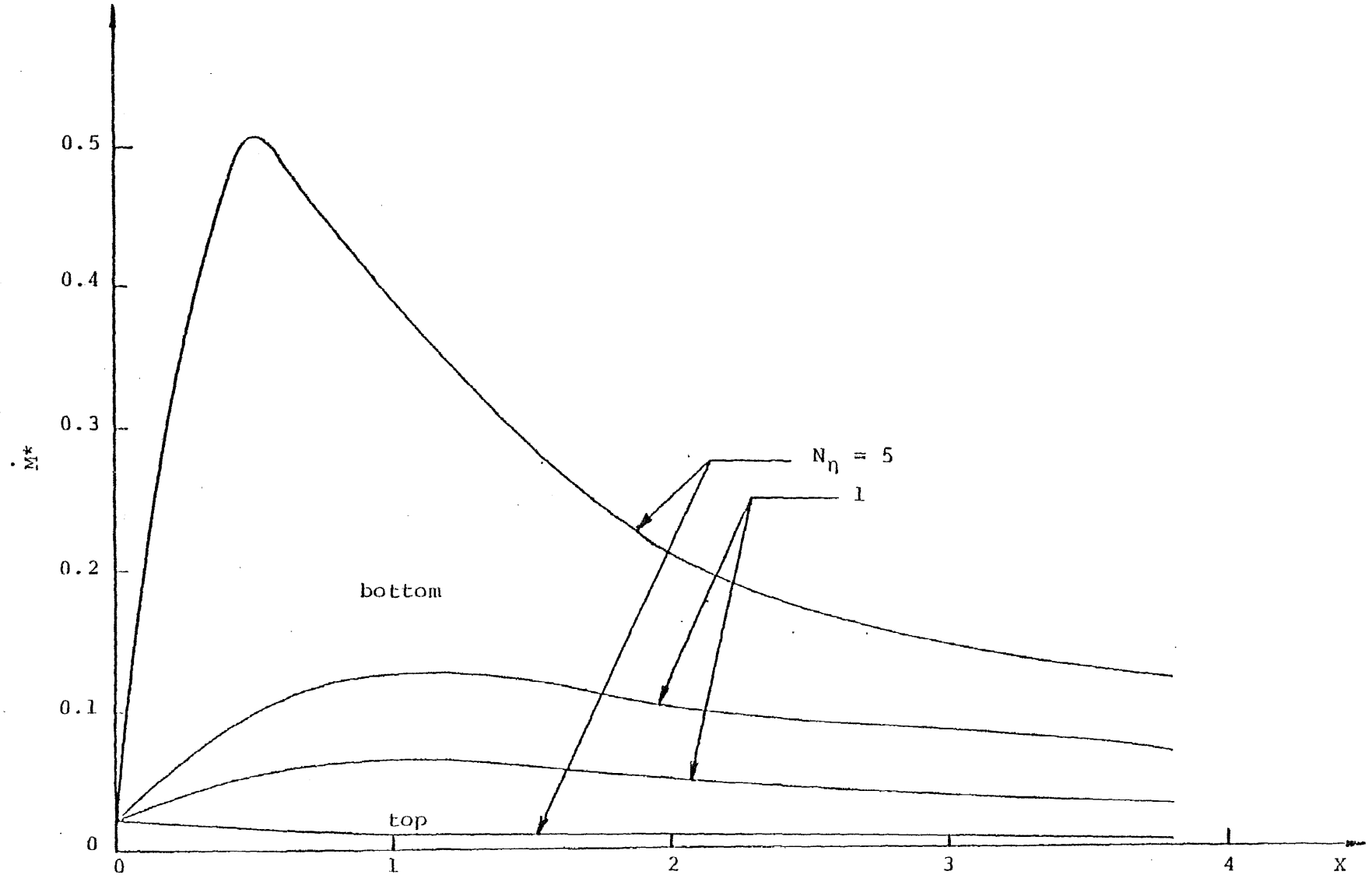

FIG. 4.13 INFLUENCE OF THE GRAVITY FLOW PARAMETER ON RATE OF DEPOSITION IN A CONVERGENT CHANNEL

(K_{np} = 0.0001, N_α = 1, θ = -7.5°, N_β = 40, N_m = 2, N_s = 1, N_R = 1000, σ = 0.5)

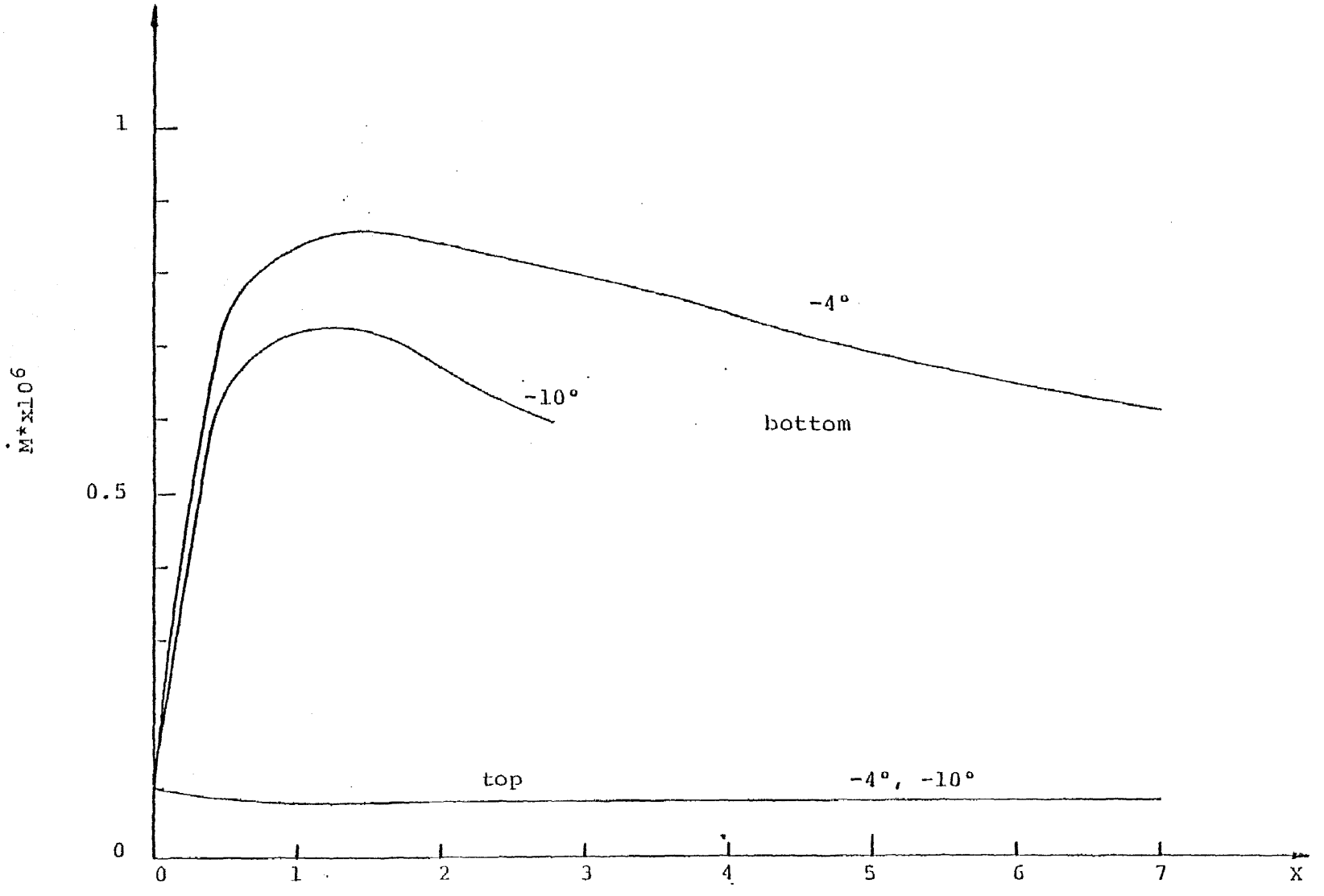

FIG. 4.14 EFFECT OF THE ANGLE OF CONVERGENCE WITH HIGH DIFFUSIVE PECLET NUMBER ON THE DEPOSITION RATE IN A CONVERGENT CHANNEL (K_{np} = 0.0001, N_α = 1, N_η = 5, N_β =10^7, N_m = 2, N_s = 1, N_R = 1000, σ = 0.5)

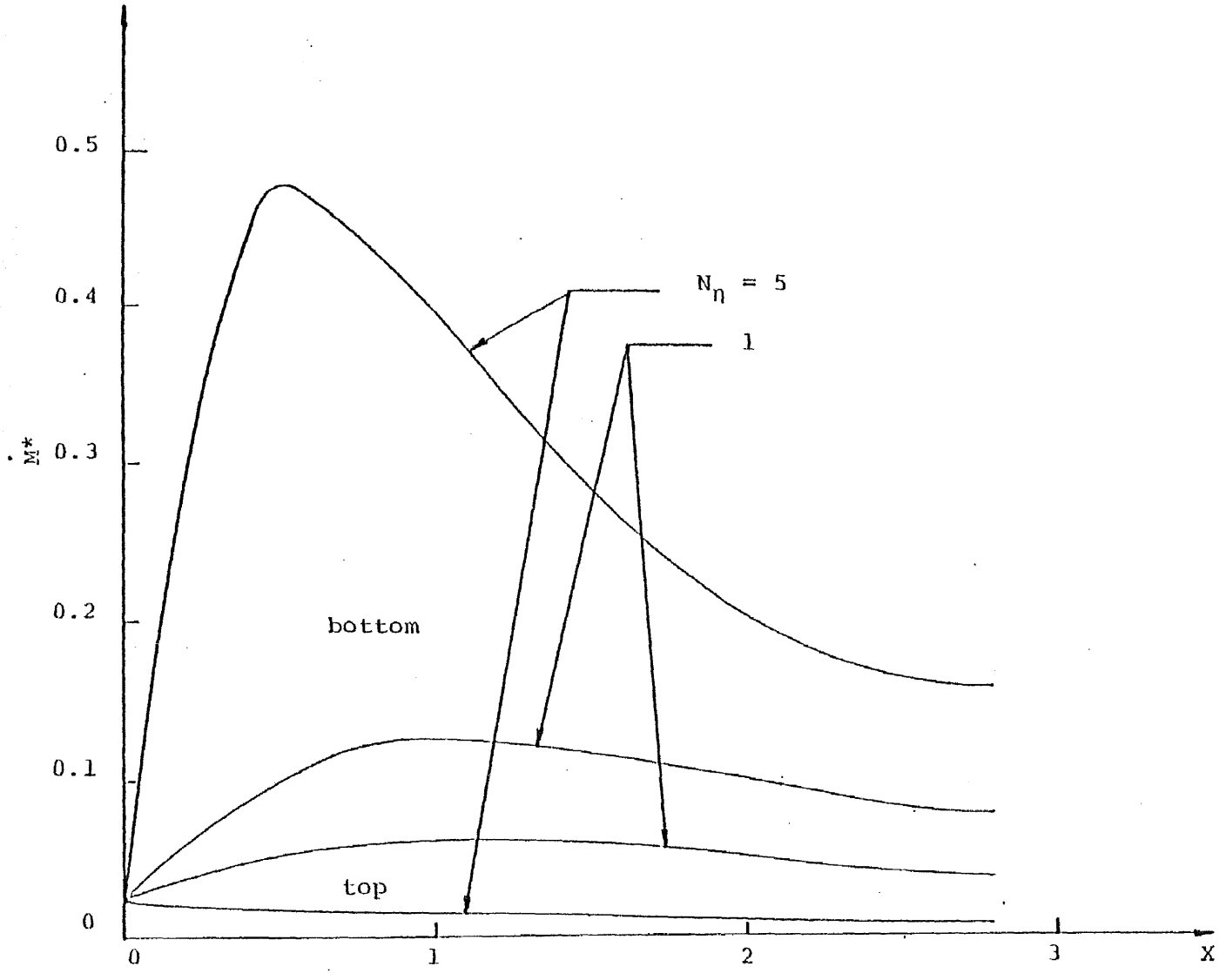

FIG. 4.15 EFFECT OF THE GRAVITY FLOW PARAMETER ON THE RATE OF DEPOSITION (K_{np} = 0.0001, N_α = 1, θ = -10°, N_β = 40, N_m = 2, $N_{\dot{s}}$ = 1, N_R = 1000, σ = 0.5)

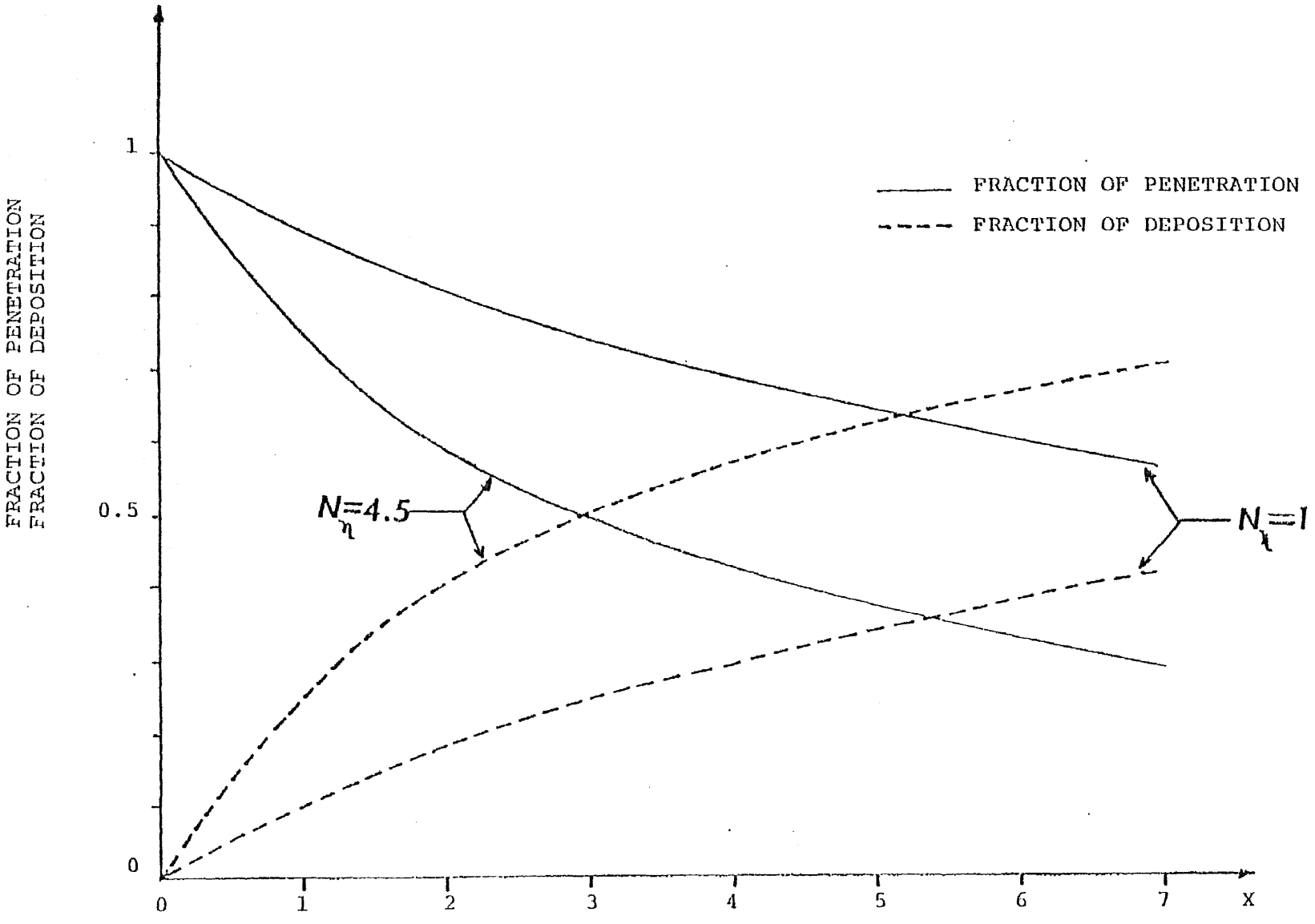

FIG. 4.16 AXIAL DISTRIBUTION OF THE FRACTION OF PENETRATION AND DEPOSITION IN A CONVERGENT CHANNEL

(K_{np} = 0.0001, N_α = 1, N_η = 4.5, θ = -4°, N_β = 40, N_m = 2, N_R = 1000, σ = 0.5)

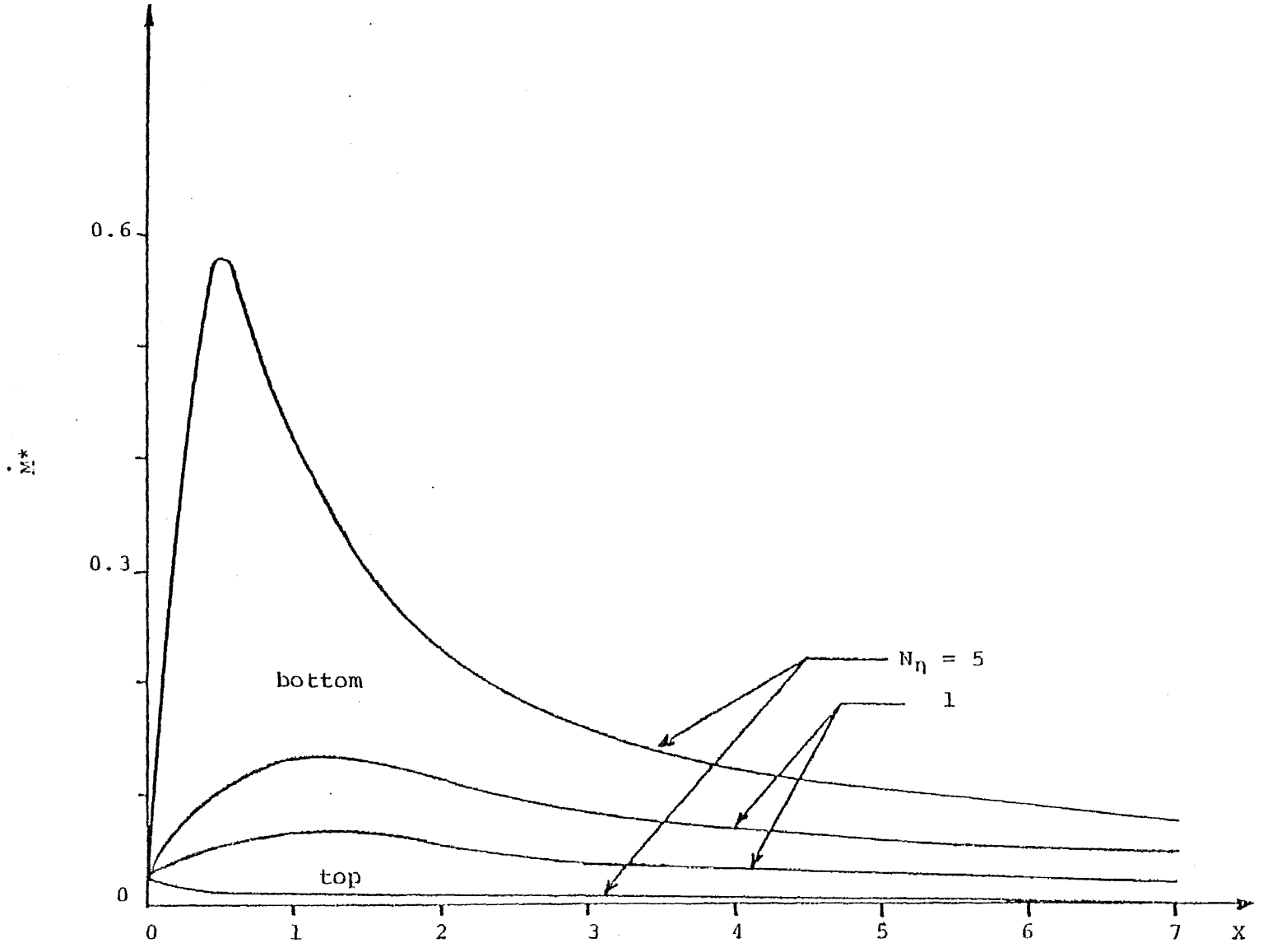

FIG. 4.17 EFFECT OF GRAVITY FLOW PARAMETER ON DEPOSITION RATE IN A CONVERGENT CHANNEL

(K_{np} = 0.0001, N_α = 1, 0 = -4°, N_β = 40, N_m = 2, N_s = 1, N_R = 1000, σ = 0.5)

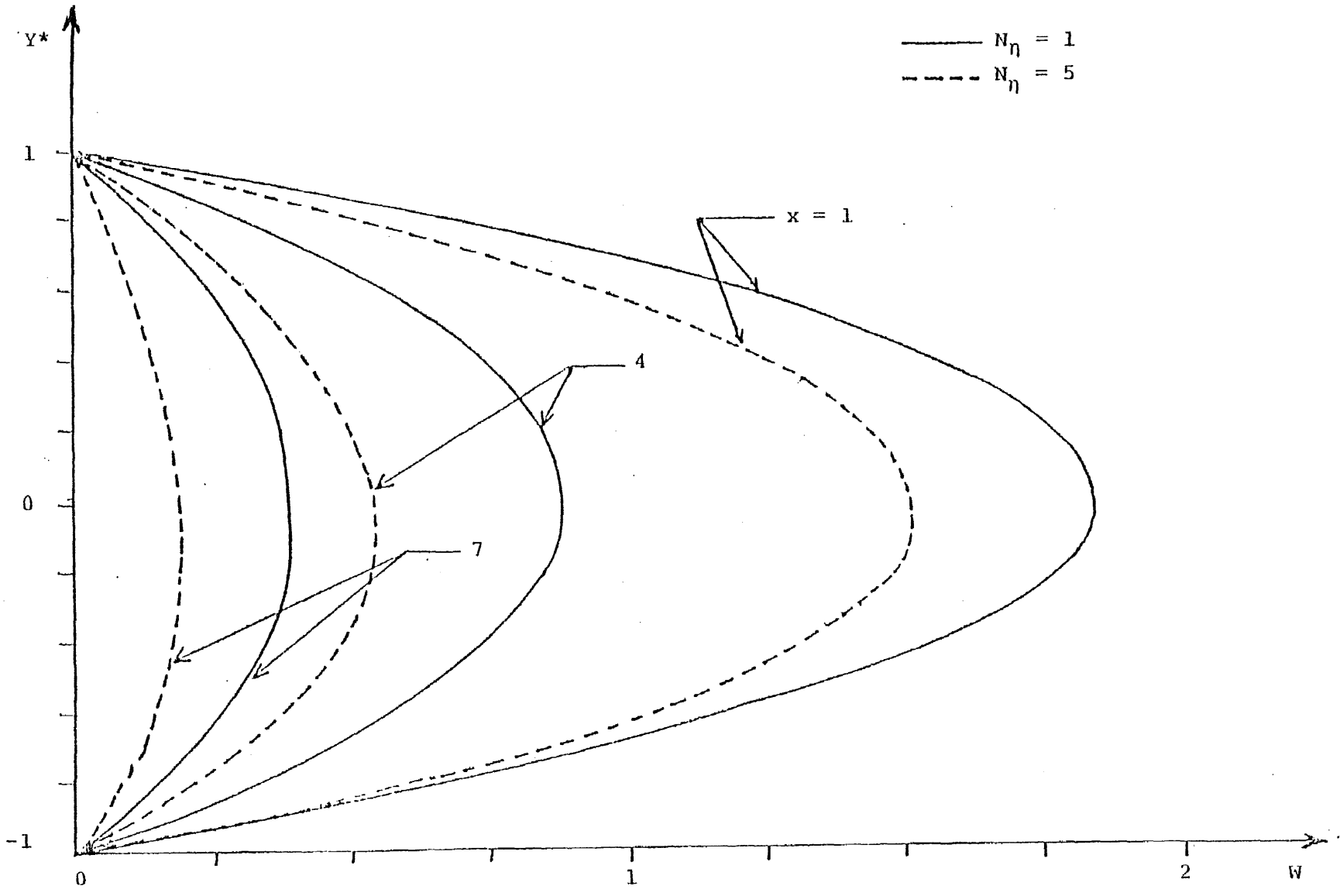

FIG. 4.18 AXIAL DISTRIBUTION OF ELECTROSTATIC POTENTIAL IN A CONVERGENT CHANNEL (K_{np} = 0.0001, N_α = 1, 0 = -4°, N_β = 40, N_m = 2, N_S = 1, N_R = 1000, σ = 0.5)

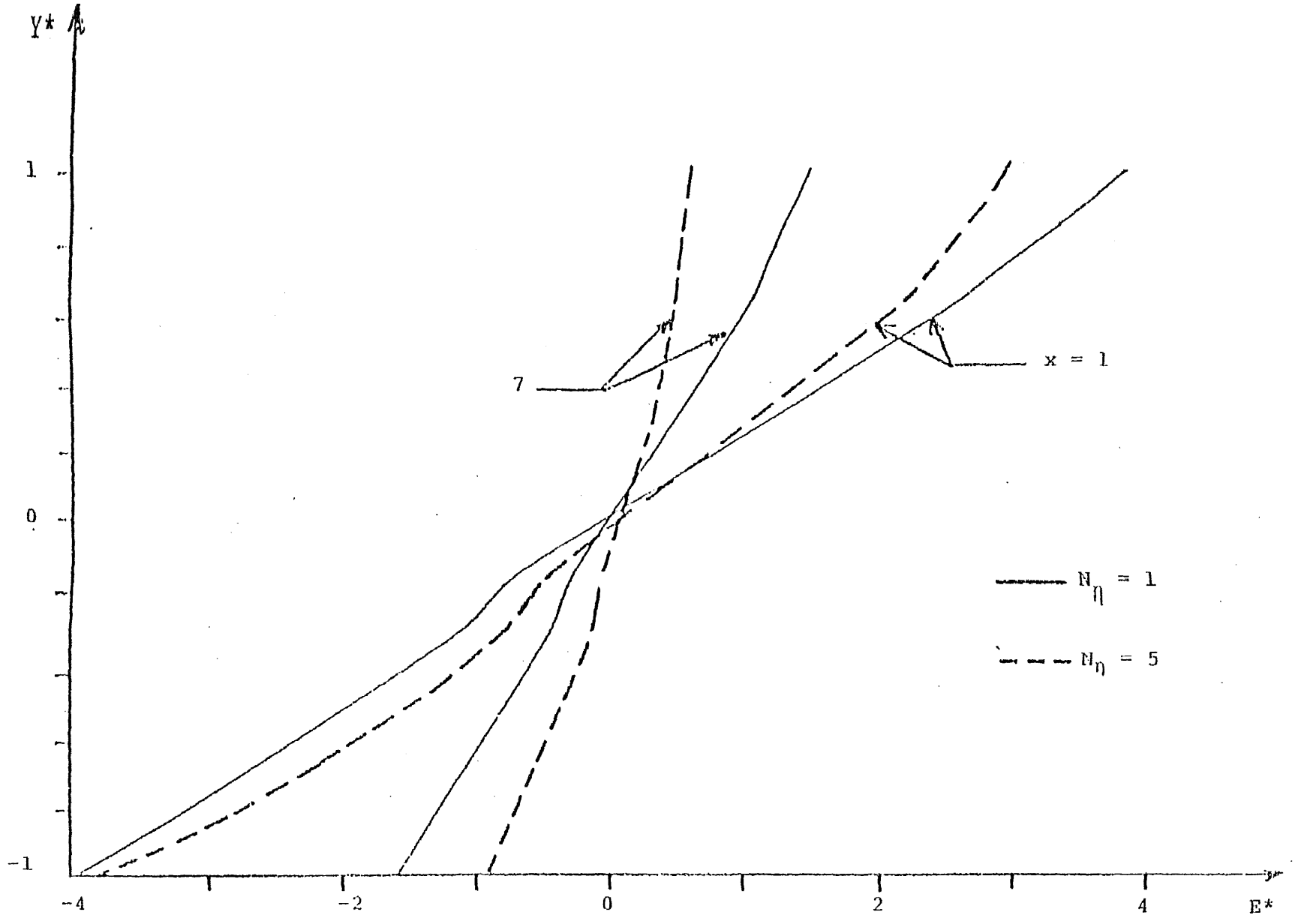

FIG. 4.19 EFFECT OF GRAVITY FLOW PARAMETER ON ELECTROSTATIC CHARGE INTENSITY IN A CONVERGENT CHANNEL (K_{np} = 0.0001, N_α = 1, θ = -4°, N_β = 40, N_m = 2, N_s = 1, N_R = 1000, σ = 0.5)

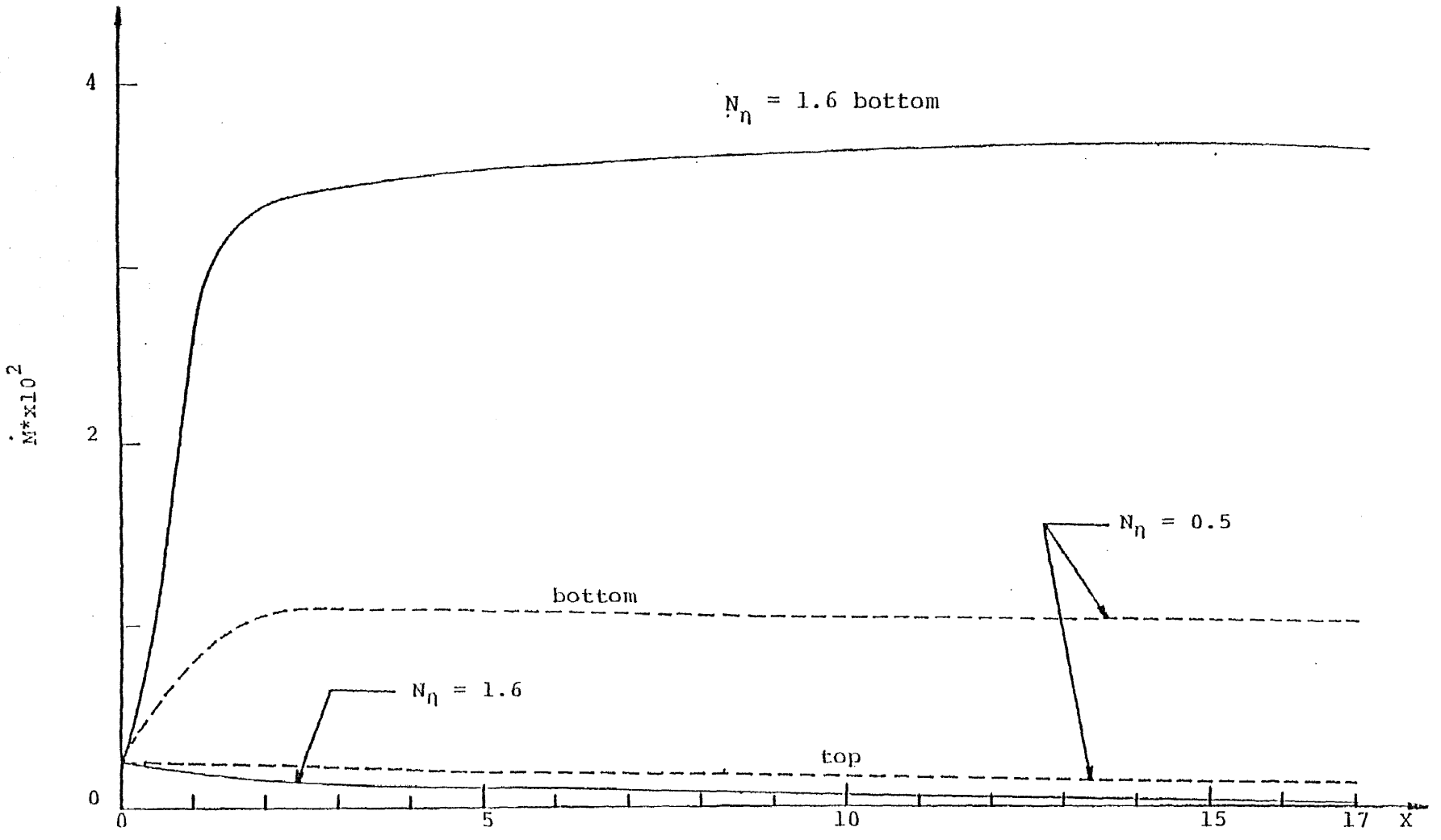

FIG. 4.20 INFLUENCE OF GRAVITY FLOW PARAMETER ON DEPOSITION RATE IN A DIVERGENT CHANNEL (K_{np} = 0.0001, N_α = 0, θ = 2°, N_β = 40, N_m = 2, N_S = 0.1, N_R = 1000, σ = 0.5)

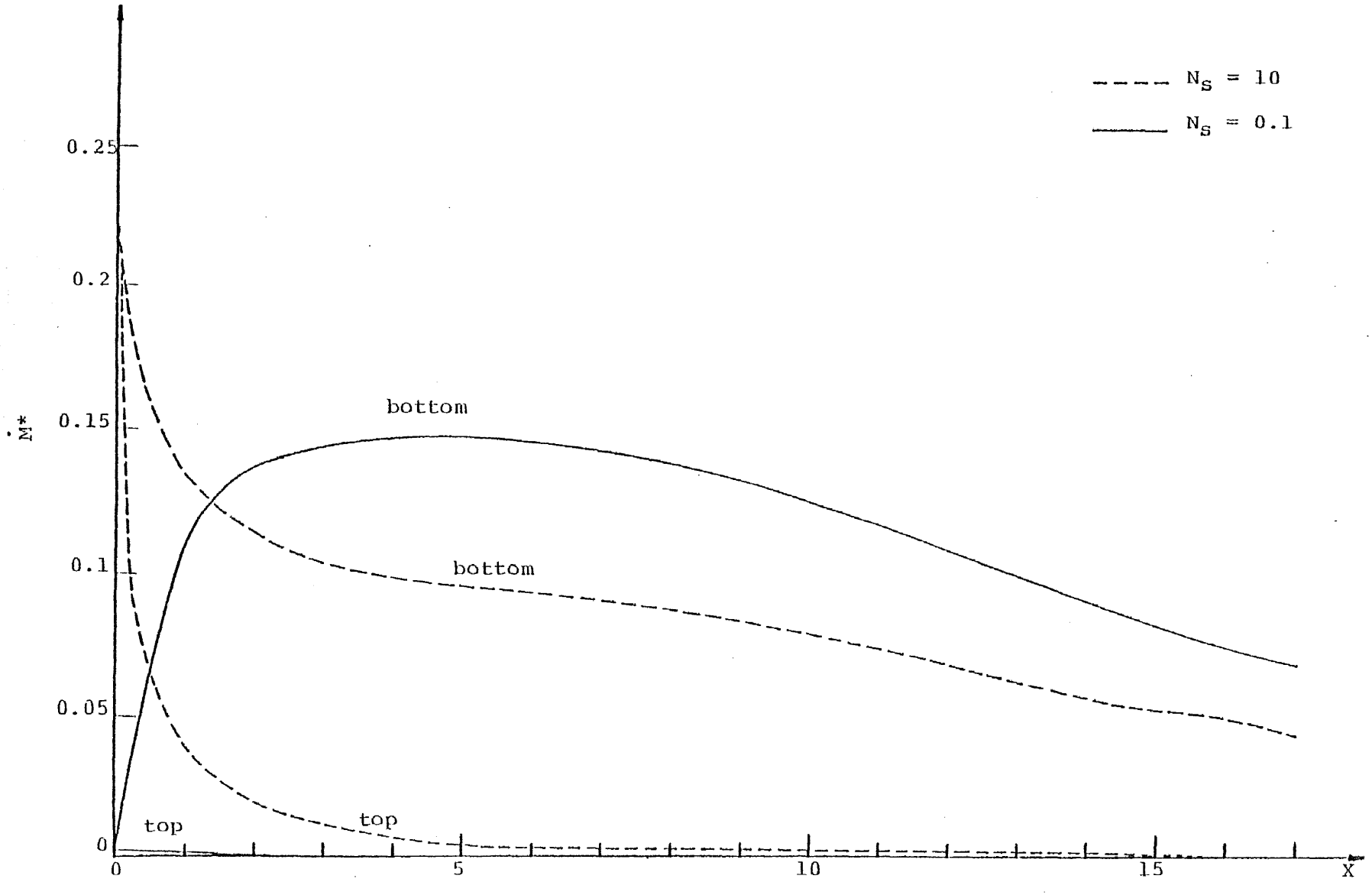

FIG. 4.21 EFFECT OF SURFACE ADHESION ON DEPOSITION RATE IN A DIVERGENT CHANNEL (K_{np} = 0.0001, N_α = 0, N_η = 4.5, 0 = 2°, N_β = 40, N_m = 2, N_R = 1000, σ = 0.5)

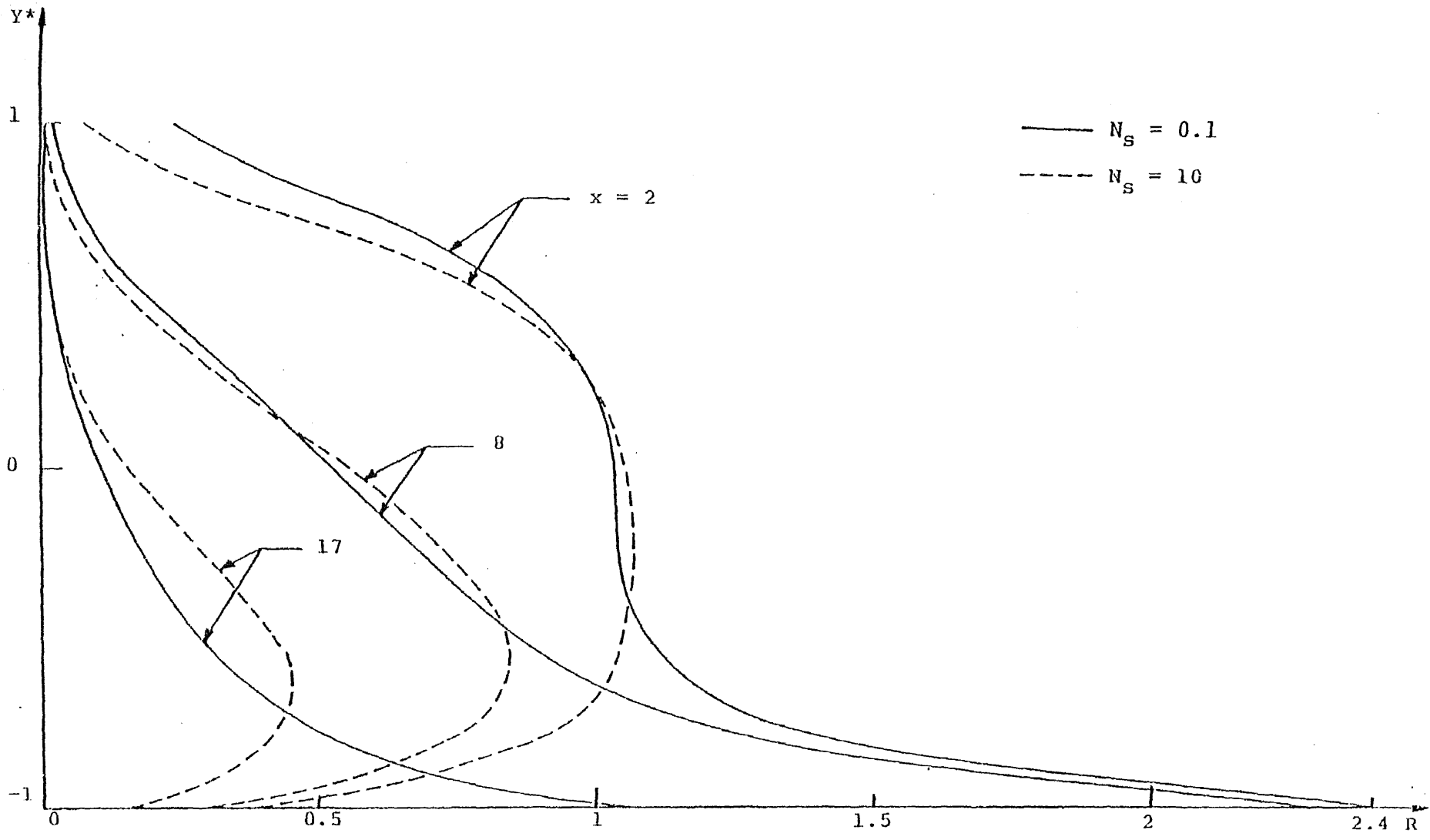

FIG. 4.22 AXIAL DISTRIBUTION OF PARTICLE CONCENTRATION WITH SURFACE ADHESION EFFECT IN A DIVERGENT CHANNEL (K_{np} = 0.0001, N_α = 0, N_η = 4.5, θ = 2°, N_β = 40, N_m = 2, N_R = 1000, σ = 0.5)

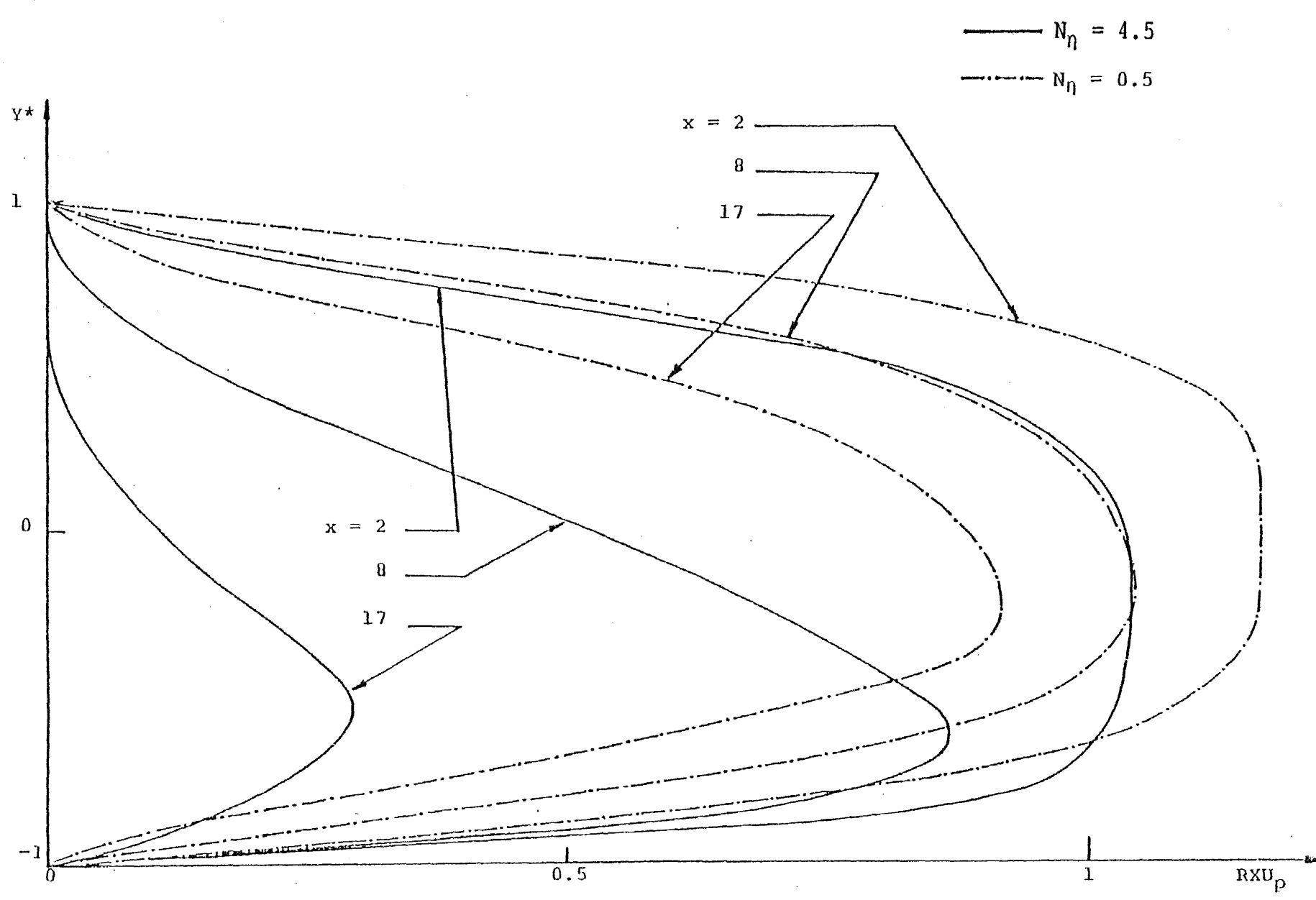

FIG. 4.23 MASS FLUX DISTRIBUTION OF SOLID PARTICLES WITH GRAVITY EFFECT IN A DIVERGENT CHANNEL

(K_{np} = 0.0001, N_α = 0, 0 = 2°, N_β = 40, N_m = 2, N_S = 0.1, N_R = 1000, σ = 0.5)

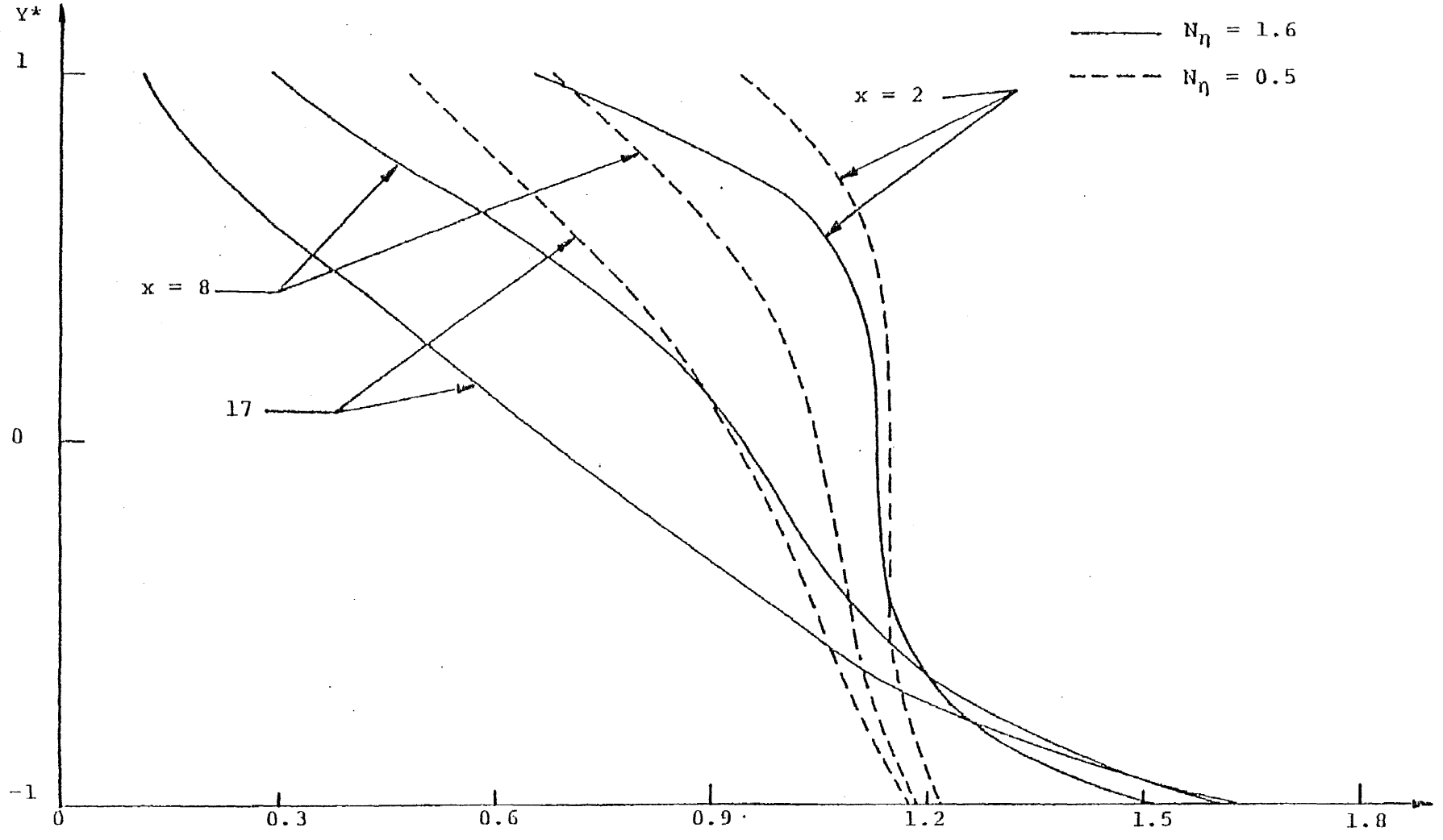

FIG. 4.24 AXIAL PARTICLE CONCENTRATION FOR A DIVERGENT CHANNEL OF 2° (K_{np} = 0.0001, N_α = 0, θ = 2°, N_β = 40, N_m = 2, N_s = 0.1, N_R = 1000, σ = 0.5)

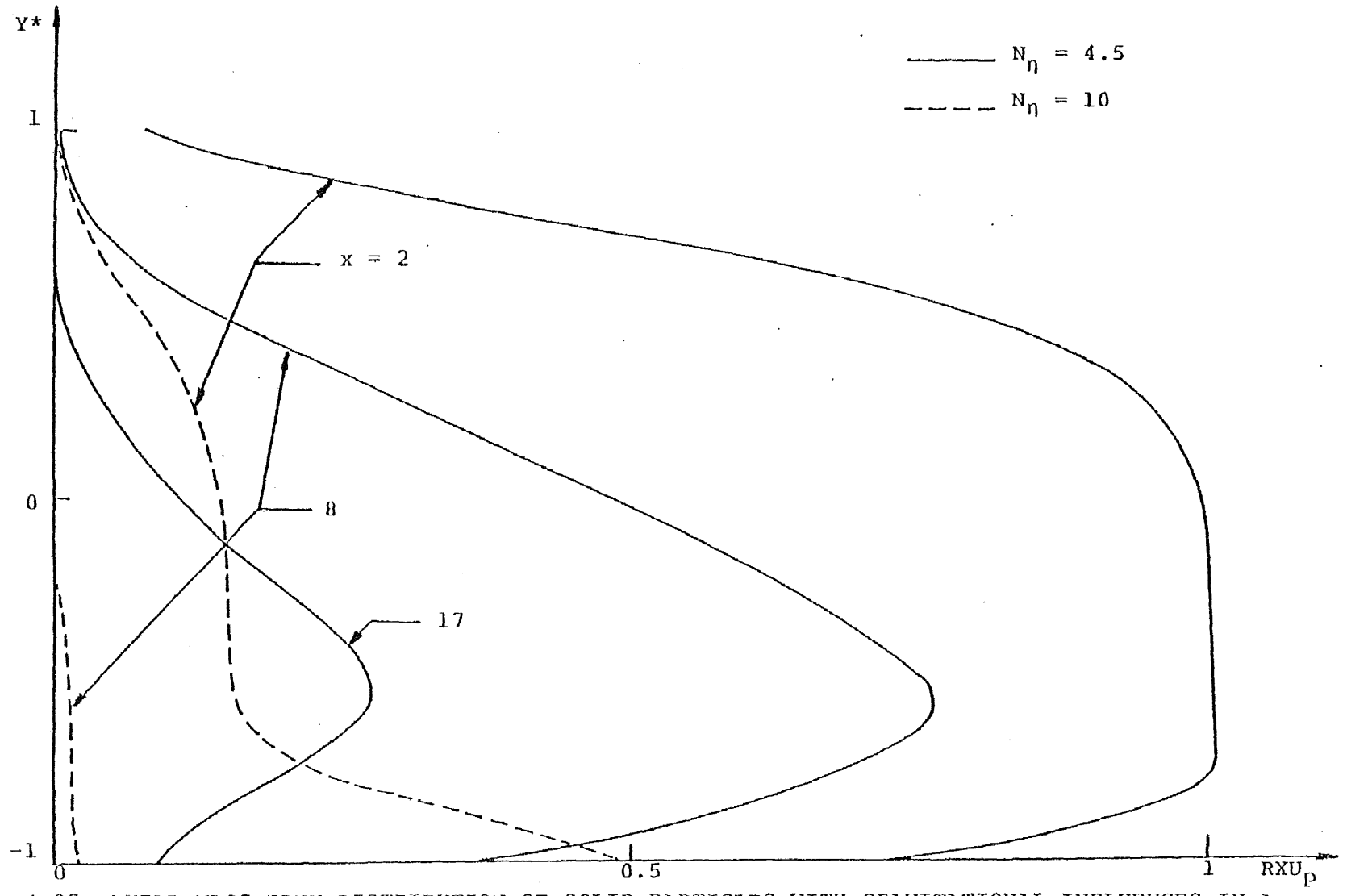

FIG. 4.25 AXIAL MASS FLUX DISTRIBUTION OF SOLID PARTICLES WITH GRAVITATIONAL INFLUENCES IN A DIVERGENT CHANNEL (K_{np} = 0.2, N_α = 0, θ = 2°, N_β = 40, N_m = 2, N_S = 1, N_R = 1000, σ = 0.5)

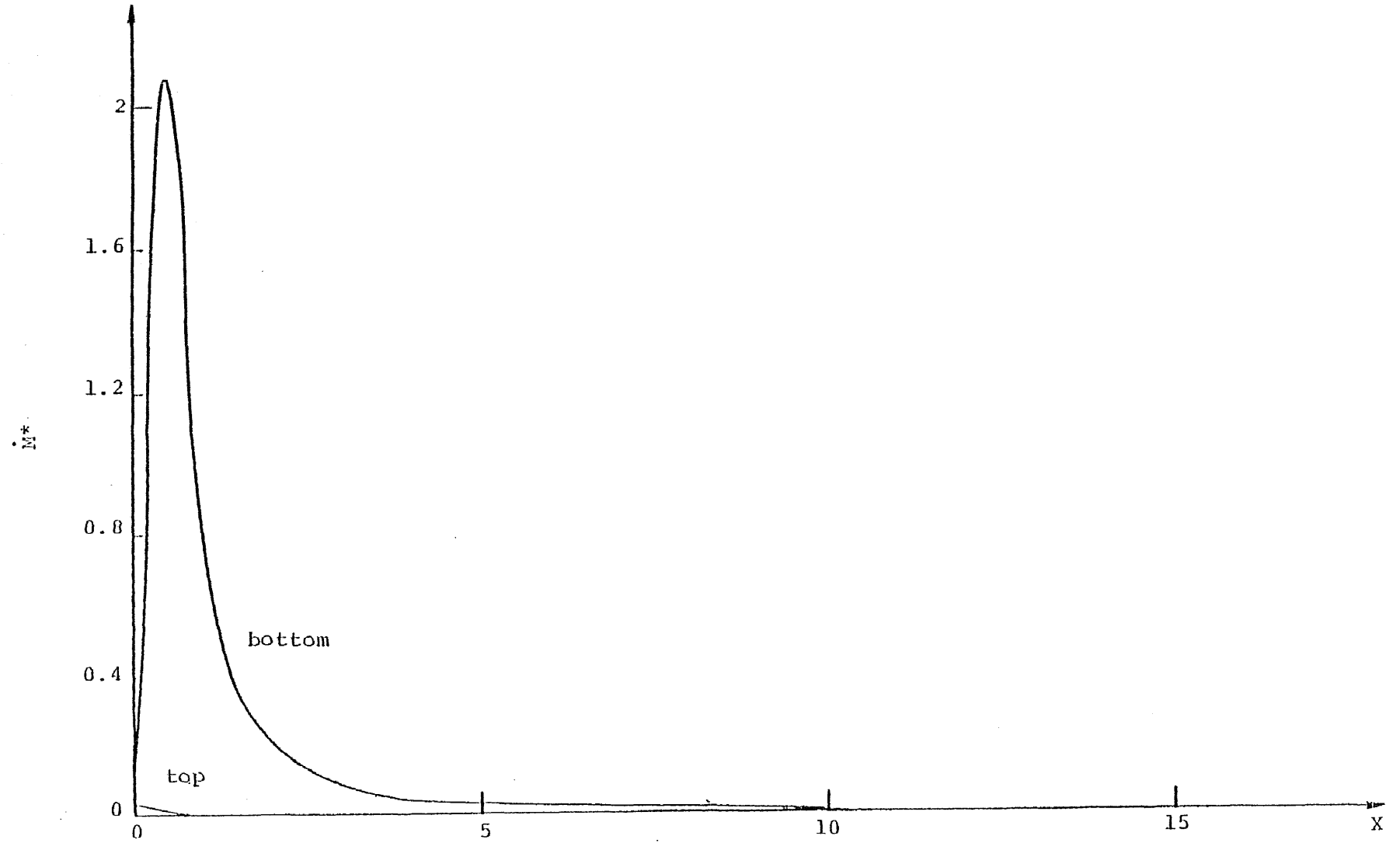

FIG. 4.26 DEPOSITION RATE IN A DIVERGENT CHANNEL WITH SIGNIFICANT GRAVITATIONAL EFFECT FOR $\theta = 2°$ AND $K_{np} = 0.2$ ($K_{np} = 0.2$, $N_\alpha = 0$, $N_\eta = 10$, $N_\beta = 40$, $N_m = 2$, $N_s = 1$ $N_R = 1000$, $\sigma = 0.5$)

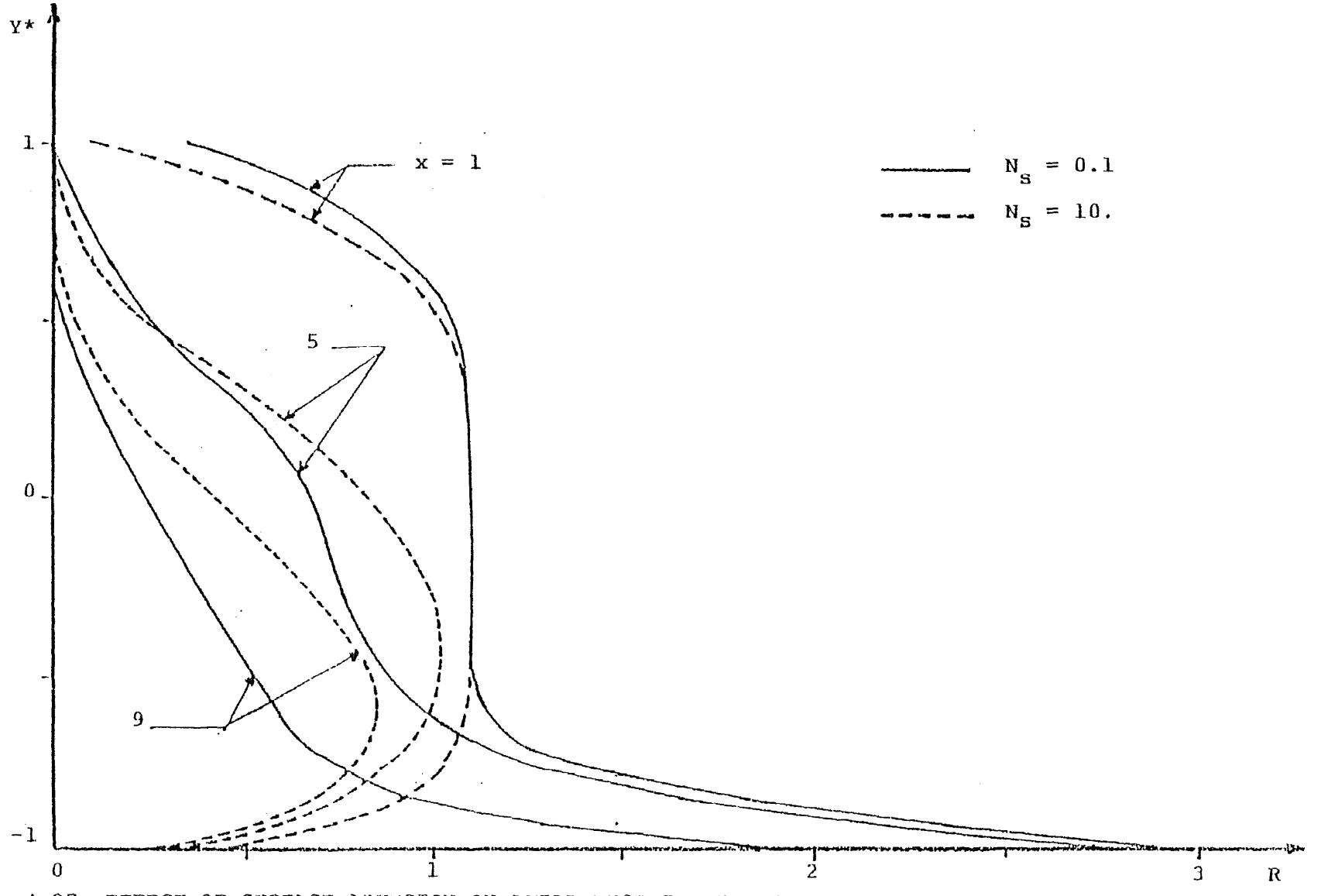

FIG. 4.27 EFFECT OF SURFACE ADHESION ON AXIAL DISTRIBUTION OF PARTICLE CONCENTRATION IN A DIVERGENT CHANNEL (K_{np} = 0.0001, N_α = 0, N_η = 5, θ = 4°, N_β = 40, N_m = 2, N_R = 1000, σ = 0.5)

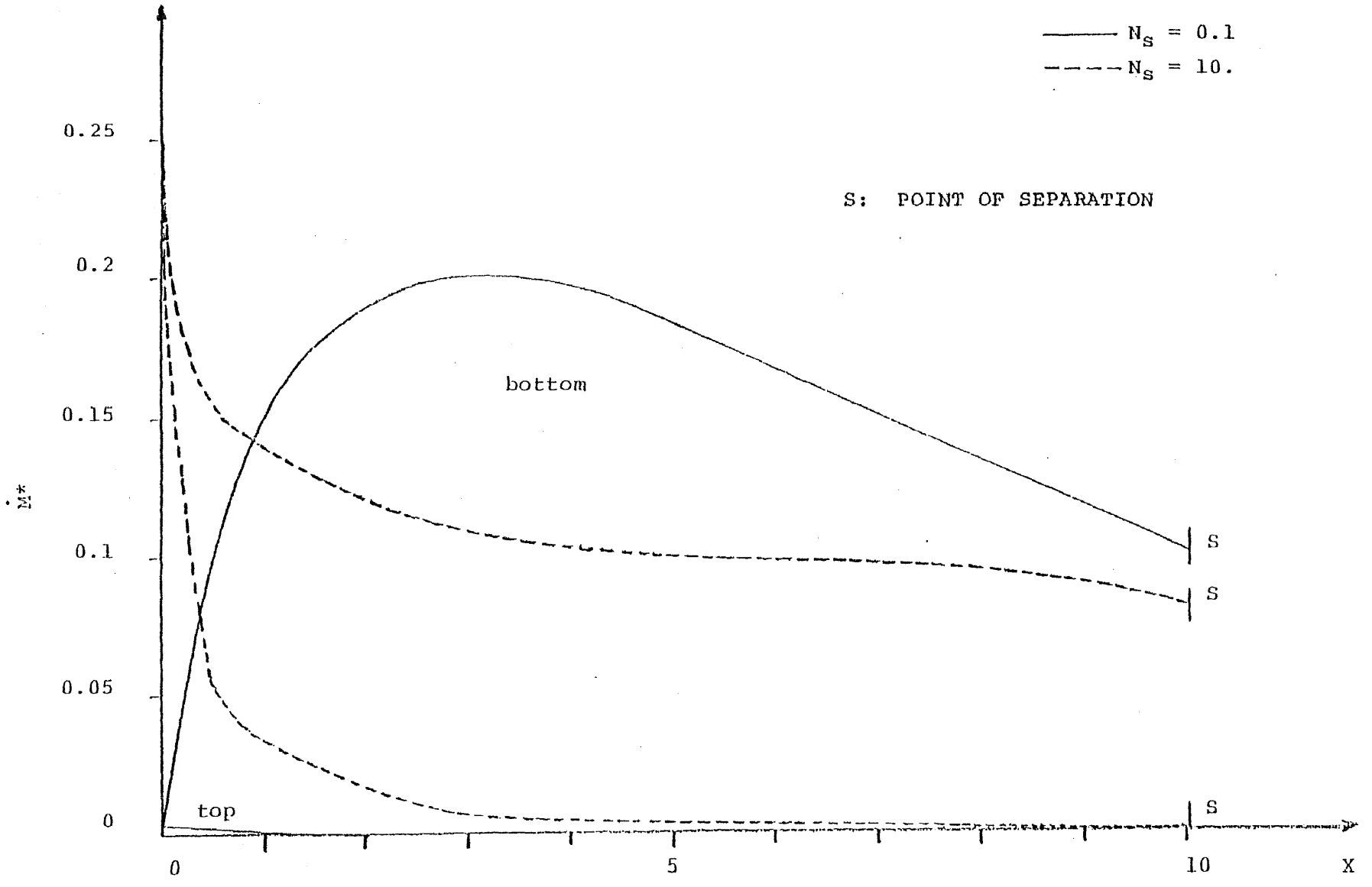

FIG. 4.28 EFFECT OF SURFACE ADHESION ON DEPOSITION RATE IN A DIVERGENT CHANNEL (K_{np} = 0.0001, N_α = 0, N_η = 5, 0 = 4°, N_β = 40, N_m = 2, N_R = 1000, σ = 0.5)

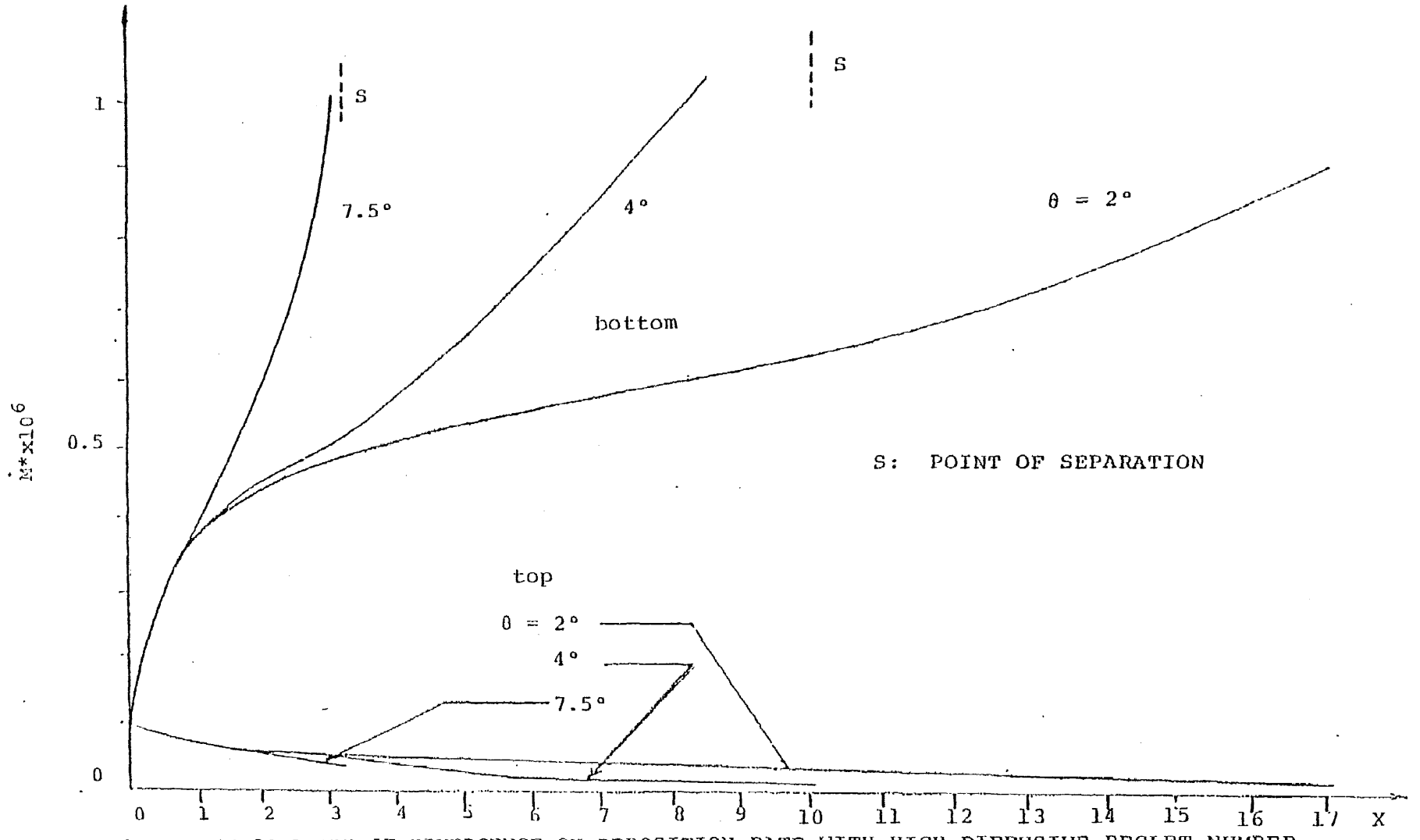

FIG. 4.29 EFFECT OF ANGLE OF DIVERGENCE ON DEPOSITION RATE WITH HIGH DIFFUSIVE PECLET NUMBER

($K_{np} = 0.0001$, $N_\alpha = 0$, $N_\eta = 5$, $N_\beta = 10^7$, $N_m = 2$, $N_s = 1$, $N_R = 1000$, $\sigma = 0.5$)

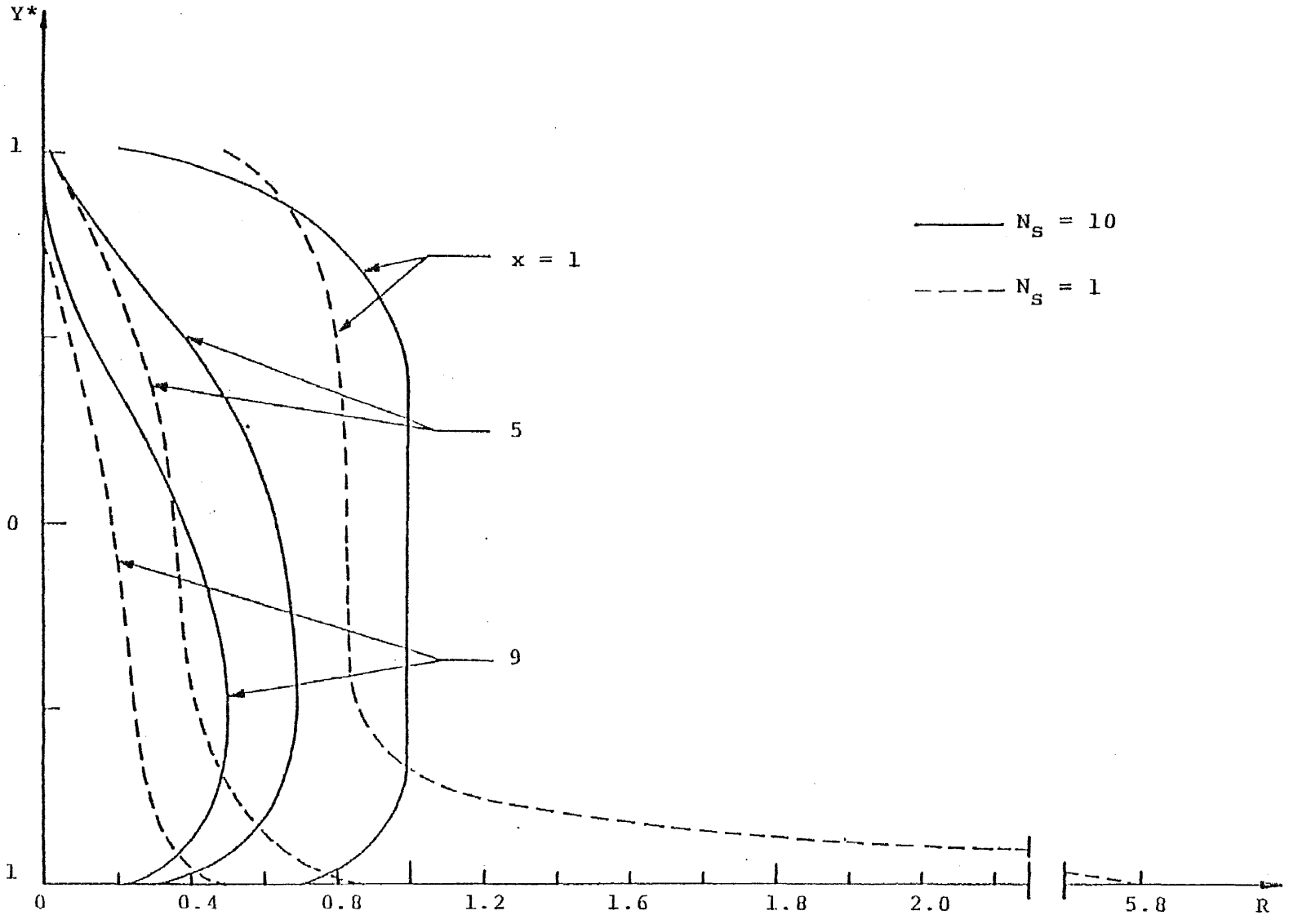

FIG. 4.30 AXIAL DISTRIBUTION OF PARTICLE CONCENTRATION WITH DIFFERENT SURFACE ADHESIONS IN A DIVERGENT CHANNEL (K_{np} = 0.0001, N_α = 1, N_η = 5, θ = 4°, N_β = 40, N_m = 2, N_R = 1000, σ = 0.5)

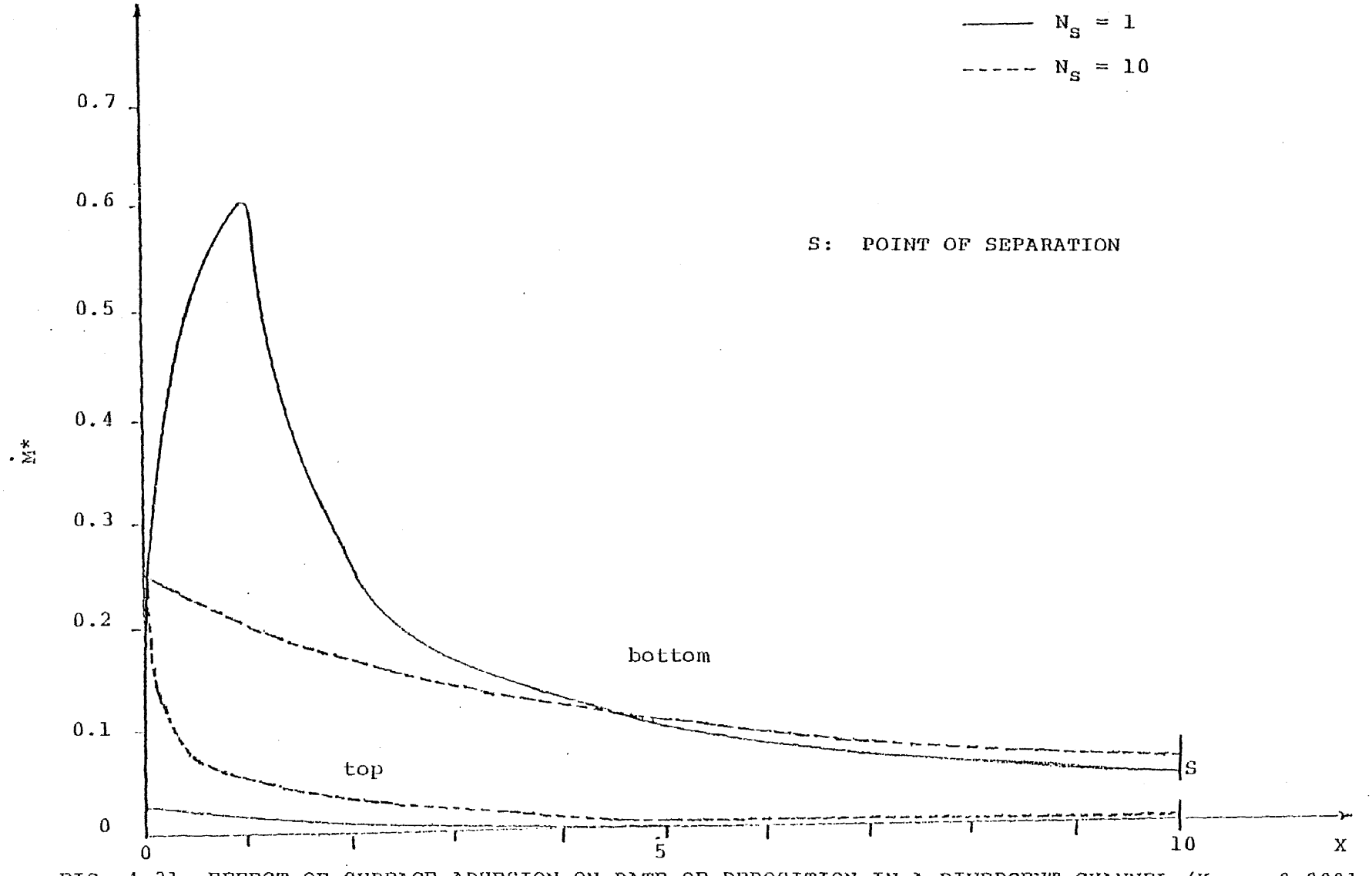

FIG. 4.31 EFFECT OF SURFACE ADHESION ON RATE OF DEPOSITION IN A DIVERGENT CHANNEL (K_{np} = 0.0001, N_α = 1, N_η = 5, 0 = 4°, N_β = 40, N_m = 2, N_R = 1000, σ = 0.5)

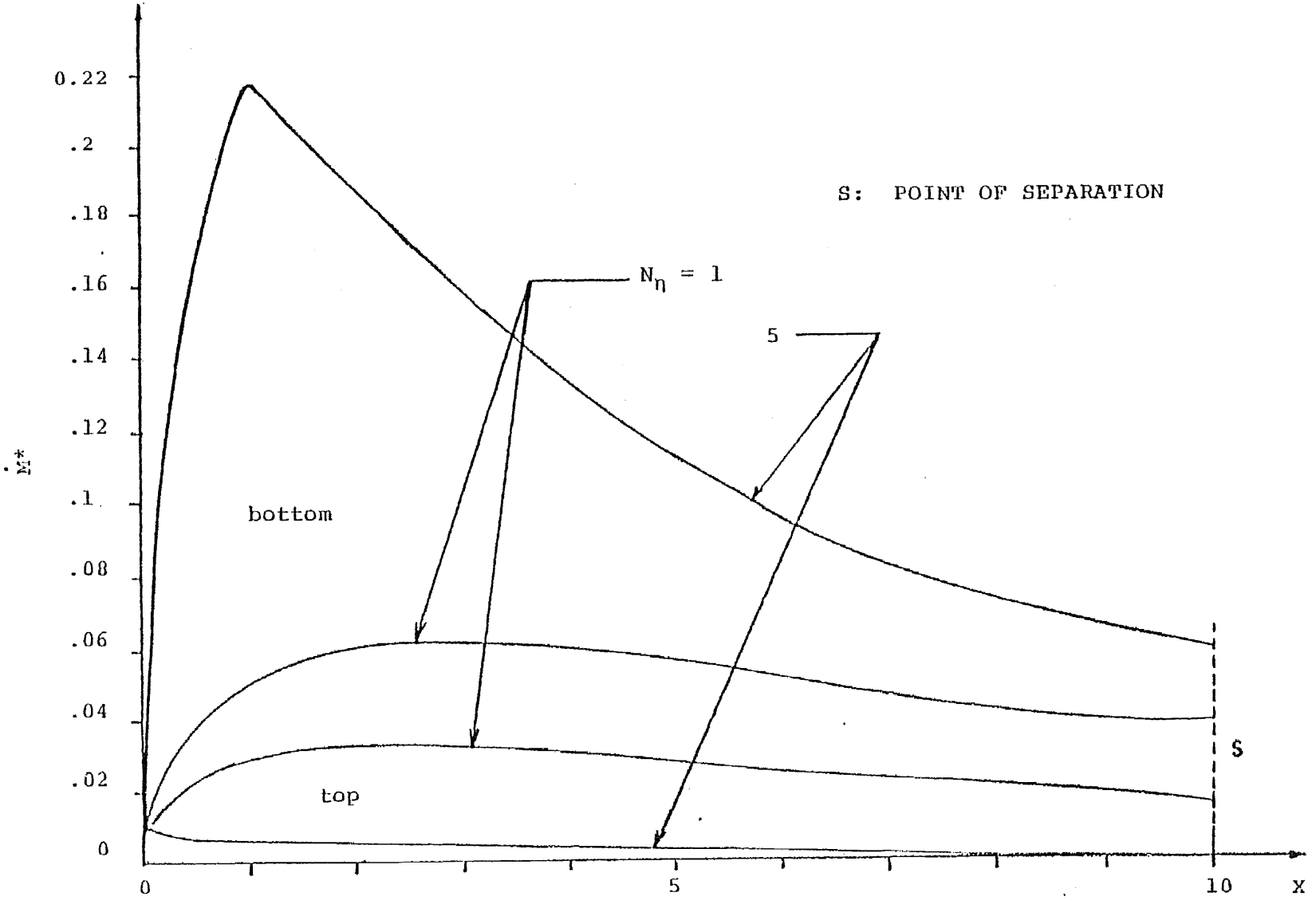

FIG. 4.32 INFLUENCE OF GRAVITY FLOW PARAMETER ON DEPOSITION RATE IN A DIVERGENT CHANNEL

(K_{np} = 0.0001, N_α = 1, θ = 4°, N_β = 100, N_m = 2, N_s = 1, N_R = 1000, σ = 0.5)

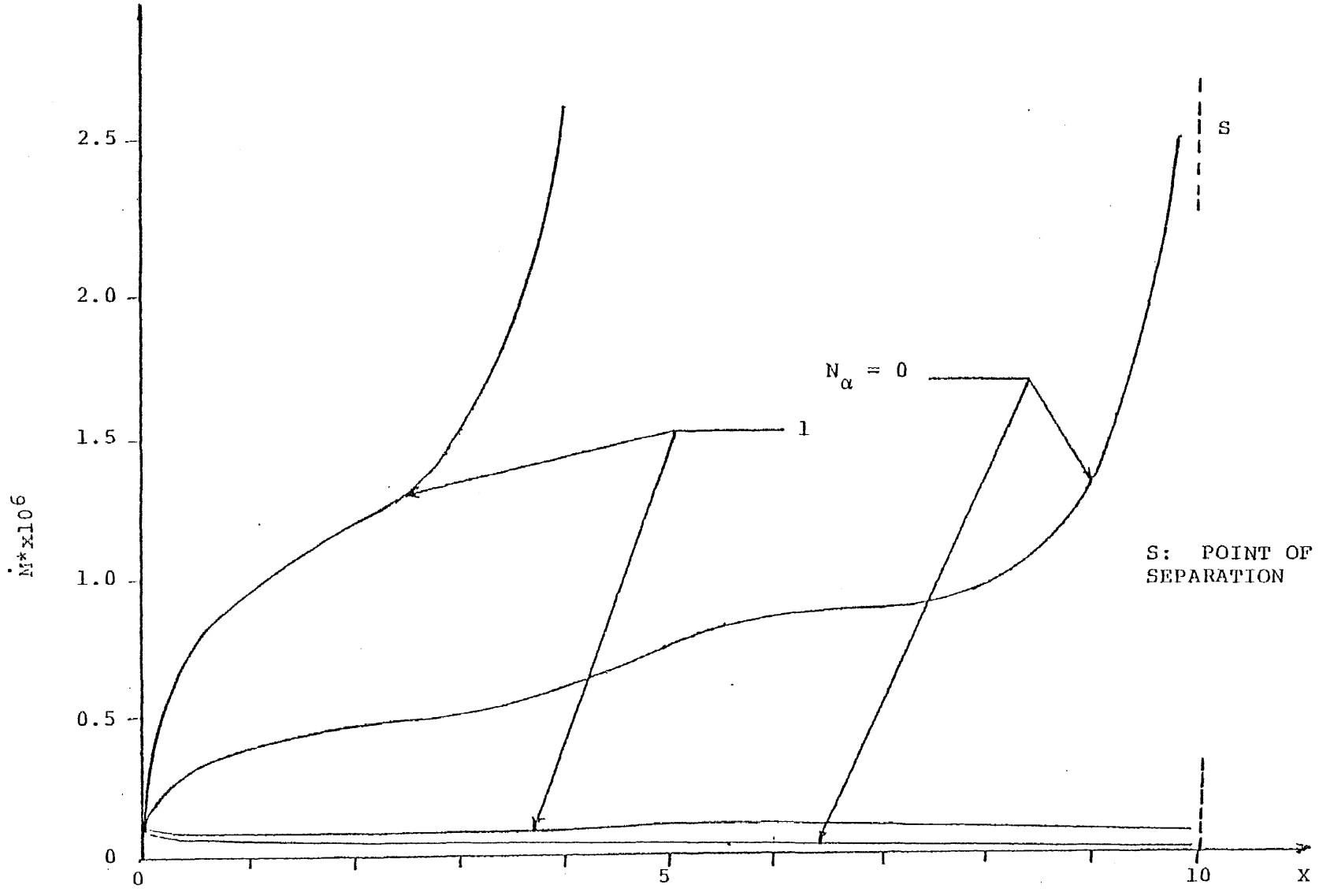

FIG. 4.33 EFFECT OF ELECTROSTATIC CHARGE ON DEPOSITION RATE WITH HIGH DIFFUSIVE PECLET NUMBER IN A DIVERGENT CHANNEL ($K_{np} = 0.0001$, $N_\eta = 4.5$, $\theta = 4°$, $N_\beta = 10^7$, $N_m = 2$, $N_s = 1$, $N_R = 1000$, $\sigma = 0.5$)

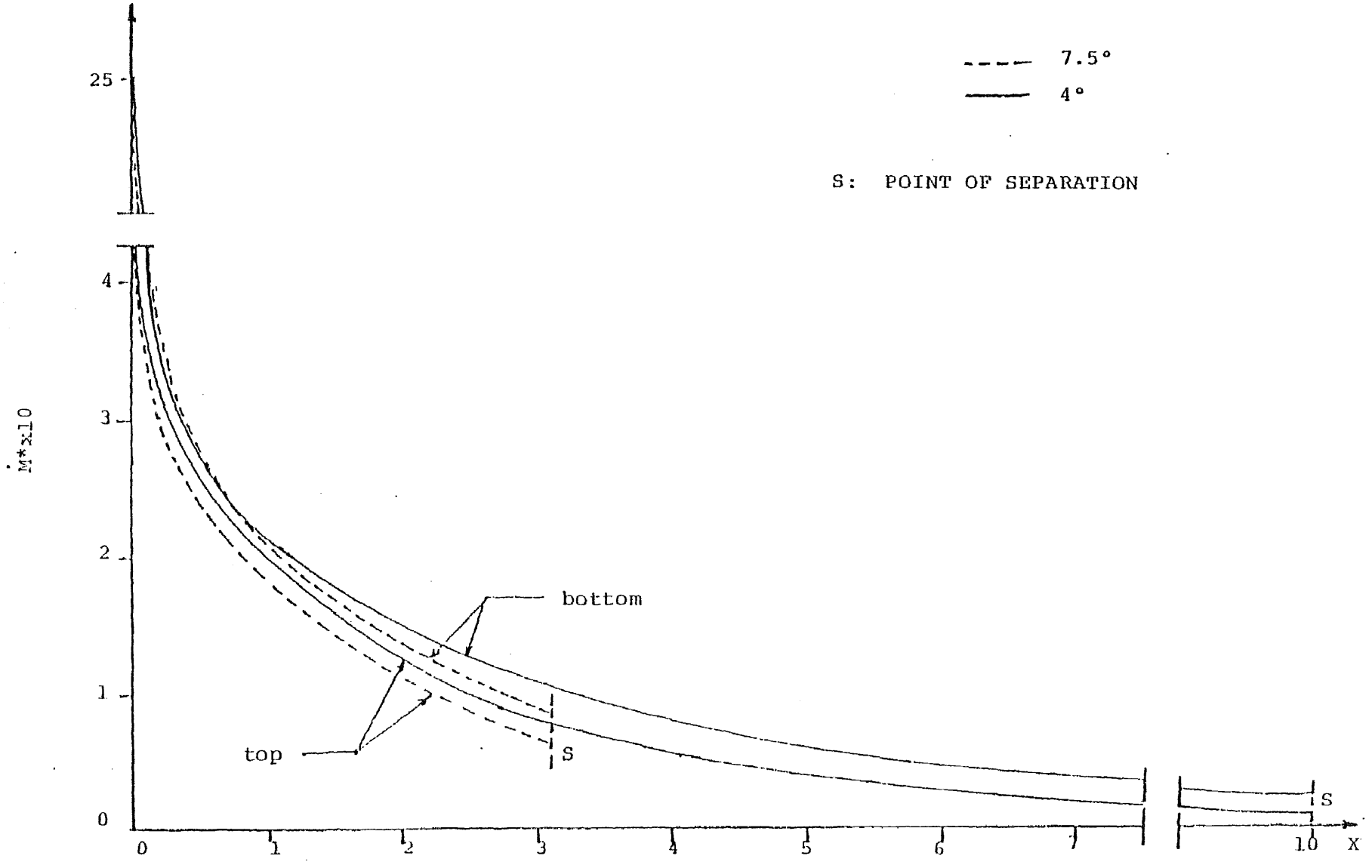

FIG. 4.34 EFFECT OF VERY HIGH ADHESION ON THE DEPOSITION RATE IN A DIVERGENT CHANNEL WITH θ = 4° and 7.5° (K_{np} = 0.0001, N_α = 10, N_η = 5, N_s = 1000, N_β = 40, N_m = 2, N_R = 1000, σ = 0.5)

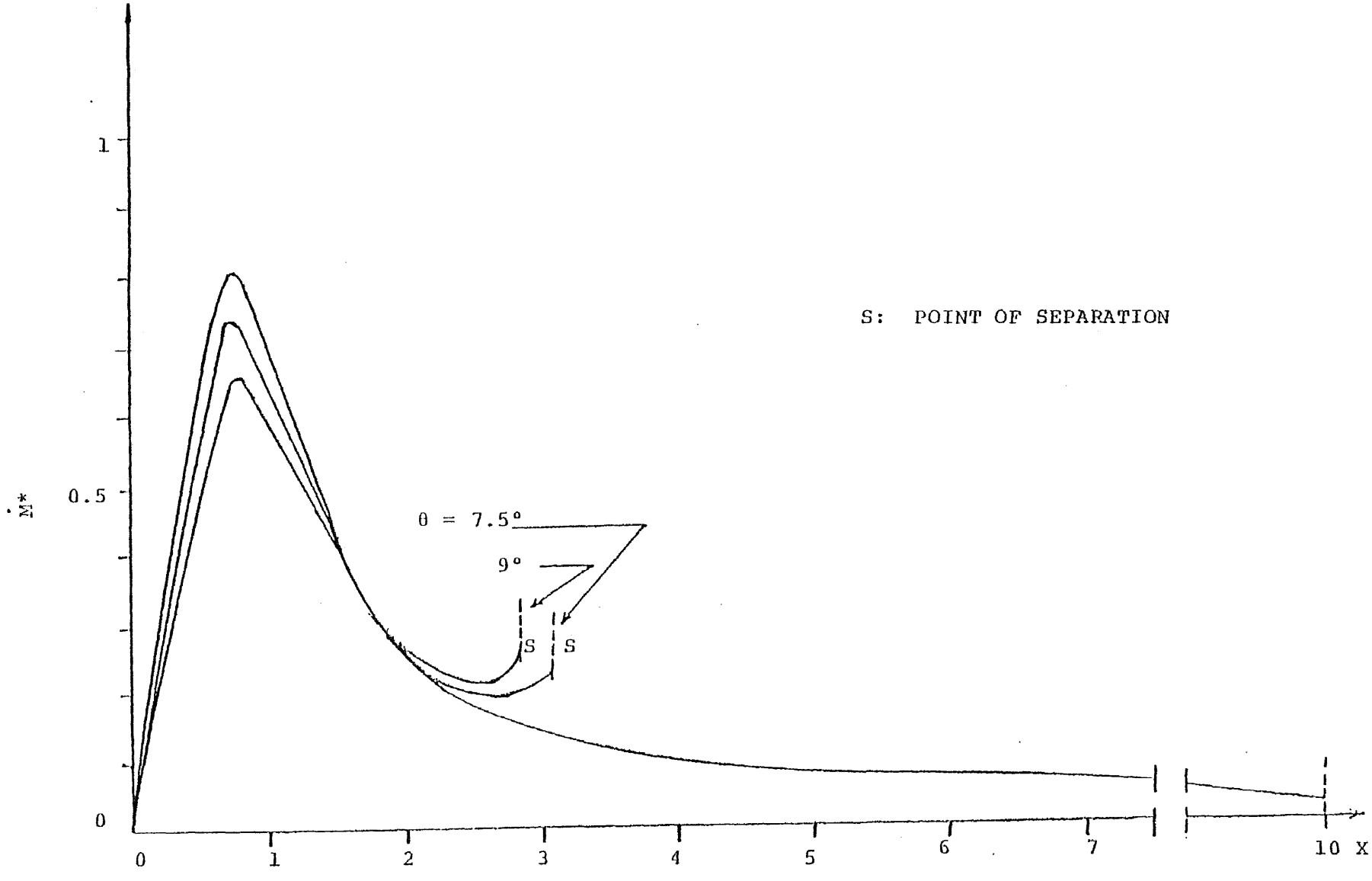

FIG. 4.35 EFFECT OF THE ANGLE OF DIVERGENCE ON THE BOTTOM DEPOSITION RATE IN A DIVERGENT CHANNEL

(K_{np} = 0.0001, N_α = 1, N_η = 4.5, N_β = 40, N_m = 2, N_S = 1, N_R = 1000, σ = 0.5)

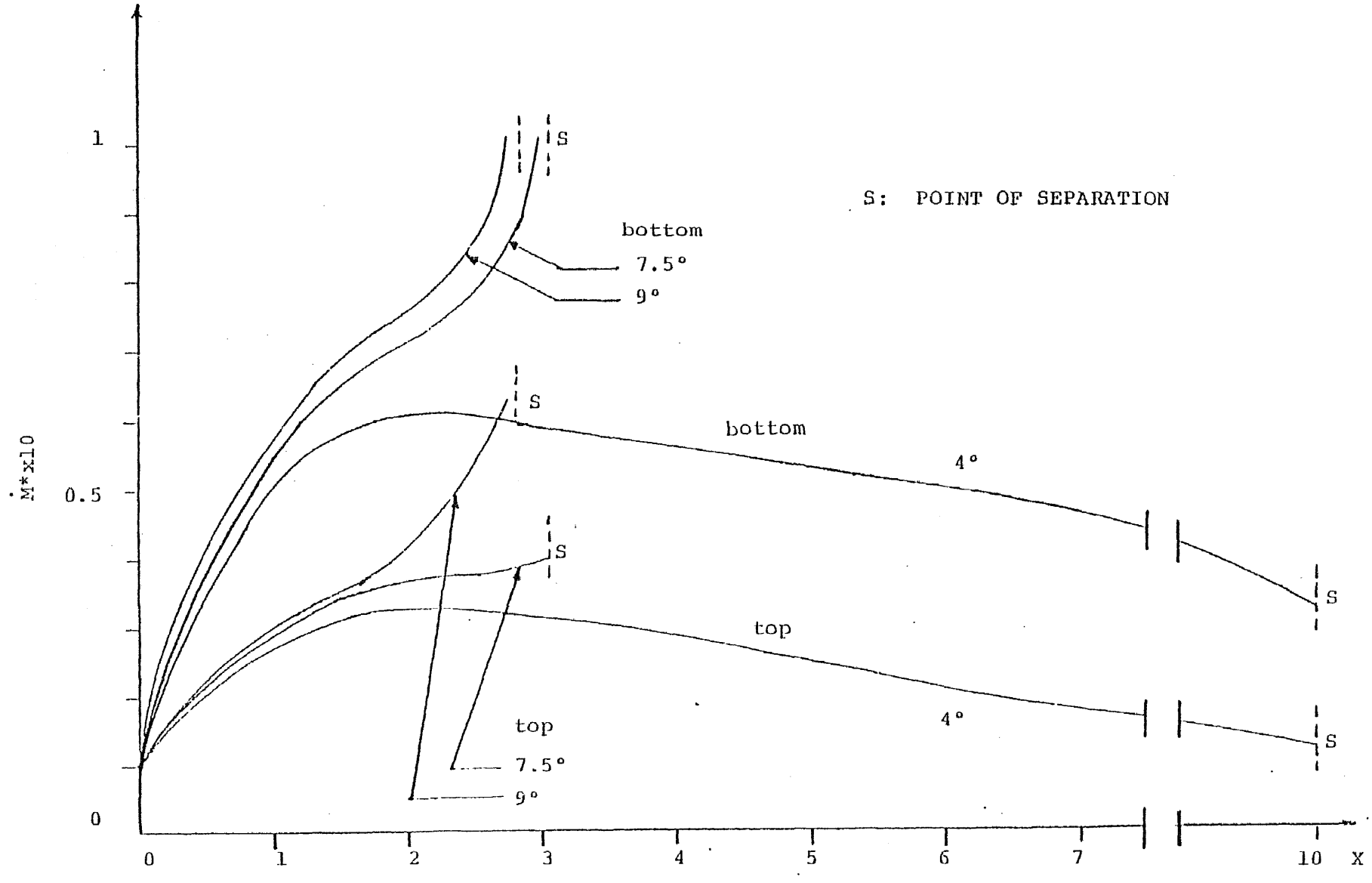

FIG. 4.36 EFFECT OF THE ANGLES OF DIVERGENCE ON THE DEPOSITION RATE IN A DIVERGENT CHANNEL
(K_{np} = 0.0001, N_α = 1, N_η = 1, N_β = 100, N_m = 2, N_s = 1, N_R = 1000, σ = 0.5)

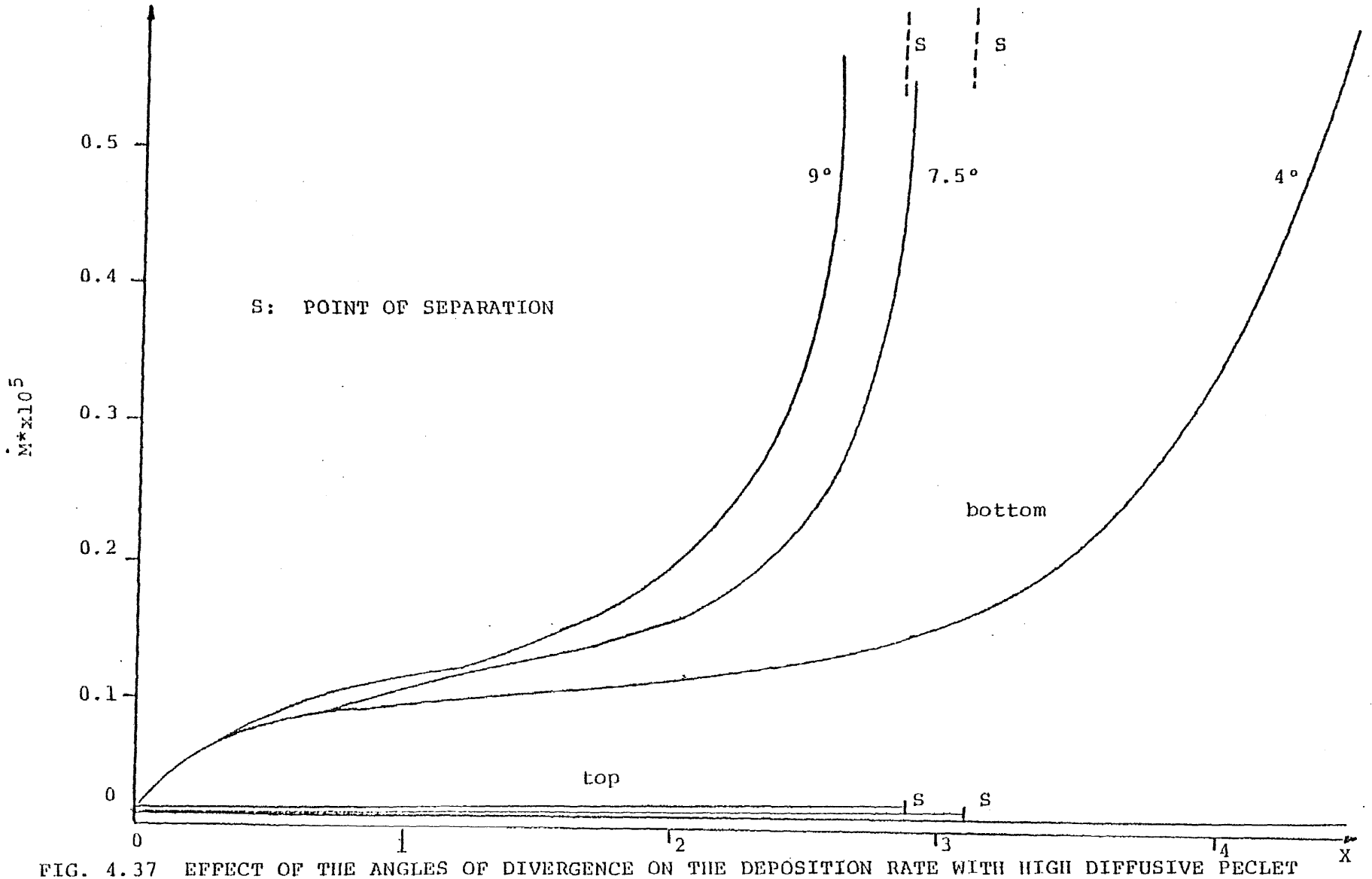

FIG. 4.37 EFFECT OF THE ANGLES OF DIVERGENCE ON THE DEPOSITION RATE WITH HIGH DIFFUSIVE PECLET NUMBER (K_{np} = 0.0001, N_α = 1, N_η = 4.5, N_β = 10^7, N_m = 2, N_s = 1, N_R = 1000, σ = 0.5)

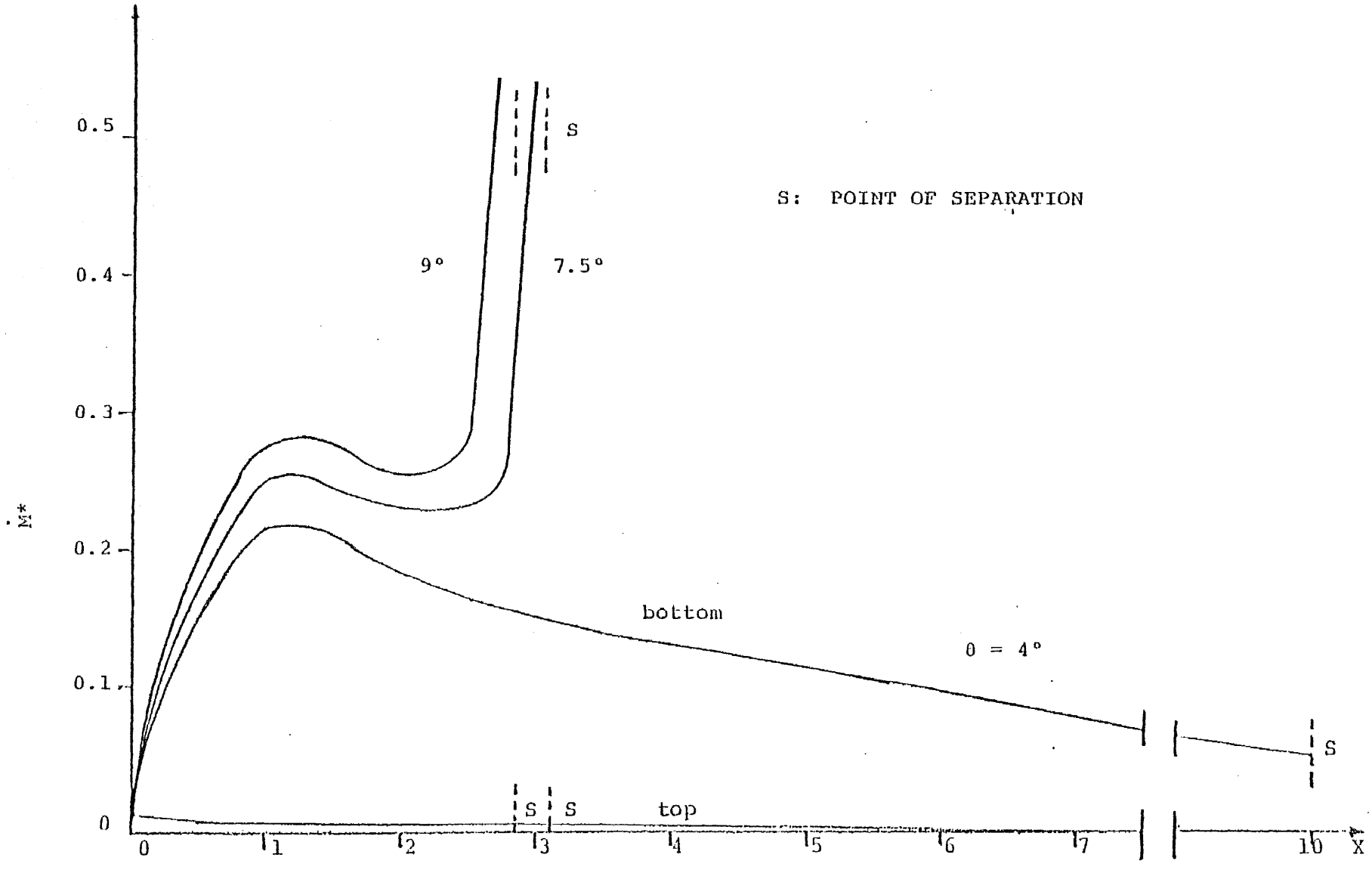

FIG. 4.38 EFFECT OF THE ANGLE OF DIVERGENCE ON THE DEPOSITION RATE IN A DIVERGENT CHANNEL

(K_{np} = 0.0001, N_α = 1, N_η = 5, N_β = 100, N_m = 2, N_s = 1, N_R = 1000, σ = 0.5)

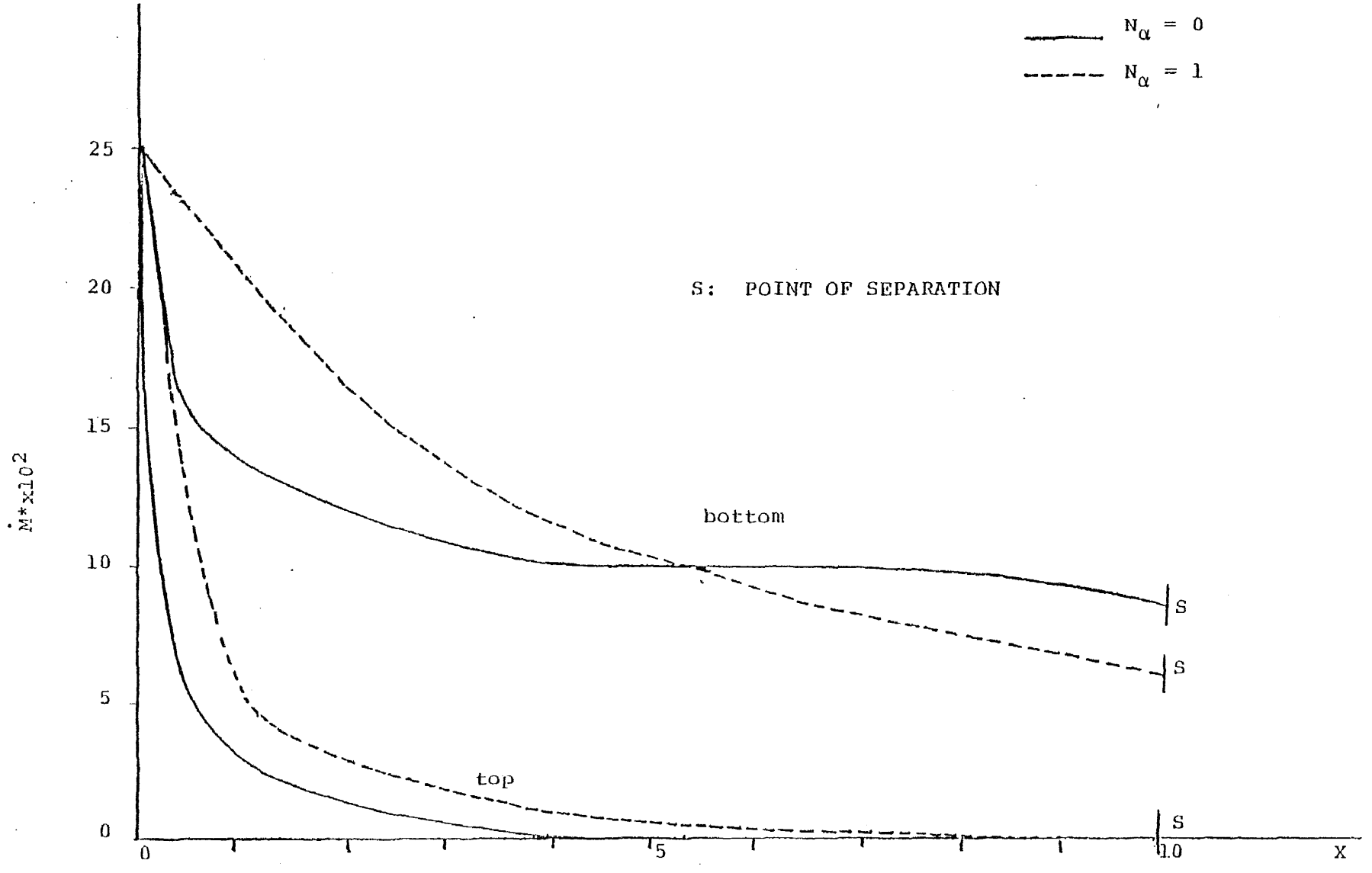

FIG. 4.39 EFFECT OF ELECTROSTATIC CHARGE ON RATE OF DEPOSITION IN A DIVERGENT CHANNEL (K_{np} = 0.0001, N_α = 1, θ = 4°, N_β = 100, N_m = 2, N_s = 1, N_R = 1000, σ = 0.5)

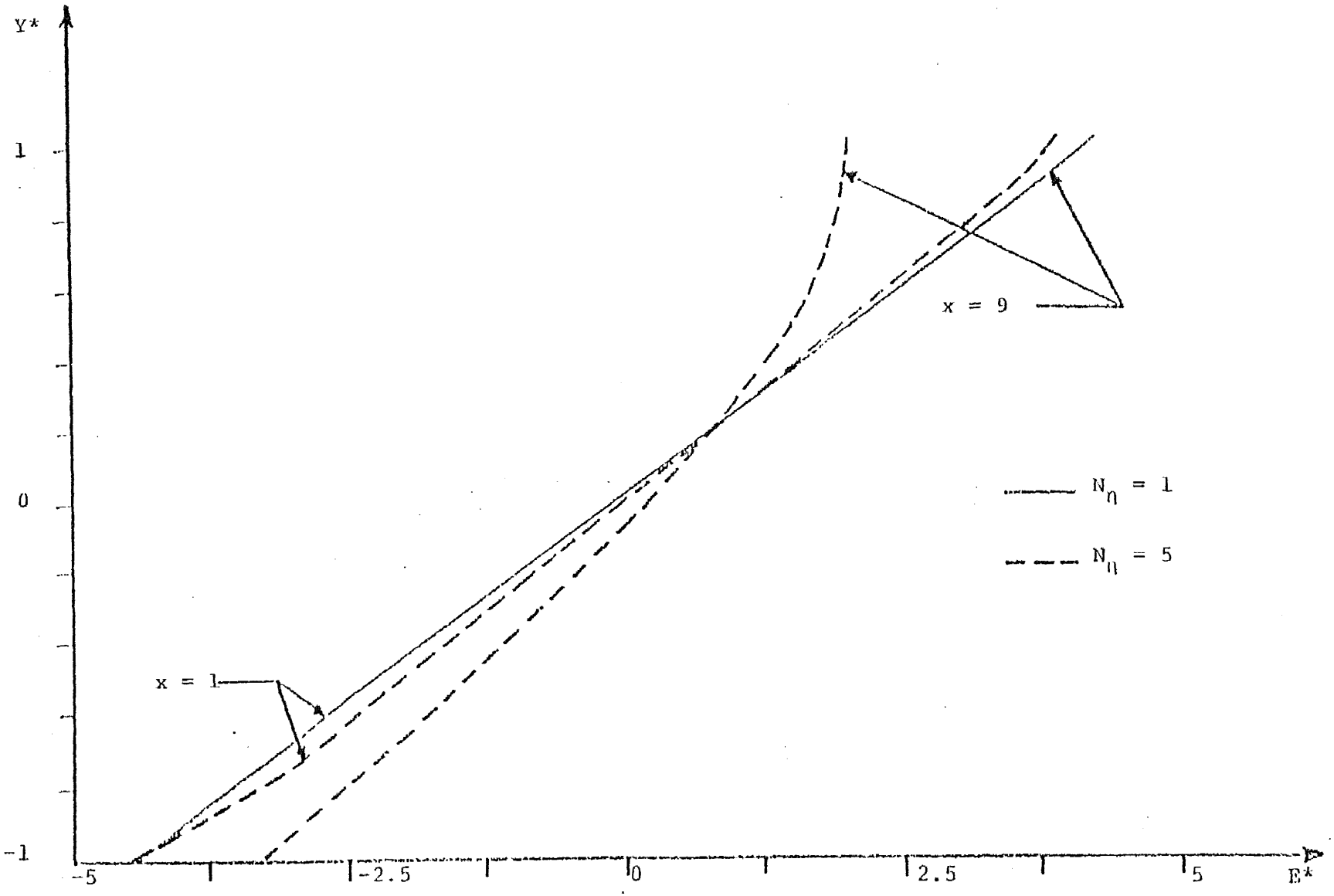

FIG. 4.40 GRAVITATIONAL INFLUENCE OVER THE AXIAL DISTRIBUTION OF ELECTRIC FIELD INTENSITY IN A DIVERGENT CHANNEL (K_{np} = 0.0001, N_α = 1, 0 = 4°, N_β = 100, N_m = 2, N_S = 1, N_R = 1000, σ = 0.5)

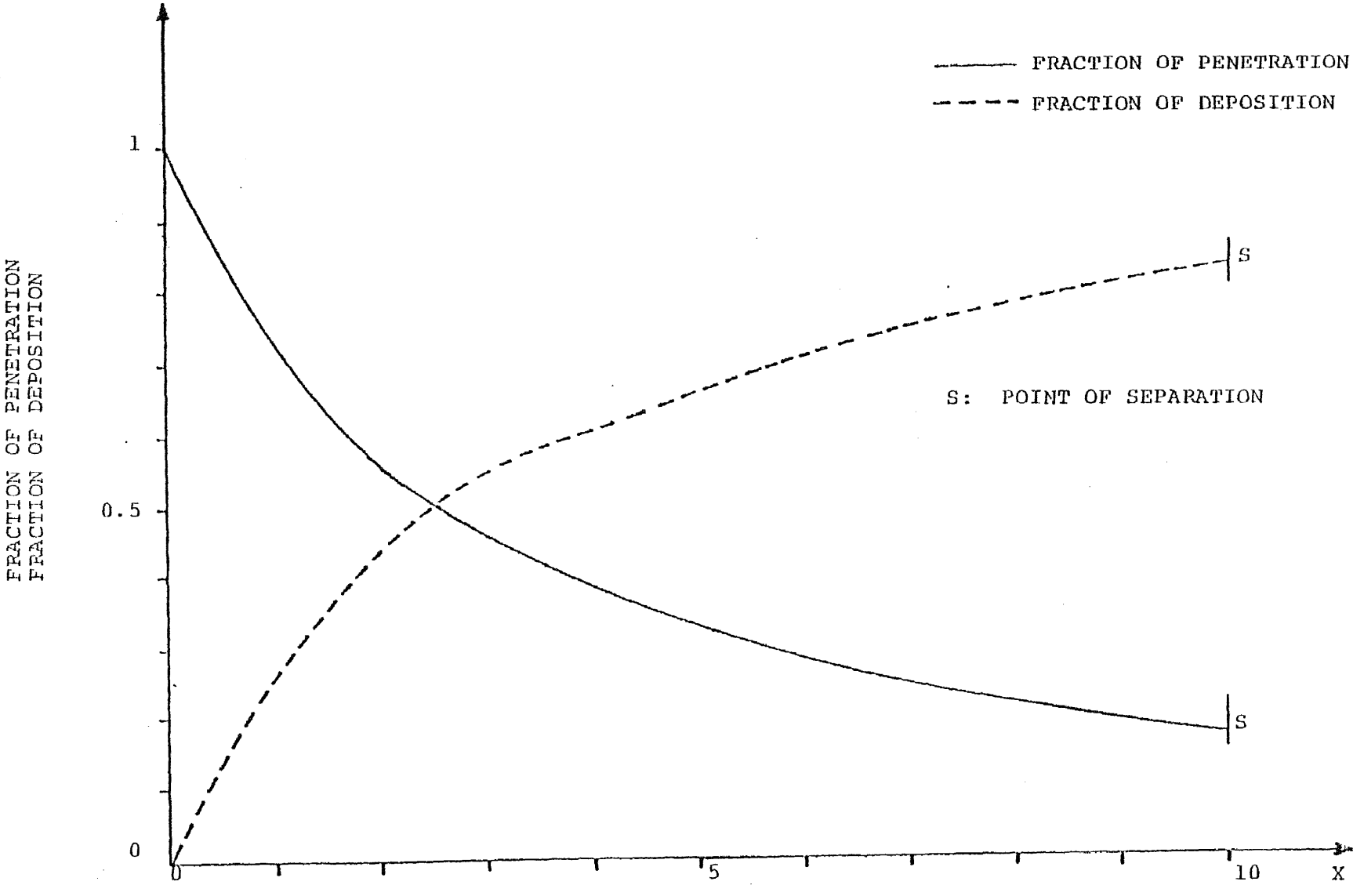

FIG. 4.41 AXIAL DISTRIBUTION OF FRACTION OF PENETRATION AND DEPOSITION IN A DIVERGENT CHANNEL

(K_{np} = 0.0001, N_α = 1, N_η = 4.5, 0 = 4°, N_β = 40, N_m = 2, N_S = 1, N_R = 1000, σ = 0.5)

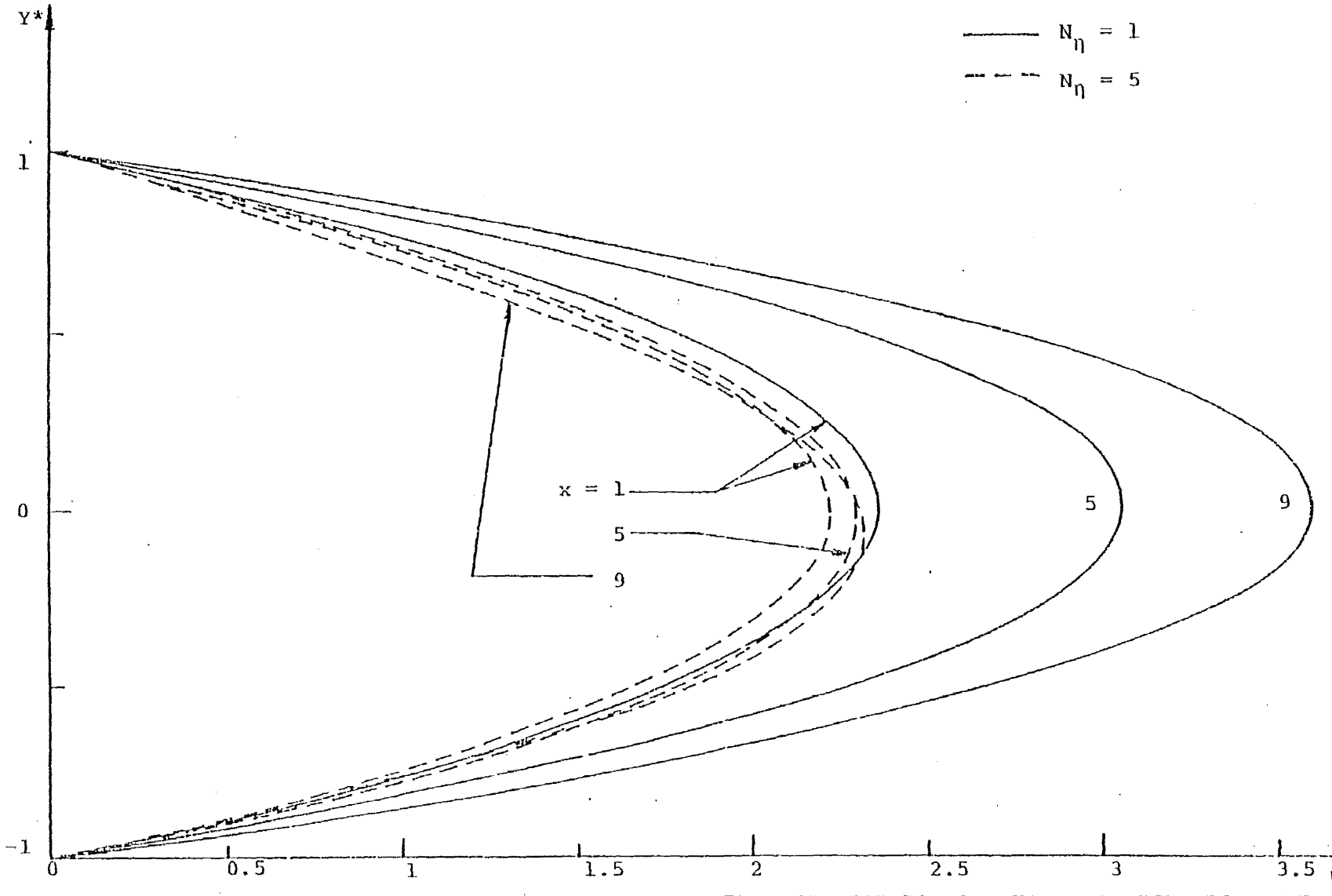

FIG. 4.42 EFFECT OF THE GRAVITY FLOW PARAMETER ON THE AXIAL DISTRIBUTION OF THE ELECTRICAL POTENTIAL IN A DIVERGENT CHANNEL (K_{np} = 0.0001, N_α = 1, 0 = 4°, N_β = 100, N_m = 2, N_s = 1, N_R = 1000, σ = 0.5)

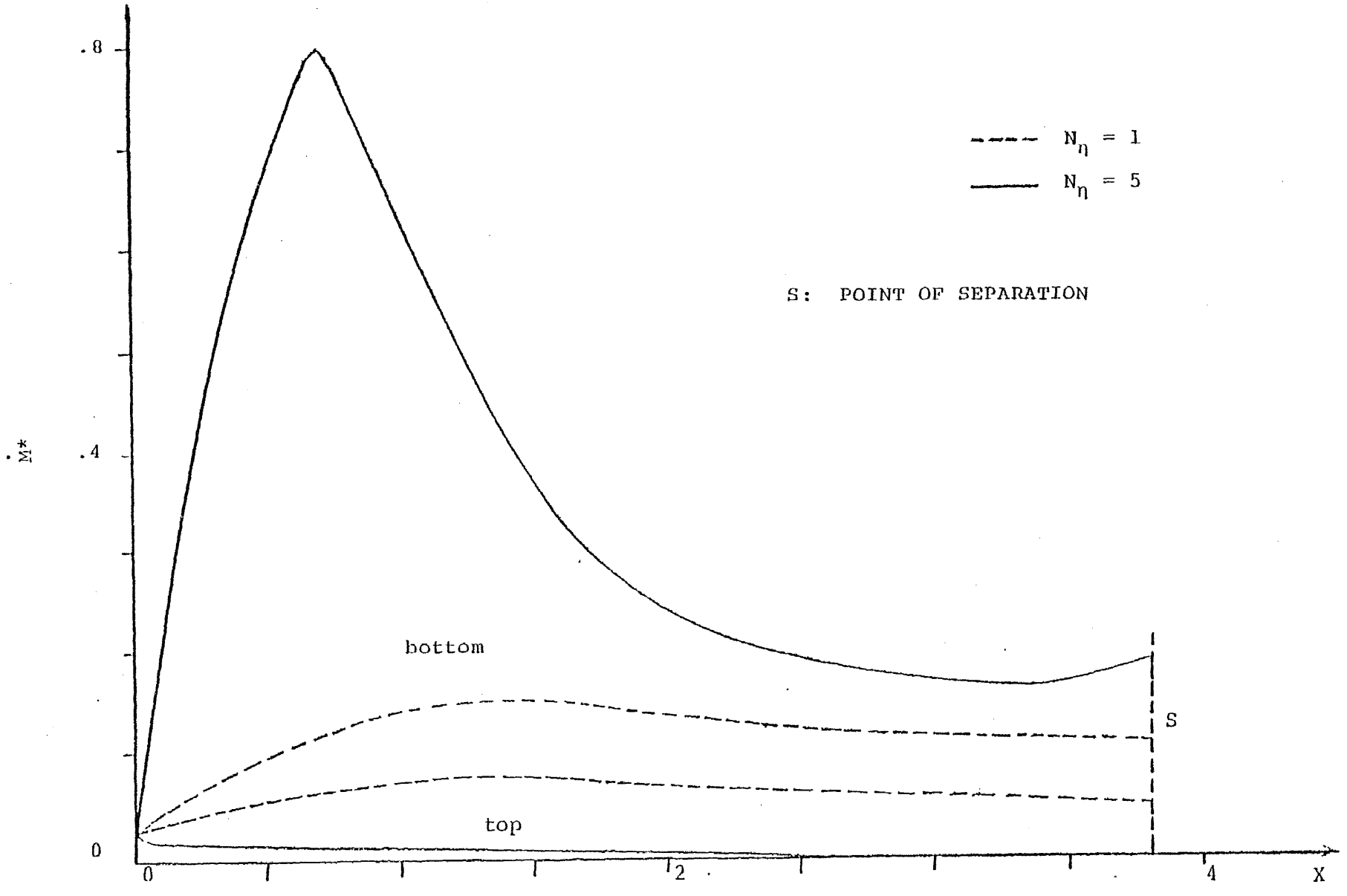

FIG. 4.43 EFFECT OF GRAVITY FLOW PARAMETER ON RATE OF DEPOSITION FOR THE CASE OF A PARALLEL CHANNEL CONNECTED TO A DIVERGING CHANNEL (K_{np} = 0.0001, N_α = 1, θ = 7.5°, N_β = 40, N_m = 2, N_s = 1, N_R = 1000, σ = 0.5)

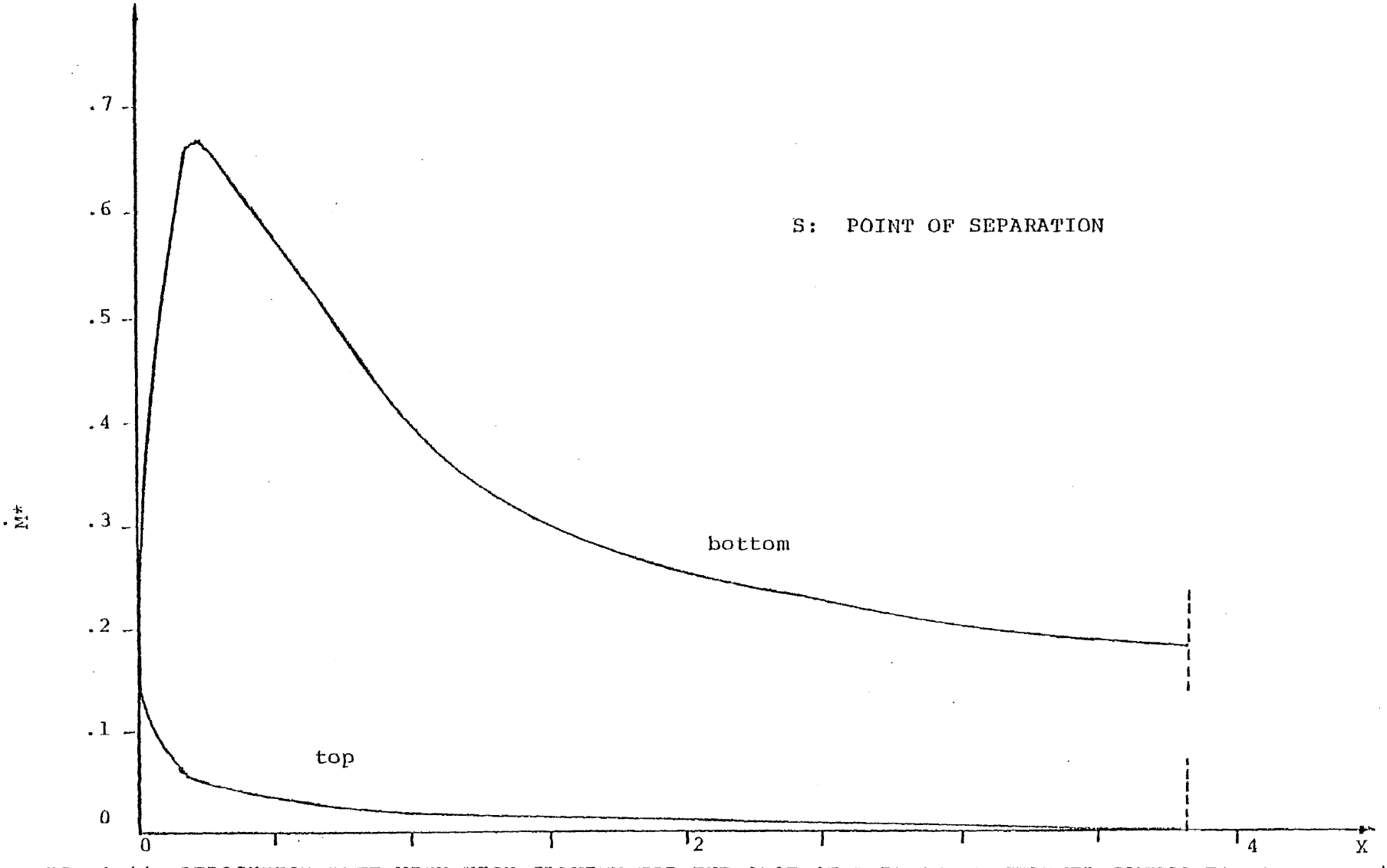

FIG. 4.44 DEPOSITION RATE WITH HIGH GRAVITY FOR THE CASE OF A PARALLEL CHANNEL CONNECTED TO A DIVERGING CHANNEL (K_{np} = 0.0001, N_α = 1, N_η = 10, θ = 7.5°, N_β = 40, N_m = 2, N_S = 7.0, N_R = 1000, σ = 0.5)

VITA

THOMAS ANTHONY KORJACK was born

. He received his B.S. Degree in Applied Mathematics at Newark State College in 1973. He received his M.S. in Applied Mathematics at Newark College of Engineering in 1974.

He was awarded a college teaching fellowship from Fall 1974 to Fall 1976, followed by an Adjunct instructoral position from Fall 1976 through Spring 1978 while serving as a research assistant during 1976-1978, all during his doctoral program in New Jersey Institute of Technology (NJIT), Newark, New Jersey, U.S.A.